PEOPLE'S DEMOCRATIC REPUBLIC OF ALGERIA

MINISTRY OF HIGHER EDUCATIONAND SCIENTIFIC RESEARCH
FERHAT ABBAS UNIVERSITY – SETIF -1-

THESIS

Submitted to Institute of Optics and Precision Mechanics
For the degree

Doctorat LMD 3rd cycle
In Applied Optics and Photonics
By

Walid Allag

Title

Study of thin films for photovoltaic solar cells

Defended on: 18/07/2022   **In front of the composed committee of**

Chairman	**BELKHIR Nabil**	**Pr.**	**Setif -1 University**
Supervisor	**GUESSAS Hocine**	**Pr.**	**Setif -1 University**
Examiners	**AZIZI Amor**	**Pr.**	**Setif -1 University**
Examiners	**NOUIRI Abdelkader**	**Pr.**	**O.E Bouaghi University**
Examiners	**KHELLADI M.Redha**	**Pr.**	**BBA University**

الجمهورية الجزائرية الديمقراطية الشعبية
République Algérienne Démocratique Et Populaire
وزارة التعليم العالي والبحث العلمي
Ministère de L'Enseignement Supérieur et de La Recherche Scientifique
جامعة فرحات عباس- سطيف1
Université Ferhat Abbas - Sétif 1

THÈSE

Présentée à l'Institut d'Optique et Mécanique de Précision pour l'obtention du
Diplôme de

DOCTORAT 3ème Cycle LMD
Domaine : Sciences et Techniques
Filière : Optique et mécanique de Précision
Spécialité: Optique et Photonique Appliqué

Par
Walid Allag

Thème

Etude des couches minces pour les cellules photovoltaïques

Soutenue, le : 18/07/2022   **Devant le jury composé de :**

Président du Jury	**BELKHIR Nabil**	**Pr.**	**F.A.U Setif -1**
Directeur de thèse	**GUESSAS Hocine**	**Pr.**	**F.A.U Setif -1**
Examinateur	**AZIZI Amor**	**Pr.**	**F.A.U Setif -1**
Examinateur	**NOUIRI Abdelkader**	**Pr.**	**Univ. O.E.Bouaghi**
Examinateur	**KHELLADI M. Redha**	**Pr.**	**Univ.BBA**

Abstract

Study of thin films for photovoltaic solar cells

Undoped and Rare Earth Elements (Er, Yb) doped ZnO thin films were deposited onto glass substrates via sol gel dip coating technique, to investigate the effect of REEs doping concentration on the structural, Morphological and optical properties of ZnO thin films. The pH was maintained at 9 for all prepared sols by controlling the amount of Monoethanolamine (MEA). The effects of Er and Yb doping concentration on the ZnO films properties was studied by using XRD, SEM, AFM, Raman spectroscopy FTIR and UV–visible spectrophotometer. The results showed that the incorporation of Er^{3+} and Yb^{3+} under alkaline pH had a great effect on the ZnO properties.

The XRD spectra of (Er3+, Yb3+) doped ZnO revealed that all synthesized samples exhibit a polycrystalline hexagonal wurtzite structure with no additional peak assigned to REEs.

Homogenous, smooth and dense granular morphology nanostructures were revealed by AFM and SEM analysis. all samples show a low roughness value which decreases when increasing Er and Yb doping concentrations. Raman spectroscopy and FTIR analysis were found very consistent with XRD results.

the optical transmittance was found to be improved by RRE (Er3+, Yb3+), A red-shift was observed in the band gap of both Er and Yb doped ZnO films with increasing doping rate.

This study allowed us to get ZnO thin films with very important structural, optical properties, which are very promising in photovoltaic applications.

Keywords*: Rare earth; ZnO; Erbium; Ytterbium; Alkaline pH; Raman spectroscopy*

Résumé

Etude des couches minces pour les cellules photovoltaïques

Des couches minces de ZnO non dopés et dopés par des éléments de terres rares (Er, Yb) ont été déposés sur des substrats de verre via sol-gel « dip coating » technique, pour étudier l'effet de la concentration de dopage en terres rares sur les propriétés structurelles, morphologiques et optiques des films minces de ZnO. Le pH a été maintenu à 9 pour tous les sols préparés en contrôlant la quantité de monoéthanolamine (MEA). Les effets de la concentration de dopage Er et Yb sur les propriétés des films de ZnO ont été étudiés à l'aide de XRD, SEM, AFM, spectroscopie Raman FTIR et spectrophotomètre UV-visible. Les résultats ont montré que l'incorporation de Er3+ et Yb3+ sous pH alcalin avait un effet important sur les propriétés du ZnO.

L'étude par DRX du ZnO pure et dopé (Er3+, Yb3+) ont révélé que tous les échantillons obtenus présentent une structure wurtzite hexagonale polycristalline.

Des nanostructures de morphologie granulaire homogènes, lisses et denses ont été révélées par analyse AFM et MEB. Tous les échantillons présentent une faible valeur de rugosité (RMS) qui diminue lorsque les concentrations de dopage Er et Yb augmentent. La spectroscopie Raman et l'analyse FTIR se sont avérées très cohérentes avec les résultats obtenus par DRX.

Tous les échantillons du ZnO dopés par Er and Yb présentent une transparence élevée par rapport aux ZnO pure (~85%), tandis que l'énergie de gap des films de ZnO dopés diminue avec l'augmentation du taux de dopage.

Cette étude nous a permis d'obtenir des couches minces de ZnO aux propriétés structurales, optiques très importantes, très prometteuses dans les applications photovoltaïques.

Mots-clés *: Terre rare ; ZnO ; Erbium ; Ytterbium ; pH alcalin ; Spectroscopie Raman*

Dedication

To my Parents and brothers

 The reason of what I become today

Thanks for your great support and continuous care.

To my sweet wife

I am really grateful to you. You have been my inspiration throughout the journey.

To my Friends.

Acknowledgements

Table of contents

CHAPITRE II: FILM GROWTH METHODS AND MATERIALS CHARACTERIZATION

CHAPITRE III: RESULTS AND DISCUSSION

List of figures

x

List of tables

General Introduction

For nearly two decades, Nanotechnology is one of the world's fastest-growing inventions. Fabrication, manipulation, and characterization of materials at the nanoscale are also part of nanotechnology (usually between 1 and 100 nm). In all fields, such as manufacturing, research, security, biomedical, and biology, nanotechnology has a profound effect on economic, educational, and social innovations. It's just one of the inventions behind the millennium's educational transition. Moreover, nanotechnology education is being integrated into engineering and science classes at many universities around the world for aspiring engineers and scientists [1].

Nanostructured materials are a major concern for individual researchers and research organizations all over the world because of their enormous potential for social benefits. Although nanostructure materials have been present in practical applications far back in human history, it is only in recent times that it has been possible to synthesize these structures in a controlled manner, to characterize them, and thereby gain a better understanding of past known and newly discovered nanostructured materials [2] Nanoscale technologies such as nanoparticles, nanotubes, nanofibers, nanocomposites, and nanofilms, which are all called the next generation of materials, have been used in a variety of industries due to their unique properties. [3,4].

The synthesis of nanostructure materials is the key innovation of the 21st century in a wide range of applications. Because of their unusual size and shape-based physiochemical properties, semiconducting metal oxides such as ZnO, TiO2, and SnO2 have been studied and commonly used. Among these, ZnO shows an excellent stability in chemically as well as thermally stable n-type semiconducting material which make it suitable for wide range of uses in optoelectronics and transparent electronics [5].

Up to now, a several methods are used to prepare ZnO thin films including pulsed laser deposition, spray pyrolysis, electrochemical method and co-precipitation method. Among these methods, sol–gel method is widely used in the laboratory and industrial production due to its advantages over other processes such as, low cost, possibility of large-scale production, the precise control over the film morphology and thickness, low fabrication temperature [6-10].

The objective of this work was to deposit undoped and rare earth element (REE) doped ZnO thin films by Sol Gel "Dip Coating" method with a careful preparation condition. In order to

understand the growth behavior of ZnO thin films, REE doping effects on ZnO thin films properties, several techniques were employed to characterize prepared ZnO films and thus investigate its optical, morphological and structural properties.

This thesis consists of three chapters, and it is organized as follows:

the first chapter includes a general overview on the properties of layered ZnO thin as well as its main applications in technological fields,

Chapter two is divided into two main sections; the first section presents a general description of the growth process of ZnO thin films via Sol gel "dip coating" technique, while the second provides a brief description of the characterization technique and the equipment employed to characterize zinc oxide.

The third chapter presents the characterization study of Zinc oxide thin films undoped and doped with different rare earth elements which are Erbium and Ytterbium; where the main objective is for finding out the effect of doping rate on the ZnO thin films; in accordance with the results have gotten enough interpretation and discussion.

Finally, we conclude our thesis by some general conclusions, a discussion, and possible perspectives.

Chapter I:

Background and literature survey

I.1 Introduction
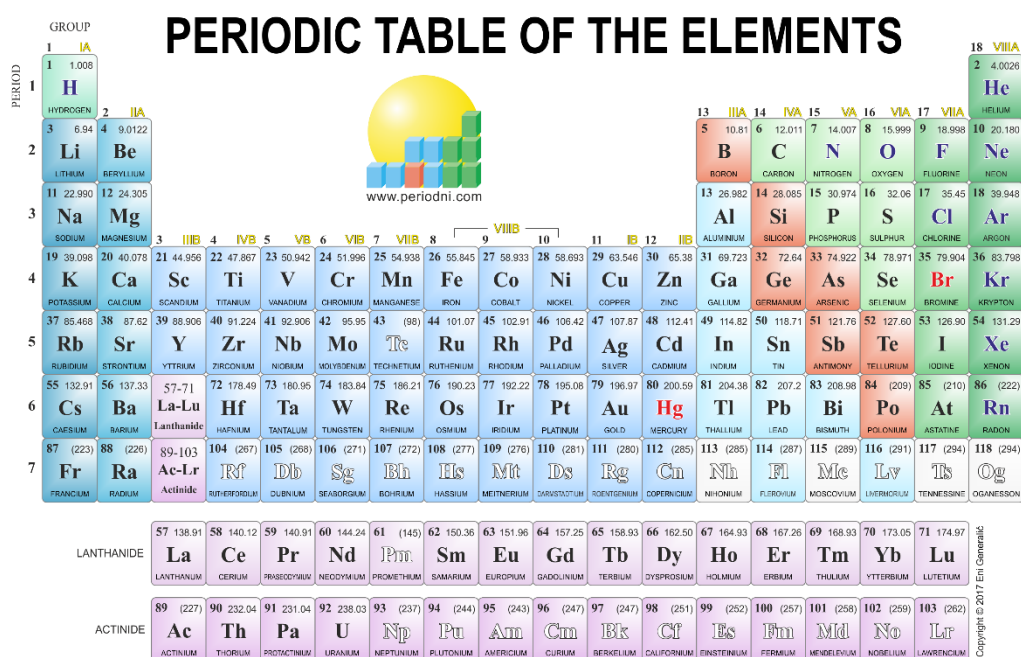
Since last three decades various groups of semiconductors have come up to play an important role in the development in the field of science and technology. Among those groups the well-known II-VI compounds' semiconductors group like ZnS, ZnSe, ZnO and ZnTe have been successfully used in many scientific applications.

The II–VI compound semiconductors, have been extensively studied due to its effective use in a variety of practical applications such as in optoelectronic industry, solar cells, passivation layers, transparent UV protection films, chemical sensors, piezoelectric transducers, transparent conductor's solid-state laser devices, photodetectors etc [11, 12]

II-VI semiconductor compounds are combinations of two atoms, one of the alkaline earth metals (group 2 of the Periodic table) or one of the group 12 elements (group 12 of the periodic table) and one atom of the Chalcogens (group 16 of the periodic table) **Fig I.1**.

In the past few decades, zinc oxide as one of the II-VI compound semiconductors have attracted considerable technological and scientific interest due to their potential applications in diversified areas. besides, ZnO based thin films is a suitable candidate as a transparent conducting oxide to be applied in solar cells industry.

Figure I. 1*. Periodic table of elements*

I.2 Zinc oxide: Fundamental properties

ZnO is a key technological material, it occurs in nature as the mineral zincite in the earth crust (**Fig I.2**). however, for most applications ZnO must be produced synthetically for specific applications. ZnO was discovered in 1810 by Bruce in Franklin Furnace (New Jersey, USA) and since then it has been commercially the most important chemical compound of zinc element [13]

Figure I.2. Photographs of an orange zincite crystal

Zinc oxide (ZnO) is a nontoxic inorganic compound belongs to the family of II–VI compound wide-gap semiconductor with a room temperature direct band gap of 3.37 eV (**Fig I.3**). and a large exciton binding energy of about 60 meV, which is almost three times greater than that of GaN (25 meV), GaAs (4 meV) and ZnSe (22 meV) at room temperature. which makes it a very attractive material for the applications to the advanced optoelectronic devices [14, 15]. Zinc oxide has attracted significant attention as a material for ultraviolet (UV) light-emitters, varistors, transparent high-power electronics, surface acoustic wave devices, piezoelectric transducers and gas sensors and also as a window material for displays and solar cells [16,17].
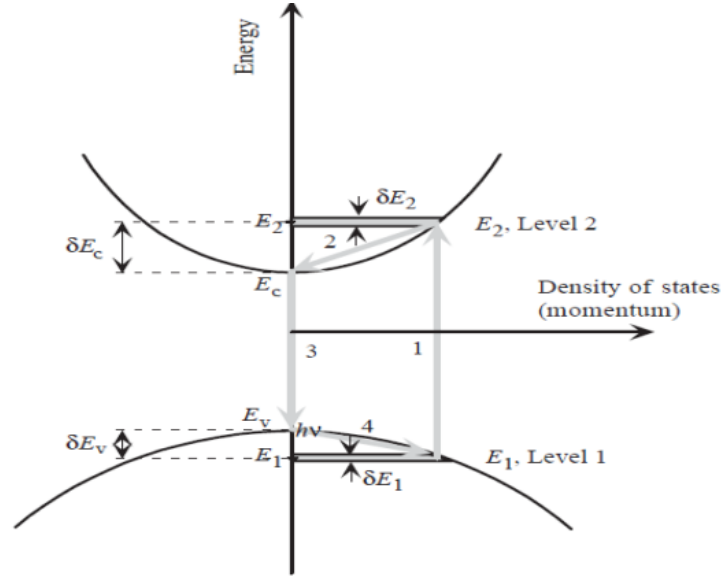
Figure I.3*: Optical transitions in a direct band-gap semiconductor on the energy versus momentum (which also represents energy versus density of states though the functional forms deviate) diagram, which is pumped beyond transparency [18]*

I.2.1   Crystal structure

Depend on the pressure and temperature conditions, Zinc Oxide crystallizes in three different structures namely: wurtzite (B4), zinc blende (B3), and rock-salt (B1) [19] **Fig I.4**. The zinc blende ZnO structure can be stabilized only by growth on cubic structures, whereas rock salt structure as a metastable phase may only obtained at relatively high pressures, as in the case of GaN [18]. At ambient temperatures and pressure, ZnO crystallizes in the thermodynamically stable phase with a wurtzite structure, which belongs to the hexagonal system [20-27]. where each anion is surrounded by four cations at the corners of a tetrahedron, and vice versa.
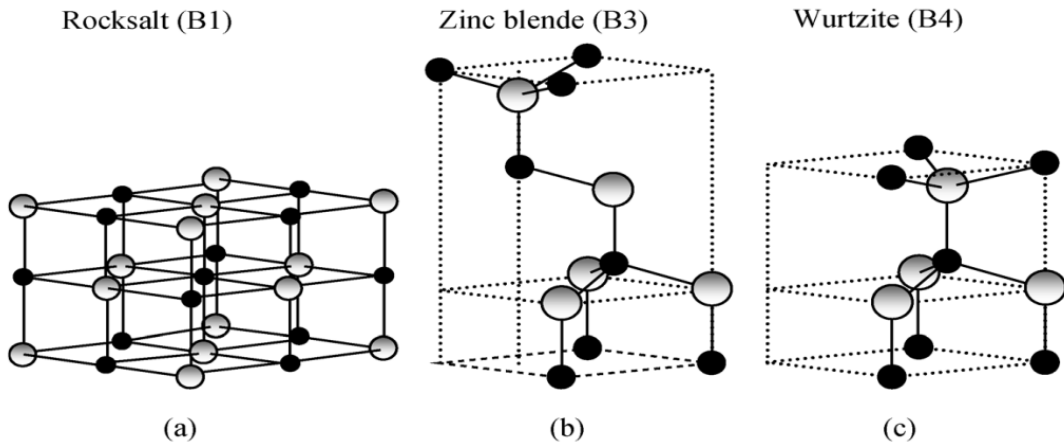
Figure I.4*: Crystal structures of ZnO: (a) cubic rock-salt(B1), (b) zinc blende (B3), and (c) wurztie (B4). The shaded gray and black spheres denote Zn and O atoms, respectively [28].*

I.2.2   The band structural and energy band gap

The optical properties of a material are greatly influenced by the energy band structure and the lattice structure. for this reason, a clear understanding of the electronic band structure is important to explain the electrical and optical properties because it determines the relationship between the energy and the momentum of the carrier. There are many reports that explain the electronic band structure of ZnO [29,30].

Naturally ZnO is an intrinsic n-type and direct wide-gap semiconductor with a bandgap energy of 3.37 eV at RT. The band structure shown below (**Fig I.5**) exhibits along high symmetry lines in the hexagonal Brillouin zone. Both the valence band maxima and the lowest conduction band minima occur at the Γ point k=0 indicating that ZnO is a direct band gap semiconductor. The bottom 6 valance bands (occurring around −6 eV) are mainly derived from the oxygen 2p bonding states. While the first two conduction band correspond to empty Zn 3s levels and the higher conduction bands are free-electron-like. [31].

These features of ZnO based material give rise to interesting optical properties which will be discussed in the next part.
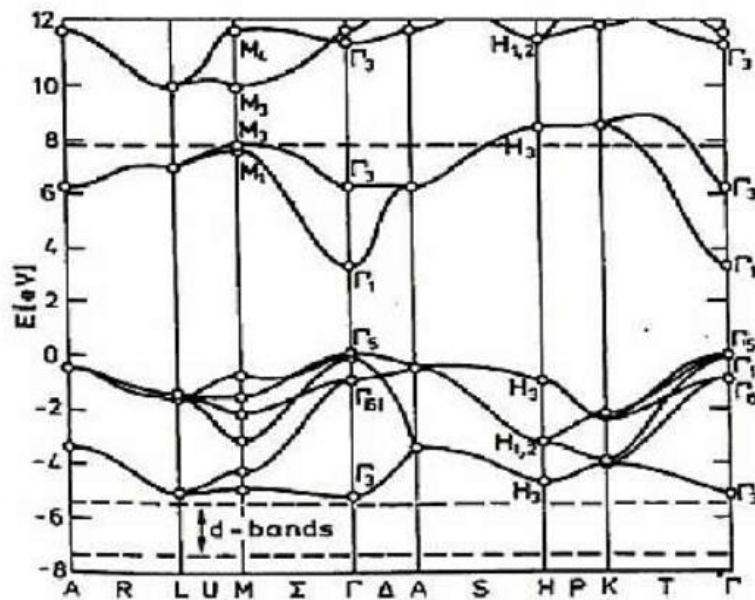
Figure I.5 : *Band structure of ZnO [32]*

I.2.3   Optical properties

Most of the applications of ZnO films are certainly related to its optical properties, optical constant such as dielectric constant (ω), refractive index $n(\omega)$, extinction coefficient $k(\omega)$ and absorption coefficient $\alpha(\omega)$. Are the main important features to determine the optical and electronic properties of the crystal. The index of refraction of a material is a number that indicates the speed at which light moves through a material compared to how it moves through a vacuum.

The extinction coefficient is an imaginary portion of the index of refraction that indicates the absorption loss when the wave passes through the sample. Optical constants give information about how the light moves through the sample and reflects off the material and can be used to measure the band gap of the material.

Many decades ago, Optical properties of ZnO based thin films were widely studied [33-35]. Since the band gap energy of ZnO is 3.37 eV at room temperature with large exciton energy of 60 meV and efficient radiative recombination, the interest in ZnO is increased and fueled as a prospect material in optoelectronics applications [36-38]. Optical transitions in ZnO have been studied by a variety of experimental techniques such as optical absorption, transmission, reflection, photo reflection, spectroscopic ellipsometry, photoluminescence, etc. actually there are two main optical transitions in ZnO : intrinsic and extrinsic. Intrinsic transitions occur between electrons from conduction band and holes in valence band, including excitonic effects due to coulomb interactions while extrinsic transitions are linked to a dopants/impurities or native defects in ZnO lattice, which lead to the creation of a discrete energy levels inside the band gap. Consequently, they influence both optical absorption and emission process.

It is well known that ZnO is transparent to light in both the visible and near ultraviolet–visible wavelength region. The transparent region corresponds to wavelengths region from 0.3-2.5 µm [29]. moreover, ZnO absorbs ultra-violet light (photoconductive under UV light) under a tailored condition, the optical transmittance of ZnO based thin films can reach 90%.

Room temperature photoluminescence spectrum of ZnO typically exhibits two luminescence bands (**Fig I.6**), a short wavelength band which is located near the absorption edge of the material ($\lambda \approx 360$ to 380 nm) which is attributed to the excitonic recombination. A broad emission band ranges from $\lambda \approx 500$-600 nm (usually in the green spectral range) which is attributed to the ZnO crystal and surface defects, such as O-vacancy (VO) [40-42], Zn vacancy (VZn) [43-45], O-interstitial (Oi) [46], Zn-interstitial (Zni) [47], and extrinsic impurities such as substitutional Cu [48].

Moreover; the morphology of ZnO nanostructures and the presence of intrinsic and/or extrinsic defects affect strongly the optical properties.
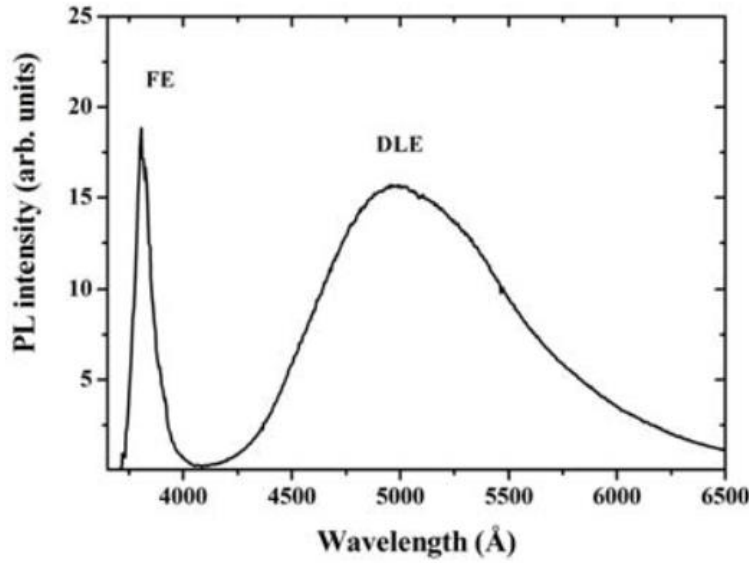
Figure I.6: *PL spectrum of single crystal bulk ZnO.*

I.2.4   Defects in ZnO

In the last decades, much attention has been focused on semiconductor materials with large band gap, due to their excellent optical and electrical features used mainly in several applications[49-54]. The understanding of both intrinsic and extrinsic defects in any semiconductor is crucial to utilize their properties in different semiconductor devices, and ZnO is no exception. Typically, defects play essential role in controlling the physical properties of ZnO based materials. [55-57].

The probability of manifestation of a defect in a semiconductor can be estimated by its formation energy. Which is defined as the difference between total energy of the crystal before and after the occurrence of that defect. The change in growth and post-growth-annealing conditions. May have a great effect on that formation energy [58]

Moreover, defects are still one of the debatable topics of semiconductors, as the measurement techniques are not able to correlate electrical or optical manifestation of defects to their origin specifically. It is highly suitable to say that the point defects in ZnO are not yet correctly understood.

I.2.4.1   Intrinsic Defects in ZnO

Native defects can be described as atomic imperfections in the material. There are three types of native defects: [59].

☐ Vacancies (V) These are missing atoms at regular lattice positions/sites

☐ Interstitials (I) These are additional atoms occupying interstices within the lattice

☐ Antisites. Is when O atoms occupying wrongly Zn lattice sites or vice versa.

I.2.4.1.1   *Zn Vacancy*

Zinc vacancy "VZn" is formed when a Zn ion breaks its bonds with four neighboring O atoms in the tetrahedral. Which introduces new partially filled states close to valence band maxima within the bandgap. As more electrons can be occupied in these partially filled states, therefore VZn acts as an acceptor in ZnO. The occurrence of VZn in n-type ZnO based semiconductors depend on the formation energy of VZn in ZnO, this energy tends to decrease when Fermi energy level moves toward the conduction band edge **(Fig I.7)**. Moreover, in n-type ZnO samples the formation energy of VZn is lowest among all other intrinsic defects which indicate the modest concentration of VZn in n-type ZnO. On contrary, in p-type ZnO samples the formation energy of VZn is extremely high when Fermi energy level is close to valence band [60].

I.2.4.1.2   *Oxygen Vacancy*

Oxygen vacancy "VO" is formed when an oxygen atom leaves the lattice site after breaking its bonds with the four neighboring Zn ions. The oxygen atoms act like a donor in ZnO lattice (see **Fig I.7**). The likelihood of the occurrence of VO in n-type ZnO also depend on its formation energy which is relatively high in n-type samples, and even in extreme Zn rich conditions the value was found to be 3.72 eV [61].

I.2.4.1.3   *Zn Interstitial*

There are two types of interstitial sites in ZnO wurtzite structure, octahedral and tetrahedral. an octahedral site has three zinc and oxygen atoms separated by a distance of 1.07 times the Zn-O bond length. while, At tetrahedral site, each Zn atoms coordinates with one oxygen and one zinc atom (as nearest neighbors) at a distance of 0.833 times the bond length of Zn-O bond along the c-axis. Consequently, there is less geometric constraints for the interstitial Zn at the octahedral site as compared with tetrahedral site, hence, octahedral site is a preferred interstitial position for Zn in ZnO. Moreover, it was found that the formation energy of Zni lower at octahedral site as compared to that of tetrahedral site, which suggests that octahedral interstitial site is the

most stable interstitial site in ZnO for Zn. Therefore, they are unlikely to be the source of unintentional n-type conductivity in ZnO [61].

I.2.4.1.4   O interstitials

There are three types of oxygen interstitials sites in ZnO: tetrahedral, octahedral and split interstitials (Oi split) site. Oxygen at the tetrahedral interstitial site is highly unstable and relaxes into a split-interstitial configuration, spontaneously. And Oi split is an electrically inactive defect which means it remains neutral at all the positions of Fermi-level. [58]. Oxygen interstitial at the octahedral site introduces states in the bandgap close to valence band and it is electrically active [61].

I.2.4.1.5   Zn and O antisites

The ZnO antisite (Zn_O, O_{Zn}) defect is formed when a zinc atom substitutes an oxygen host atom and vice versa. Zn_O have been predicted to act as donor-type intrinsic defects; however, the formation energy of Zn_O is quite high (as shown in **Fig I.7**) and it is very unlikely to have zinc antisites under equilibrium conditions in ZnO. Whereas, O_{Zn} behave as an acceptor-type intrinsic defect with a relatively high formation energy even in O rich conditions. Therefore, the occurrence of O_{Zn} is extremely rare in equilibrium conditions. However, in non-equilibrium process such as ion implantation or radiation, O_{Zn} defect may exist -in ZnO.[58]. As mentioned above, intrinsic defects within a crystal greatly affect their electrical and optical properties and consequently have a bearing on doping, minority carrier lifetime and luminescence efficiency.[60]
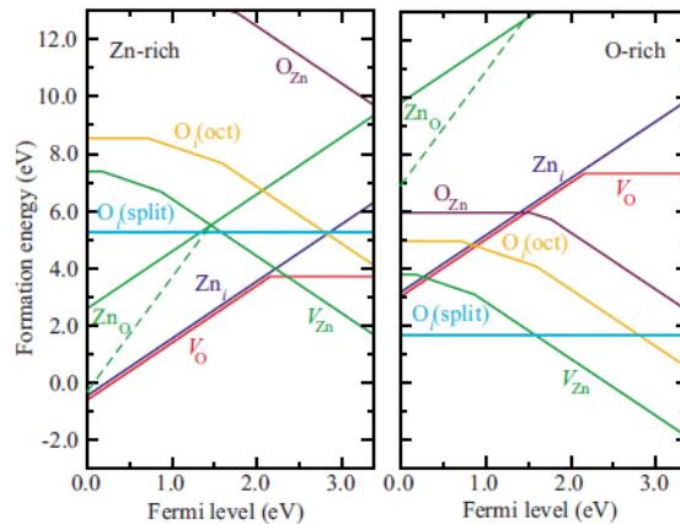
Figure 1.7: *The formation energies of various native defects in Zn-rich and O-rich conditions in ZnO [61].*

I.2.4.2   Extrinsic defects in ZnO : doping process

Doping refers to the process of adding impurities into the host material with the aim of improving the physical properties [62], and it can thus be a suitable and an effective way of controlling the electrical conductivity, optical luminescence and magnetic properties [63].

There are a wide Selective element doping which can offers a method for controlling and tailoring ZnO properties making it the most desired semiconductors in optoelectronics devices [64]

I.2.4.2.1   N-type doping

N-type doping in ZnO can be achieved by substituting Zn with group III elements such as aluminum (Al), gallium (Ga) and indium (In) [65,66] to have a significant effect on their electrical properties. n-type conductive can also be realized in ZnO by replacing O with group VII elements such as fluorine (F), chlorine (Cl), bromine (Br) and iodine (I)[67-70]. Many researchers [71-75] have reported highly electron concentration of ZnO n-type doped films (~1020-1021 cm^{-3}) and also a Low resistivity films (~10-4 W cm) [58].

I.2.4.2.2   P-type doping

To achieve p-type conductivity, which is extremely difficult to realize compared to n-type, ZnO maybe doped with acceptor impurities like group I elements: lithium (Li) and sodium (Na) [76], group V elements: nitrogen (N), phosphorus (P), antimony (Sb) and bismuth (Bi) [77-80] and group IB elements: copper (Cu) and silver (Ag) [81]. the success rate for realizing p-type conductivity in ZnO is extremely low. Reliability, stability and reproducibility of p-type doping is also an enormous issue. Therefore, inaccessibility of p-type conductivity in ZnO, limits its commercialization for the optoelectronic applications. [58]

I.3   Rare earth element

Relatively abundant in the Earth's crust and available in larger quantities than silver, gold and platinum, Rare Earth (RE) elements are a group of chemically similar metallic elements that occur naturally. Their chemical similarity comes from the fact that they have the same number of electrons in their outer atomic shell so they behave in a similar way during a chemical reaction. they inevitably exist in minerals as mixtures of different REs and strikingly behave as a single chemical entity, which means that they are not a pure metal. Moreover, the extraction of pure RE elements is tremendously difficult; hence the word "rare" was adopted to refer to such difficulty in extracting. As a consequence of such difficulty the discovery of all REs took approximately 160 years (from 1788 to 1941) to be completed. presently, ion-exchange and solvent extraction methods are used to produce highly purity (99.999 % pure) and low-cost RE elements. [82] It was

found that bastnaesite, monazite and xenotime ores (**Fig I.8**) are the main significant resources to produce REES [83]. The largest economic resources in the world for REs is localized   in China and the United States [84]

Figure I.8: Typical pictures of two rare earth ores [84].

In fact, the RE elements occur in two series known as lanthanides and actinides. where each series consists of fifteen elements as shown in **Fig I.9**. The name of lanthanide was derived from the Greek word lanthano which means hidden. [85]. RE elements are characterized by the successive filling of their incomplete 4f and 5f shells. The lanthanides which is characterized by a partially filled *4f* shell [86], start with the element lanthanum which has the atomic number ($Z=$ 57) and it ends with the element lutetium ($Z=70$). The actinide group which is identified by the progressive filling of the 5f-shell begins with actinium ($Z=89$) and end with element lawrencium ($Z=103$). [83]. Erbium and Ytterbium, belonging to the lanthanide's series are the focus of this thesis.

Figure I.9: Rare earth elements.

Theoretically, elements are characterized by their atomic number, the number of electrons orbiting in shells around the nucleus depends on the atomic number. Normally, the average radius of an atomic shell gradually increases as more electrons are added to it. But in the case of the lanthanide series, a steady decrease in the size of atoms and ions is observed. when going from lower to

higher atomic numbers This phenomenon is called the lanthanide contraction. [82, 85] Such reduction of the atomic and ionic radii is ascribed to the imperfect shielding of the valence f-orbitals [87]. As the number of 4f electrons successively increases the nuclear charge rises as well. As a result, the effective nuclear charge increases due to poor shielding and hence the 4f electrons tend to be more and more firmly bound to the nucleus causing the contraction phenomenon [82,88,90]. RE ions are widely accepted as optically efficient luminescent candidates due to its large number of accessible states in the ground and the first excited configurations which producing many emissions over a wide spectral range. It is known that RE elements are strongly reactive and can be easily oxidized when exposed to air. [83] By far, the most common stable valance state of the majority of RE elements in solids is the trivalent state RE^{+3}. [91]

The majority of trivalent lanthanides are luminous, but some are less emissive than others. the radiative transitions within the 4f manifolds is the main transition which dominate the optical properties of lanthanide ions. Therefore, many scientists have focused their efforts on researching RE-related transitions in order to create a useful energy level diagram. (**Fig I.10**) which shows the energy of the different states for several RE3+ ions [92]. Lanthanide doped luminescent materials can emit light in the ultraviolet (UV) to near infrared light field, depending on the excitation. [93]. Moreover, the shape of the emission spectra will vary significantly depending on the ion's chemical environment. but the energy of the transitions remains relatively insensitive [94].
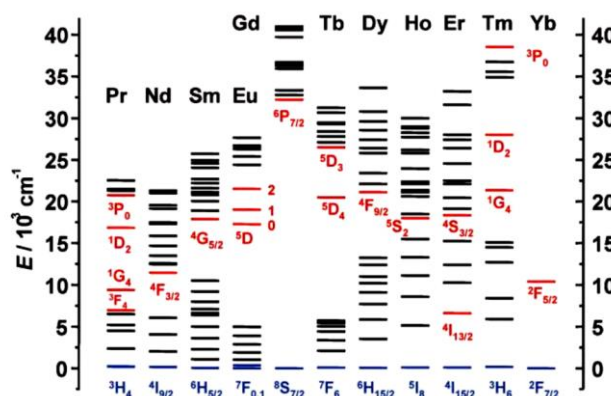
Figure I.10: Partial energy diagrams for the trivalent lanthanide. The main

luminescent levels are drawn in red, while the fundamental level is indicated in blue.

II-VI compound semiconductors have been found to be unique host materials for doping of optically active impurities, which exhibit luminescence at room temperature [84]. Rare earth ions in II-VI semiconductors compounds have been studied since more than 50 years [86] in powders [88], bulk crystals [89], thin films [91], and epitaxial layers [95]. Recently, rare earths

(RE) doped semiconductors have long been the topic of research owing to their prominent and desirable optical and magnetic properties.

Typically, the steady emissions, of the trivalent rare earth elements makes it possible; to incorporate them into various hosts with different lattice and still preserve the typical rare earth emissions. Semiconductors such as ZnO, GaN, ZnSe doped with rare earth ions show evidence of electroluminescence; these materials are candidates for traditional semiconductor light emitting diodes and enable new technologies for highly distinguishable emissive flat panel displays. [31]

Recently, the ZnO presented an interesting subject for doping with various RE elements. This is of course very suitable to improve both the optoelectronic and luminiscent properties because the incorporation of dopants generates lattice defects and changes consequently the band gap energy [96]. In particular, the doping with rare-earth elements has been extensively investigated, experimentally as well as theoretically. [97-103]

I.3.1 Erbium

In 1843 Carl Gustav Mosander, a Swedish scientist, discovered the erbium (Er) element. It is a shiny silvery white metal, as shown in **Fig I.11** which can be extracted from various sand ores such as Monazite and Xenotime. It is estimated that the average concentration of Er in the Earth's crust is about 3 parts per million by weight. it is considered to be fairly reactive when exposed to air. Table I.1 outlines some physical and chemical features of Er.
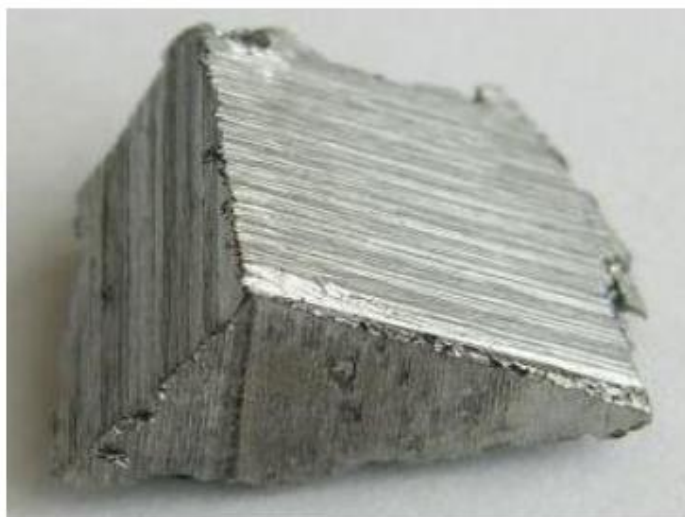
Figure .I.11: A picture of pure erbium metal

Er ions have several important uses in a variety of technological fields. For example, in the optical communication systems, Er-doped fibre amplifiers have been used. Er can efficiently emit at 1.5

μm due to the transition from its first excited state to the ground state. Interestingly, at this particular wavelength the commonly used silica-based fibre optic has minimum loss, nearly zero dispersion and maximum transparency, thus Er ions are considered as an important component to successfully amplify high frequency telecommunication signals. Moreover, lasing of Er ions when doped into aluminum garnet (Er:YAG) is safely and popularly used by dermatologists for skin treatments.

Table I.1 *Some physical and chemical properties of Erbium.* [31]

Symbol	Er
Atomic number (Z)	68
Density (g/cm^3)	9.066
Atomic Mass	167.26
Atomic volume (cm^3/mol)	18.449
Melting point (°C)	1529
boiling point (°C)	2863
Coefficient of thermal expansion (K^{-1})	12.2 x 10^{-6}
Thermal conductivity W/(cm.k)	0.145
Electrical resistivity (μΩ•m)	0.860
Crystal structure	Hexagonal closed-packed (hcp)
Ionic radius of Er^{3+} (Å)	0.89
Electronic configuration of Er atom	Xe 4f12 6s2

Erbium's everyday uses are varied. It is commonly used as a photographic filter, and because of its resilience, it is useful as a metallurgical additive. Other uses:

- Used in nuclear technology in neutron-absorbing control rods [104, 105].
- When added to vanadium as an alloy, erbium lowers hardness and improves workability [106].
- Erbium oxide has a pink color, and is sometimes used as a colorant for glass, cubic zirconia and porcelain. The glass is then often used in sunglasses and cheap jewelry [106].

I.3.2 Ytterbium

Ytterbium (Yb) was isolated in 1878 by Jean Charles Galissard de Marignac at the University of Geneva. The story began with yttrium, discovered in 1794, which was contaminated with other rare-earth elements (aka lanthanoids). In 1843, erbium and terbium were extracted from it, and then in 1878, de Marignac separated ytterbium from erbium. He heated erbium nitrate until it decomposed and then extracted the residue with water and obtained two oxides: a red one which

was erbium oxide, and a white one which he knew must be a new element, and this he named ytterbium. Even this was eventually shown to contain another rare earth, lutetium, in 1907. In common with many lanthanide elements, ytterbium is found principally in the mineral monazite. It can be extracted by ion exchange and solvent extraction. A tiny amount of ytterbium metal was made in 1937 by heating ytterbium chloride and potassium together but was impure. Only in 1953 was a pure sample obtained. it is a soft, silvery metal as shown in **Fig I.12**. It slowly oxidizes in air, forming a protective surface layer.

Figure I.12: *A picture of pure ytterbium metal*

Ytterbium is beginning to find a variety of uses, such as in memory devices and tunable lasers. It can also be used as an industrial catalyst and is increasingly being used to replace other catalysts considered to be too toxic and polluting. [107]

Table I.2 *Some physical and chemical properties of Ytterbium.* [108]

Symbol	Yb
Atomic number (Z)	70
Density (g/cm^3)	6.90
Atomic Mass (amu)	173.045
Atomic volume (cm^3/mol)	24.79
Melting point (°C)	824
boiling point (°C)	1196
Coefficient of thermal expansion (K^{-1})	25.1 10^{-6}
Thermal conductivity W/(m.k)	39
Electrical resistivity (μΩ•m)	0.25
Crystal structure	fcc: face-centered cubic
Ionic radius of Yb^{3+} (Å)	1.008
Electronic configuration of Yb atom	[Xe] 4f146s2

I.3.3   Common applications of rare earth elements

There is a variety application for which REEs are used, from the ordinary domains (automotive catalysts and petroleum cracking catalysts, flints for lighters, pigments for glass and ceramics and compounds for polishing glass) to the highly specialized (miniature nuclear batteries, lasers repeaters, superconductors and miniature magnets) Furthermore, REEs are now particularly relevant and widely used in the defense industry. Some of their specific defense applications include anti-missile defense, aircraft parts, communications systems, electronic countermeasures, jet engines, rockets, underwater mine detection, missile guidance systems and space-based satellite power (Table I.3).

Table I.3 *Common applications of rare earth elements*. [31]

N⁰	Element	Symbol	Uses
1	Cerium	Ce	Catalyst, Fuel additive, Optical polish, Ceramic, Glasses And Phosphors
2	Dysprosium	Dy	Lasers, Magnets, Ceramic, Phosphors And Nuclear Applications
3	Erbium	Er	Ceramic, Glasses dyes, Optical Fibers, Lasers, Photography And Nuclear Applications
4	Europium	Eu	Phosphors, Lasers And Phosphors
5	Gadolinium	Gd	Lasers, Ceramic, Optical, Magnetic Detection And Medical Image Visualization
6	Holmium	Ho	Lasers, Ceramic, Magnets, Optics And Nuclear Applications
7	Lanthanum	La	Catalyst, Ceramic, Glasses , Phosphors And Pigments
8	Neodymium	Nd	Catalyst, Lasers, IR Filters And Magnets
9	Praseodymium	Pr	Ceramic, Glasses And Pigments
10	Promethium	Pm	Phosphors, Nuclear Batteries And Measuring Devices
11	Samarium	Sm	Magnets, Microwave Filters, Lasers And Nuclear Applications
12	Scandium	Sc	Aerospace, Lighting, Nuclear Applications And Semiconductors
13	Terbium	Tb	Lasers, Lighting And Phosphors
14	Thulium	Th	Electron Beam, Lasers And Medical Image Visualization
15	Yttrium	Y	Capacitors, Phosphors, Radars And Superconductors
16	Ytterbium	Yb	Lasers, Chemical Industry And Metallurgy
17	Lutetium	Lu	Catalyst And Medicine

I.4   ZnO Based devices

Up to now, Zinc oxide as a TCO has triggered a remarkable interest for its wide array of applications in various technical fields such as transparent electrodes used for luminescent devices [109], solar cells [110,111], gas sensors [112], spintronic devices [113], photo-detectors [114], acoustic devices [115], and lasers [116], etc. It's a remarkable multifunctional and biocompatible direct-, wide-band gap semiconductor with a unique set of properties and Nano structuring potential. [117]. ZnO has showed to be a boon for materials science as It possesses a special set of characteristics, such as UV absorption. Anti-microbial properties, steady thermal and optical

properties. ZnO has made a major contribution to a variety of industries. (ceramics, lubricants, ointments, adhesives or the rubber industry) [118-120]. ZnO films could be doped with a variety of elements in the intended target to achieve such desired and potential properties which make it a key element in many industrial manufacturing processes. we are now moving into an era where ZnO devices will become increasingly functional and exotic [121].

I.4.1 ZnO-based light emitters

In the past decade, light-emitting diodes (LEDs) based on wideband gap semiconductor have attracted considerable attention due to its potential optoelectronic applications in illumination, mobile appliances, automotive and displays [122]. The wide bandgap and large exciton-binding energy at room temperature of ZnO make it a very promising candidate for fabrication of blue and UV LED, which requires that the junction devices provide high electron and hole concentration in the active region. ZnO is widely available and cheap, so it has an advantage over GaN from the cost point of view which also make the fabrication of ZnO-based optical devices an attractive prospect. The commercial success of GaN-based optoelectronic and electronic devices trig the interest in ZnO-based devices [123].

In contrast, the lack of stable and reproducible p type ZnO become a limiting factor in realising ZnO based LED. n-type ZnO thin film which is grown on other p type materials like Si, GaN, zinc telluride, copper(I) oxide and GaAs was a suggested alternative approach [124,125]. Various ZnO based heterojunction and homojunction light emitters in the UV and visible ranges (red, blue, green or white) have been reported. [126-131].

I.4.2 Solar cells

Based on the converting of sunlight into electricity, photovoltaic effect has been recognized as a promising way to meet rising energy demands while also addressing the concerns about carbon dioxide emissions from fossil fuel use [64]. Thin-film solar cells are one of the more appealing innovations for producing electricity by collecting photons from sunlight. Unlike batteries or fuel cells, solar cells do not utilize chemical reactions or require fuel to produce electric power, and, unlike electric generators, they do not have any moving parts.

Solar cells, whether used in a central power station, a satellite, or a calculator, have the same basic structure. Light enters the device through an optical coating, or antireflection layer that minimizes the loss of light by reflection; it effectively traps the light falling on the solar cell by promoting its transmission to the energy-conversion layers below. The three energy-conversion layers below the

antireflection layer are the top junction layer, the absorber layer, which constitutes the core of the device, and the back junction layer. Two additional electrical contact layers are needed to carry the electric current out to an external load and back into the cell, thus completing an electric circuit. The overwhelming majority of solar cells are fabricated from silicon with increasing efficiency and lowering cost as the materials range from amorphous (no crystalline) to polycrystalline to crystalline (single crystal) silicon forms. The recent research centered on the use of a variety of new, low cost materials, such as zinc oxide (ZnO). ZnO is a material of considerable interest for applications in low cost photovoltaics.

The simplest use of ZnO-based materials in thin film solar cells is antireflection and/or light-trapping coatings and contacts. For applications as transparent contacts in solar cells, doping with group III elements is usual. Whereas, doped ZnO electrodes are commonly used both as contacts and to enhance light trapping in thin film solar cells via textured electrode surface.

ZnO can be used in the formation of relatively low cost photovoltaic cells such as dye-sensitized solar cells and hybrid organic–inorganic nanostructure solar cells. Inorganic solar cells have been the subject of the majority of ZnO-based electrode research topics [132]. n-type ZnO films may also be used within the photovoltaic structure itself, for example as a tunnel junction in amorphous silicon cells or as part of the p/n junction in some solar cells. [64]

As an example, the well-known Cu (In, Ga) Se2 (CIGS: Copper Indium Gallium Selenide) solar cell, the basic structure of a thin-film solar cell CIGS is illustrated by the **Fig I.13**. Soda-lime glass of about of 1–3 millimeters thickness, a molybdenum (Mo) metal layer is deposited which serves as the back contact and reflects most unabsorbed light back into the CIGS absorber. Following molybdenum deposition, a p-type CIGS absorber layer. A thin n-type buffer layer is added on top of the absorber, the buffer is typically cadmium sulfide (CdS). Al doped ZnO serves as a transparent conducting oxide to collect and move electrons out of the cell while absorbing as little light as possible.
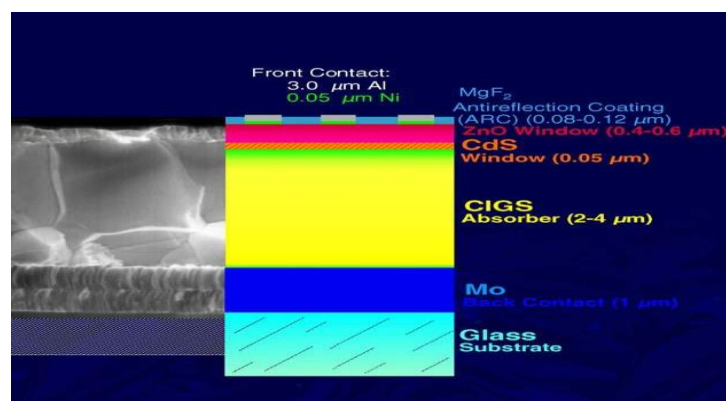
Fig I.13 Exemple devive sttructure of a CIGS solar cell

I.4.3   Gas Sensors

Tremendous increase in environmental pollution due to the rapid expansions of industrialization and growing population in cities and combustion of fuels from vehicles; etc., which is an alarming threat to ecosystems present in biosphere.[133]. Therefore, there is an urge for clean air supply to maintain our ecosystem. On the other hand, leakages of explosive and flammable gases are extremely dangerous for human beings and their belongings [134]. Early detection of these poisonous chemicals is thus required for environmental security purposes. Nowadays, gas sensors have become more popular because of their various applications in fuel cells (for the detection of hydrogen gas), in mining industries (for the detection of methane), in automobile industries (for the detection of NO2 from vehicle exhaust), in oil refineries (for the detection of hydrocarbons), and in fertilizer industries (for the detection of ammonia) [135]. Scientific community and researchers around the globe thus are trying to develop novel chemical sensors with superior performances. These chemical sensors also play other important and vital roles in other areas gas alarms, sensors for water and soil pollutants, human health, temperature sensor, speed sensor, magnetic field sensor, and emissions control .

A variety of Semiconductors oxide have been extensively studied and applied for gas sensing applications as these materials under operating conditions possess high electron mobility, non-toxic nature, high-specific surface area, good chemical, and thermal stability [136,137]. zinc oxide shows up as an interesting material displaying considerable possibilities of application in sensor structures sensitive to some chosen gases [138]. Being physically and chemically stable, ZnO is a suitable candidate for thin film gas sensors. Many researchers have found out that doping ZnO with suitable elements in appropriate amounts enhance the sensing selectivity and response time of the film. Several reports of ZnO thin film-based gas sensors for detecting species such as

ammonia, ammonium, nitrogen dioxide, water, ozone, carbon monoxide, hydrogen, hydrogen sulfide and ethanol for various applications [139]. Al-doped ZnO thin film was found to be suitable breath analyzer (sensing ethanol). Also, Sn-doped ZnO thin film gas sensor was employed for NO2 detection [136]. Other reported works include Pd-doped ZnO gas sensors for H2 detection by Al-zaidi et al. [137] and a ZnO thin film gas sensor by rf sputtering for H2, NO2 and hydrocarbon detection by Sadek et al. [140]. Balakrishnan et al. [141] reported the detection of NH3 gas by a p-type ZnO thin film.

I.4.4   laser

ZnO-based thin films are indeed interesting for use in semiconductor, photoconductor or piezoelectric and optical waveguide materials. Recent examples include surface acoustic wave devices, bulk acoustic wave devices, acoustic optical devices, and short wavelength semiconductor diode lasers (SDLs) [142]. wide bandgap materials are ideal for short-wavelength semiconductor laser diodes [143]. GaN compo unds are currently used in blue and UV lasers [144]. Due to the higher exciton binding energy of 60 meV compared to GaN (25 meV), ZnO could be a promising material for UV and blue laser applications. It was found that the lasing phenomenon in ZnO occurs due to exciton-exciton scattering, and a stimulated emission from ZnO was observed under optical pumping [145] Therefore, ZnO-based lasers have a low threshold value [144]. Cao *et al.* [146] observed a random stimulated emission from a ZnO polycrystalline thin film. Gadallah *et al.* [147] in 2013 reported surface and edge emission under optical pumping from a ZnO thin film grown on a sapphire substrate by PLD with the highest gain and lowest loss (at that period). Despite the fact that there are a variety of publications on lasing via ZnO, there are no reports on ZnO-based laser diode due to the limitation in achieving a stable p-type ZnO thin film. But now with the various reports on p-type ZnO [148–151], it is expected that a ZnO-based laser diode will be available soon.

Chapter II :

Film Growth Methods and Materials Characterization

II.1 Introduction

Currently, deposition techniques have evolved too much following the growth of industrial demand in different disciplines such as: microelectronics, optics, mechanics, chemistry biomedical..., constantly requiring the use of new materials of all kinds: insulators, semiconductors, conductors, superconductors ..., as well as new structures ranging from mono to multilayers.

Considering the wide range of applications for ZnO, Several methods have been previously applied for the synthesis of ZnO nanostructures which can be divided into two groups based on the nature of the deposition process viz, physical or chemical., The physical methods include physical vapour deposition (PVD), laser ablation, molecular beam epitaxy, and sputtering. The chemical methods comprise gas-phase deposition methods and solution techniques (**Table II.1**). The aim of any deposition technique is the preparation of thin films in reproducible, controllable and predictive ways [152-157]

Unfortunately, many of the mentioned techniques are problematic because they need high temperatures for synthesis, have long reaction times, use toxic materials, and involve expensive equipment.Consequently, sol gel as a solution method has gained much interest compared to other techniques for ZnO thin films growth. Due to its simplicity, low-cost and and easy way to manipulate for producing highly nanostructured thin films, with uniform morphology, high homogeneity, and particle size controlling.

In this chapter, a brief description of the most common methods used in the growth of thin films. The thin films growth techniques discussed include both sol gel techniques "dip and spin coating", Particle morphology, elemental composition, and structure of the Rare earth doped ZnO were studied using scanning electron microscopy (SEM), Raman spectroscopy , energy dispersive spectrometer (EDS), X-Ray diffraction (XRD), Atomic Force Microscopy (AFM) . The optical properties were studied using the UV-Vis spectroscopy and FTIR technique.

II.2 Synthesis of ZnO thin film

There are many applications for thin film processing. The most popular for ZnO thin films are pulsed laser deposition (PLD), chemical vapor deposition (CVD), metalorganic chemical vapor deposition (MOCVD) and molecular-beam epitaxy. These processing parameters allow for the production of high performance ZnO materials. Recently, new processing techniques have

popularized, such as chemical spray pyrolysis, screen printing, electrochemical deposition, and sol-gel synthesis with the later offering a low cost, resource efficient process. [158]

Table II.1 . Methods of thin flms deposition.

Physical deposition	Chemical deposition
1. **Evaporation techniques**	1. **Sol-gel technique**
a. Vacuum thermal evaporation.	2. **Chemical bath deposition**
b. Electron beam evaporation.	3. **Spray pyrolysis technique**
c. Laser beam evaporation.	4. **Plating**
d. Arc evaporation.	a. Electroplating technique.
e. Molecular beam epitaxy.	b. Electroless deposition.
f. Ion plating evaporation.	5. **Chemical vapor deposition (CVD)**
2. **Sputtering techniques**	a. Low pressure (LPCVD)
a. Direct current sputering (DC sputtering)	b. Plasma enhanced (PECVD)
b. Radio Frequency sputering (RF sputtering)	c. Atomic layer deposition (ALD)

II.2.1 Physical Vapour Deposition process (PVD)

PVD processes encompass a wide range of vapor-phase technologies, and is a general term used to describe any of a variety of methods to deposit thin solid films by the condensation of a vaporized form of the solid material onto various surfaces. PVD involves physical ejection of material as atoms or molecules and condensation and nucleation of these atoms onto a substrate. The vapor-phase material can consist of ions or plasma and is often chemically reacted with gases introduced into the vapor, called reactive deposition, to form new compounds. [159]

II.2.1.1 Vaccum Evaporation

Vacuum evaporation is one of the most commonly used methods for deposition of functional films on to various substrates (**Fig II.1**). The vacuum is used to allow vapor particles to deposit directly on to the substrate, where vapor particles condense back to a solid state, forming a functional coating. The vacuum evaporation process involves two basic stages: the evaporation of a functional material and the condensation on the substrate. In high-vacuum evaporation, electrical heating or electron beam heating is used to melt, gasify and evaporate the coating materials. The vapor of the coating material then travels to the surface of the substrate and gradually cools, a thin film layer of good quality is finally formed . Vacuum is used to prevent the collision of the evaporated particles with the background gas or other unwanted particles.

25

Evaporated functional materials deposit on to the surface of the substrate. Various high quality thin films of ZnO have been successfully obtained using Thermal vacuum evaporation [160-162].
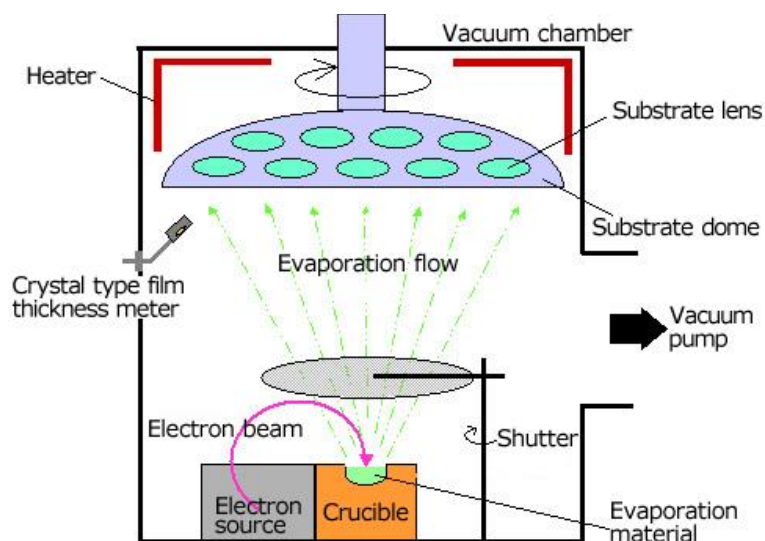
Figure II.1: Schematic of vacuum evaporation process with E-beam heating [163]

II.2.1.2 Laser Ablation

Laser ablation, also known as pulsed laser deposition (PLD), a high intense, pulsed laser beam irradiates the target and ejecte micron-sized particulates during the ablation process. These particulates are ejected from targets due to the high intensity laser pulse and are believed to seriously degrade the optical properties of the grown films[164]. When a target absorb laser pulse, the convertion of energy into thermal, chemical, and mechanical sources of energy takes place, resulting in evaporation, ablation, plasma generation, and even exfoliation [165] A simple diagram of a typically PLD process is shown in **Figure II.2**: a vacuum chamber with a chamber window that has a holder for the substrate and a target material. To limit interaction of impurity gas molecules, a vacuum chamber is required. The substrate holder fixes the substrate in location and can alter the substrate in different ways such as heating or applying an electrical current. The target is used as source material to be deposited on the substrate. Finally, a pulse laser beam is directed at the target, resulting in the creation of an ablation plume towards the substrate which begins to form a film [166]

The PLD targets are usually fabricated by thorough mixing of predetermined quantities of finely ground powders of the materials of interest and then compressing into pellets followed by a well-defined heattreatment process called sintering[167]. PLD technique has the advantage to be able to use high oxygen pressures and to produce crystalline ZnO films of high quality with a high growth rate even at low temperature.
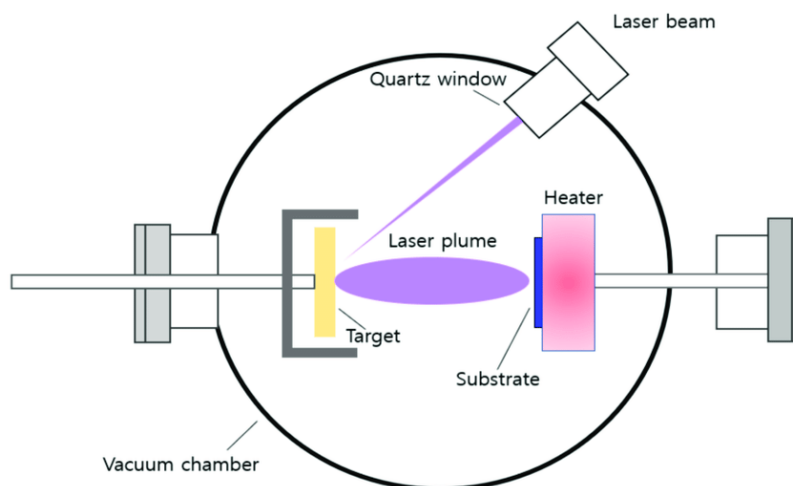
Figure II.2: *Schematic of the PLD process [168].*

II.2.1.3 Sputtering Technique

Sputter deposition is a physical vapor deposition (PVD) method for depositing thin films, which is one of the most popular growth techniques due to its low cost, simplicity, large area,and low deposition temperature [167,168]. Sputtering means to eject material from a target and then deposit it on the substrate [169]. The simple form of the sputering system consists of an evacuated chamber containing metallic anode and cathode [168] in order to obtain a glow discharge in the residual gas in the chamber. Also, an applied voltage in the order of several KeV with pressure more than 0.01 mbar is sufcient for flm deposition. The sputtering process depends on the bombardment of the ions released from the discharge to the molecules in the cathode leading to the liberation of the molecules from the cathode with higher kinetic energy. The atomic weight of the bombarding ions should be nearly to that of the target material in order to maximize the momentum transfer. These molecules move in straight lines and strike on the anode or on the substrate to form a dense thin flm [168]. The diagram of the sputtering system is shown in **Figure II.3**.
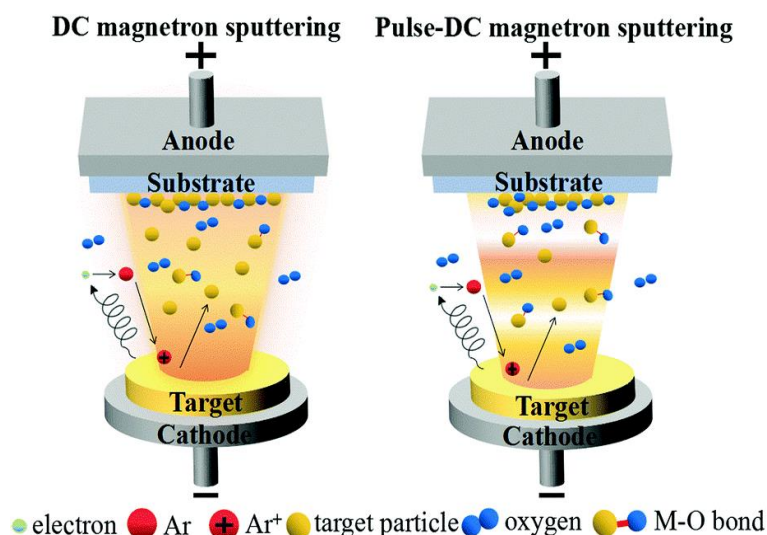
Figure II.3: Sputering system diagram [170]

II.2.2 Chemical vapor deposition (CVD)

Although the production of thin flms via physical methods as previously described gives good quality and functionalizes properties, it is highly expensive and perhaps requires a large amount of material target. dating back the late 1800's Chemical Vapor Deposition (CVD) is a very old processing technique [171]. it was mostly used to produce high-purity refractory materials such as titanium and zirconium. Most of them do not require expensive equipment. After World War II, researchers started to note the likely advantages of CVD, and its use and success increased.

The CVD method (**Fig II.4**) is used to deposit thin and thick films with thickness ranging from Angstroms to fraction of a millimeter with controlled structure. onto a heated surface. Since the growth of the film can be on any side based on the attainment of gas precursor, this method allows for deposition on complex surfaces, which will be more useful in industries.

In these methods the film composition depends on precursors and the stoichiometry can be achieved by controlling the precursors and rate of deposition. It can allow for codeposition of elements and does not require a high vacuum. CVD techniques are used to grow thin films at normal atmospheric conditions. Organic, inorganic insulating films and semiconductor films are deposited by this technique[172,173]. There are four key steps of a typical CVD process:

1. A thermal activation of the chemical precursors to form a vapor.
2. This vapor is then transported through a heated chamber where the substrate is located.
3. In this chamber, the desired gas phase reactions occur and the reactants are deposited onto the substrate surface resulting in film formation.

4. Volatile byproducts are desorbed from the film and removed from the chamber through convection.

There are many CVD techniques viz: atmospheric-pressure CVD, low-pressure CVD, ultrahigh vacuum CVD, plasma-enhanced CVD, microwave plasma-assisted hot filament CVD, metaleorganic CVD, photo-initiated CVD, atomic layer deposition, spray pyrolysis, liquid-phase, epitoxy, etc. [174]

Unfortunatly, high operating temperatures (which can exceed 1000 ° C) for the gas phase reactions to occur limits the types of substrates that the thin film can be grown on. Which increase the cost of CVD processing . Many researchers have developed LPCVD and PACVD with very localized heating [175]. Moreover, The Chemical precursors with high vapor pressures, which are required in CVD, are usually toxic and dangerous to handle. Finally, the by-products from the gas phase reactions that do not remain on the thin films can also be toxic and even corrosion. Often it is required that these by-products be neutralized which adds to the cost of production.
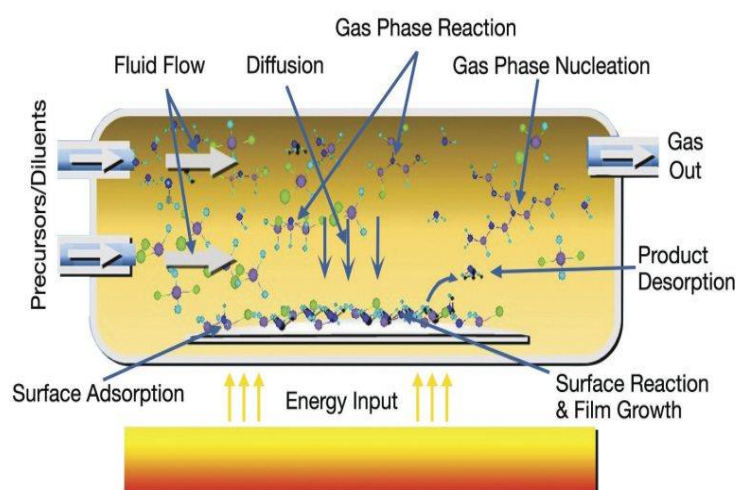
Figure II.4: Aspects of a CVD process.

II.2.3 Sol gel

Sol-gel process has been broadly used for the synthesis of metal oxide nanostructures since the first introduction of the concept of silica gel by Ebelmen [176] and Graham [177] in the mid-19th century. Sol-gel process is one of the famous wet-chemical methods. The advantage of this is synthesizing the nonmetallic inorganic materials, ceramics, glass ceramics, etc. and it can produce
large quantities of nano-materials, large areas of coatings at low cost, also, It works under lower-temperature processing, gives beter homogeneity for multicomponent materials. and offers the

potentials for a simplified, low energy, resource efficient processing route. The method has been widely applied to the production of metal oxides such as ZnO, SnO2, TiO2, and ZrO2 [178-181]The word 'sol' means the formation of a colloidal suspension and 'gel' means the conversion of 'sol'via hydrolysis and condensation reactions to viscous gels or solid materials [182]. Using a variety of methods, this sol gel can then be added to a desired substrate. After that, the samples go through several phases of drying and annealing to obtain the desired properties.

Two routes are used to prepare transition metal oxides (TMOs) as follows:

a.   Preparing of inorganic precursors via inorganic salts in aqueous solution.

b.   Preparing of metal alkoxide precursors via metal alkoxides in nonaqueous solvents.

A sol is defined as a dispersions of colloidal particles in a liquid . These particles can range from amorphous to crystalline. They can be dense, porous, or even form polymer chains. [183,184]. A gel is an interconnected and rigid solid network with pores of submicrometer dimensions surrounding and supporting a continuous liquid phase [185]. In typical sol-gel solutions, when sols partciles form covalent bonds, the formation of gels, or gelation, take place. The morphology of of these sol particles have a great effect on the final structure of the gel network Sol-gel is also known as soft chemistry or solution chemistry. It is the process of taking the metal acetate or metal alkoxide based precursors into a gel and then converts it into the desired final product, following five main stages of formation which are hydrolysis, polymerization, condensation, nucleation, and growth. Two types of precursors can be used which will typically determine the solution used. Metal alkoxides are generally used with organic solvents and metallic salts are used with aqueous solutions [186-188].

This is process is typically done at either room temperature or up to no more than 100ºC, depending on the solvent used. **Figure II.5** shows a typical sol-gel process for both thin films and powders [189].
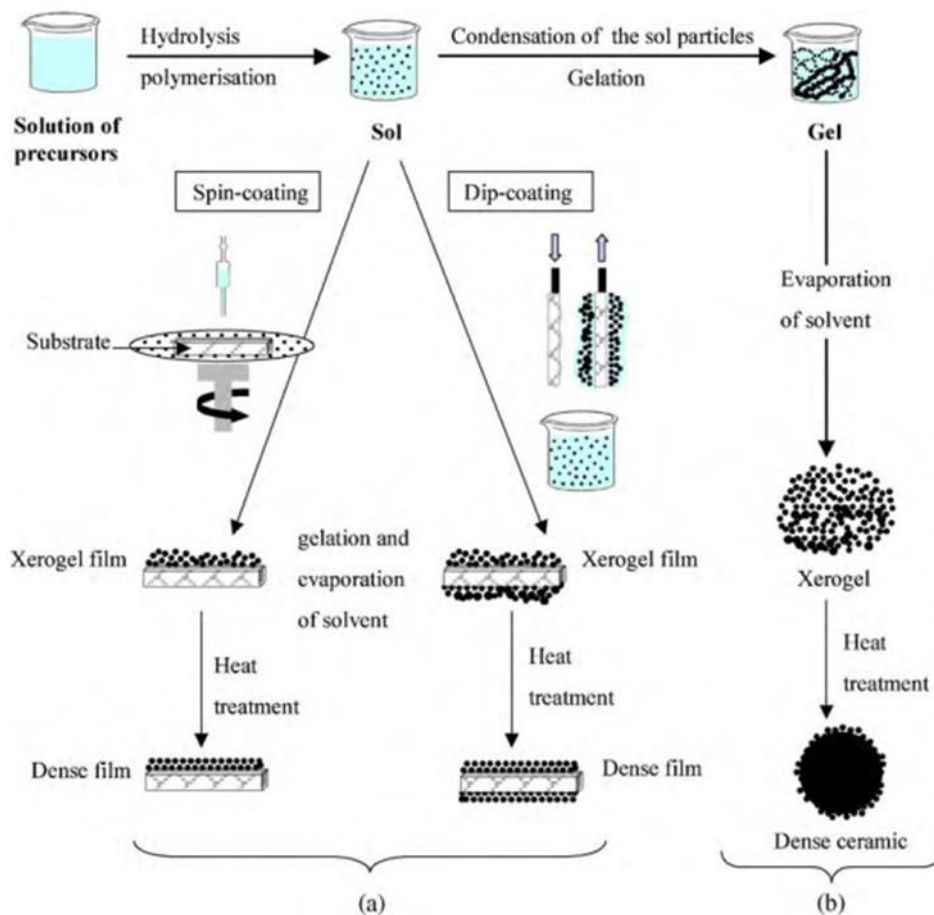
Figure II.5*: Overview showing two synthesis examples by the sol–gel method; (a) films from a colloidal sol; (b) powder from a colloidal sol transformed into a gel [189]*

The three main steps of sol gel process are:

1. preparation of the start solution with a solvent, a precursor, and the required additives.
2. Deposition of the prepared solution on substrates by several techniques with dip-coating (M. Ohyyama, 1997) [190], spin coating (M.N.Kamalasanan, 1996) [191].
3. The samples are then pre-heated at an elevated temperature to evaporate the solvent leaving behind a xerogel film or matrix.

The process of applying the solution to the film/substrate and then dried is repeated several times until a desired film thickness is achieved. The sample is then post-heated, or annealed, to form the final crystal structure and remove any unwanted organic material.

To make powders, the gels are normally dried at room temperature. In the sol-gel process, It's hard to distinguish between primary particles, which are a small grains or crystallites, and secondary particles, which are agglomerates of primary particles . because, the grain growth occur

at the same time as agglomeration [187]. **Figure II.6** shows the primary particles of about 2 nm in diameter that agglomerate in secondary particles of about 6 nm.
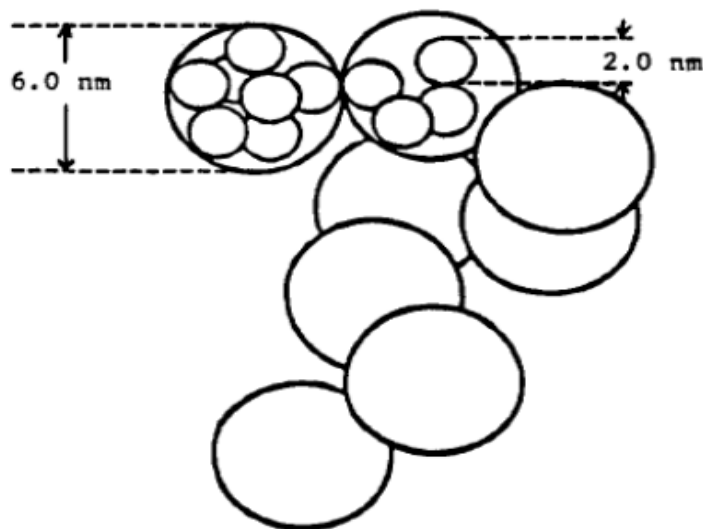
Figure II.6: Schematic representation of primary and secondary particles in alkoxide gel [183].

There are several possible options of available precursors to synthesized ZnO, which can affect the characteristics of the final product. Zinc alkoxides seem like good options since alkoxides are typically used with alcoholic solutions. However, metal alkoxides are generally not desirable as they are, "sensitive to moisture, highly reactive explosive materials and remain expensive" [189]. Fortunaty, The metal salt is used as an alternative to alkoxides because its hydrolysis is easier to work with. Metallic salts, both organic and inorganic, are cheaper and readily available. Among these metalis salts, nitrates and chlorates are possible candidate for use; however, It may be difficult to avoid anions of these species from remaining in the final product. This leaves organic zinc salts like zinc acetate. The remaining acetate groups will generally decompose during the annealing process.that is why zinc acetate (ZnAC), specifically dihydrate, is the most commonly used precursor in ZnO thin film sol-gel [189]. zinc acetate dihydrate has the advantage of giving homogeneous crystallization and less random than nitrate [192]

A large number of solvants were used In the synthesis of ZnO, viz, ethanol, methanol, isopropanol and two 2-methoxyethanol [193-196].

The use of additive(s) such as monoethanolamine (MEA) [197] and diethanolamine (DEA) [198] or acids such as acetic acid or hydrochloric acid [199]. can be employed to help facilitate shortcomings that may exist for certain precursor-solvent pairings. These additives can control the pH level, act as a chelating agent, or aid in dissolving the precursor in the solvent.

The properties of a particular sol–gel network are related to a number of factors that affect the rate of hydrolysis and condensation reaction, such as [64]:

➢ Nature of the precursor and its concentration,

➢ Type of solvent and the acidity of the medium,

➢ Type of additive species and their concentrations,

➢ Aging temperature and time of the early mixture,

➢ Method of coating of substrates and its speed,

➢ Nature of the substrate,

➢ Pre- and post-heat treatment of the materials.

II.2.3.1 Reaction processes involved in the formation of ZnO

By definition, the colloidal state is a semi-liquid state of matter. A solution colloidal is a dispersion of matter in a liquid (solvent). Obtaining such solution is governed by a phenomenon of solvation. Solvation is a close association between the molecules of the solvent and the molecules or ions of the solute. The stability of a colloidal solution results from the balance between attractive and repulsive interactions which exerted between the particles.

The principle of the sol-gel method is quite different. This process uses molecular precursors in solution which gradually transform into a network oxides by polymerization reactions.

The starting solution consists of a precursor generally an alkoxide metallic, in our case it is Zn-$(OC_2H_5)_2$. The reactions involved in the formation of zinc oxide are hydrolysis and condensation.

The hydrolysis of a substance is its decomposition by water using H^+ and OH ions from the dissolution of water [200]. Hydrolysis of Zn- $(C_2H_5O)_2$ alkoxide will be accompanied by the consumption of water, the release of alcohol and the formation of hydroxyl group (HO-Zn (OC_2H_5)) as shown by the following chemical reaction:

$$Zn\text{-}(C_2H_5O)_2 + H_2O \rightarrow HO\text{-}Zn\text{-}(OC_2H_5) + C_2H_5\text{-}OH \qquad (1)$$
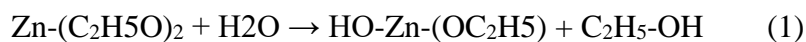
During condensation, certain hydroxyl groups (HO-Zn (-OC2H5)) generated during hydrolysis react with each other to give a water molecule (reaction 3 called oxolation reaction), while others react with Zn (- OC2H5) which have not yet reacted to give an alcohol molecule (reaction 2 known as reaction alkoxolation) [201]. The two reactions of oxolation and alkoxolation result in the creation of (OC2H5) -Zn-O-Zn- (OC2H5) bridges where each oxygen atom becomes a bridge connecting two Zinc atoms.

At room temperature, these reactions are written:

(OC2H5)-Zn-OH + C2H5-Zn-(OC2H5)→(OC2H5)-Zn-O-Zn-(OC2H5) + C2H5-OH   (2)

(OC2H5)-Zn-OH + HO-Zn-(OC2H5)→(OC2H5)-Zn-O-Zn-(OC2H5) + H2O   (3)
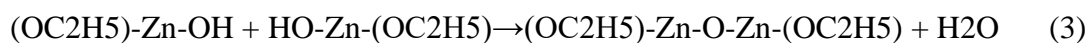
During the progress of the hydrolysis and condensation reactions there is creation of polymeric clusters that increase in size over time, when one of these clusters reaches an infinite dimension (critical size) the viscosity also becomes infinite this is the sol-gel transition point. From this point on, the cluster continues to evolve by incorporating the smaller polymeric groups. Once all the links have been used, the hydrolysis and condensation reactions complete and a gel is formed [202].

II.2.3.2 Dip coating

Dip coating or immersion coating, technique (see **Fig II.7**) is a simple classic way of depositing onto a substrate, especially small slabs and cylinders, a uniform thin film of liquid for solidification into a coating. It is the most commonly used technique in both academia and industry for many chemical and nanomaterial engineering research projects. typically, the procedure refers to the immersing a substrate in a tank containing coating material, withdrawn the piece from the tank under controlled speed, temperature and atmospheric conditions The basic flow is steady, and in it film thickness is set by the competition among viscous force, capillary (surface tension) force and gravity. Thickness and uniformity can be sensitive to flow conditions in the liquid bath and gas overhead. The faster the substrate is withdrawn, the thicker the film deposited. This can be countered by using volatile solutes and combining rapid enough drying with the basic liquid flow. Then the physics grows more complicated, theoretical prediction of process performance more difficult, and control of the process more demanding. [203, 204]
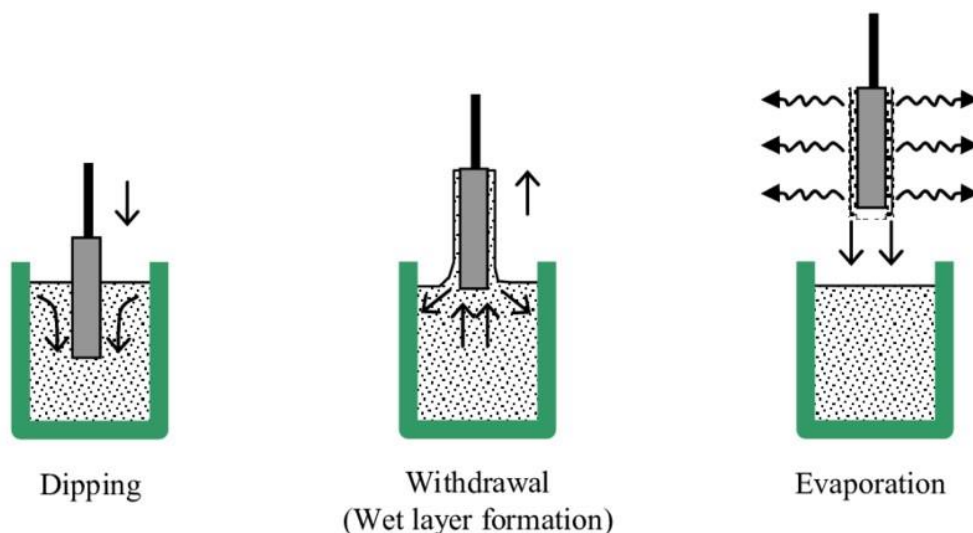
Figure II.7: Overview of the dip coating process: dipping of the substrate into the coating solution, wet layer formation by withdrawing the substrate and gelation of the layer by solvent evaporation [205].

II.2.3.3 Spin coating

Spin coating technique is used to develop thin, uniform coating for solution-based anti-reflection applications. it is a simple process for rapidly depositing thin coatings onto relatively flat substrates. the substrate is mounted horizontally on a rotating platform and spins at high speed until the coating solution is uniformly dispensed as shown in **Figure II.8** and the coating solution is dispensed onto the surface; the action of spinning causes the solution to spread out and leave behind a very uniform coating of the chosen material on the surface of the substrate [204,206]
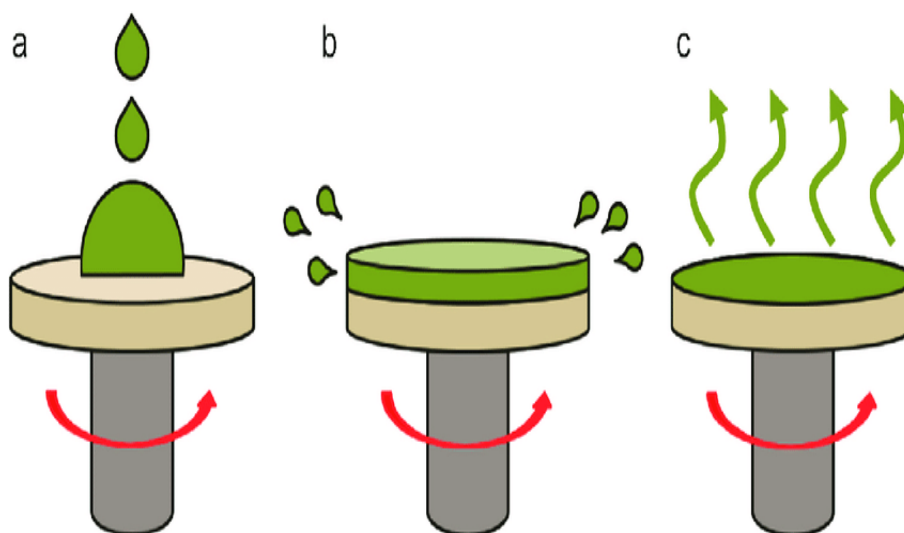
Figure II.8 Typical spin coating procedure. a) depositing coating solution; b) spinning to form material solution layer; c) evaporating to produce thin film [207]

II.3 Characterization Methods of Thin Films:

Nanoscale characterization is an important area in nanoscience and nanotechnology because it enables fundamental understanding of material properties and functions at the atomic and molecular level [208]. In this chapter, The structural, electrical, and optical properties of the grown samples were investigated using a variety of characterization techniques, a brief description for each characterization techniques, We will see through a few theoretical survey, the interest they present and the information they can provide for the characterization of our samples.

II.3.1 X-ray diffraction (XRD)

Structural characterization plays an essential role for growth-correlated properties of low dimensional semiconductor structures [209]. X-ray diffraction is one of the widely used experimental techniques for determining lattice parameters, preferred orientation of the crystal, phase composition (qualitatively and quantitatively), grain sizes, lattice strain and residual stress etc. [210]. It is an efficient non-destructive analytical technique used for the identification of crystalline structure of compounds by their diffraction pattern [211]. It can be applied to a wide range of materials, even liquids. It is very important to understand how atoms are arranged into a crystal structures, which make the understanding of of the synthesis, structure and properties of materials much easier. Until now, the most powerful experiments which explain the spatial arrangement of atoms in a materials network is "Diffraction", A diffraction pattern is produced when a material is irradiated with a collimated beam of x-rays having a wavelength (λ) close to the crystal lattice spacing, as shown in **Fig II.9**. The x-ray spectra generated by this technique provide a structural fingerprint of the material (unknown).[212]. The relative peak height is generally proportional to the number of grains in a preferred orientation and peak positions are reproducible [211]. The outgoing diffracted x-rays is recorded with a detctor as a function of diffraction angle 2θ and the specimen's orientation. Constructive or destructive interference then occurs along different directions as scattered waves are emitted by atoms of different types and positions [213]. Bragg's law was used to explain the interference pattern of X-rays scattered by crystals, diffraction has been developed to study the structure of all states of matter with any beam, e.g., ions, electrons, neutrons, and protons, with a wavelength similar to the distance between the atomic or molecular structures of interest. The process is governed by the equation:

$$\lambda = nd \sin\theta \tag{1}$$

where **n** is diffraction series, θ is diffraction angle, λ is the wavelength of X-ray, d is interplanar distance. In single crystal, **d** is the lattice constant [214].

This is the basis of **Bragg's law**, which relates the spacing between the 'planes' of atoms from which diffraction is occurring (d) to the angle (θ) at which the incident beam must probe the plane to give constructive interference.[64]
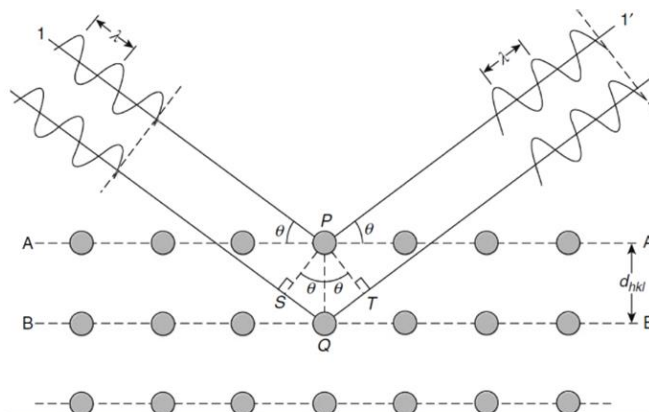
Figure II.9 *Image depicting an X-ray beam interacting with a sample [215]*

In order to obtain more structural information details, the crystallite size G along the c –axis can be obtained using Scherer formula [214].

$$G = \frac{0.9\lambda}{\beta \cos\theta}$$

(2)

Where λ is the X-ray wavelength (1.5406 Å), θ (°) is the Bragg angle of (002) peak and β (°) the FWHM of the diffraction peak.

The lattice parameters *a* and *c* were calculated using the relation for the plane spacing equation [214]:

$$\frac{1}{d^2} = \left(\frac{4}{3}\right)\frac{h^2 + hk + k^2}{a^2} + \frac{l^2}{c^2}$$

(3)

h, *k* and *l* are the Miller indices, and are the lattice parameters [214].

Experimentally the generated XRD pattern of the sample is compared with a standard XRD powder pattern 'Joint Council Powder Diffraction Standards (JCPDS)' which gives information of different crystallographic phases and preferred orientations.

In this work, The structural properties were studied by X-ray diffractometer (Siemens D5000 diffractometer) with CuKα (λ = 1.5406 Å) radiation in the Bragg-Brentano geometry in the range (10º < 2θ < 80º) from the University of Mentouri-Constantine. (**Fig II.10**).

37

Figure II.10 *The X-ray diffractometer*

II.3.2 Scanning Electron Microscope

Morphology characterization techniques vary in both cost, resolution and the type of the obtained information. When higher resolution is required, advanced microscopic techniques can be used [64]. Typical optical microscopes usually have a limit of around 1,000x to 2,000x magnification due to the nature in which they collect the image. Electron microscopes on the other hand can easily achieve 500,000x magnifications and the upper limit is only bound by the equipment used and the skill of the operator. Scanning electron microscopy (SEM) is a basic tool in several branches of Science, it is a method for high-resolution imaging of surfaces. using electrons beam that is focused on an area of a sample [215].

There is a large diversity of SEM equipment available but in generally they all follow the same principle , a beam of incident electrons produced from various types of electrons guns in an electron column and then is condensed into a beam or fine probe through a combination of electromagnetic lenses and apertures above the sample chamber. The electrons are produced by a thermal emission source, such as a heated tungsten filament, or by a field emission cathode. The energy of the incident electrons can be as low as 100 eV or as high as 30 keV depending on the evaluation objectives. The electrons are focused into a small beam by a series of electromagnetic lenses in the SEM column [215].After the electron beam interacts with the sample individual electrons then go on to hit the detector. High vacuum conditions is paramount for SEM which reduce the number of collisions between the electron beam and the atmosphere in the sample

chamber. **Figure II.11** depicts a cross-section view for an SEM set-up showing its important components.

As SEM depend on the sample being characterized , the types of sample and its condition of the are more important for SEM. the sample must exhibit some conductivity. Therefore, non conducting materials like polymers and ceramics may require a coating with a thin (~2-5nm) layer of a conductive material such as iridium or a gold-palladium alloy. Moreover, sample being bombarded with electrons must perfectly clean from dust and fingerprints.

For this work, the SEM images of ZnO thin films (doped and undoped) were obtained from the Scanning electron microscope SEM (Bruker Quanta 650) equipped with energy dispersive X-ray spectrometer (EDX) from the university Saad Dahleb- Blida. (**Figure II.12)**
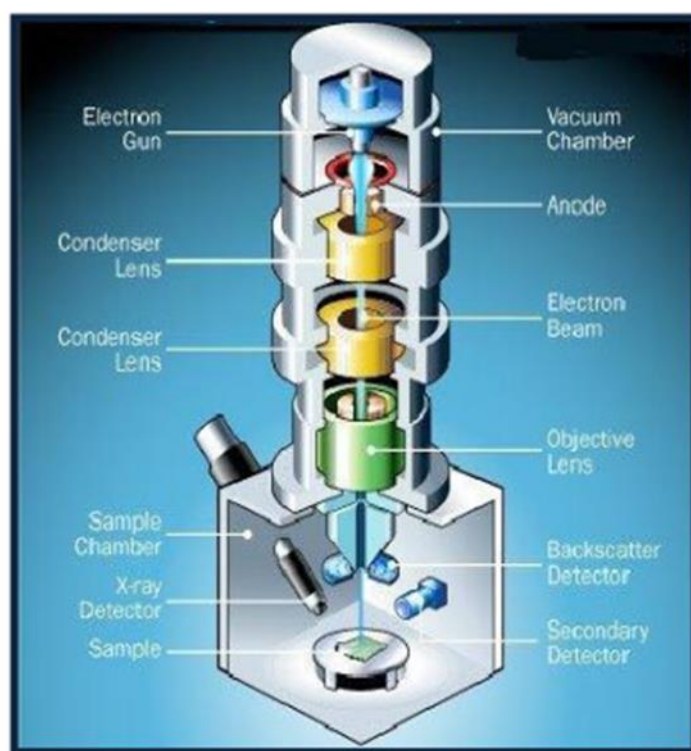
Figure II.11. Schematic cross-section of a typical scanning electron microscope [64]

***Figure II.12.** The scanning electron microscope equipment.*

II.3.3 Energy Dispersive Spectroscopy

Energy-dispersive spectroscopy (EDS or EDX) are commonly paired with SEM equipment as the same principle for sample analysis is used. It is an analytical technique used for the elemental analysis of a sample. Its characterization capabilities are due in large part to the fundamental principle that each element has a unique atomic structure allowing X-rays that are characteristic of the element's atomic structure to be identified uniquely from one another [64].

These characteristic X-rays occur when the electrons from the electron beam strike the electrons of an inner orbital of the specimen's atom. The force of this strike will knock the electron out of the orbitals of the atom and becomes a "free" electron. The ionized atom then compensates for this by adjusting and electrons from higher orbitals begin to drop down to lower orbitals releasing energy in several forms, including X-rays. Realesed X-ray photon energy is equal to the energy difference between the two levels involved [216]. The X-ray released by the electron is then detected by a solid state detector and converted into signals which are processed into an X-ray energy spectrum (**Fig II.13**).

Thus, by measuring the amounts of energy present in the X-rays being released by a specimen during electron beam bombardment, the identity of the atom from which the X - ray was emitted can be established. Characteristic x-rays from each element are used to determine the concentrations of the different elements in the specimen. Each of these peaks is unique to an atom and therefore corresponds to a single element. The higher a peak in a spectrum, the more concentrated the element is in the specimen [217].

There are a couple of things to note about EDS, EDS is not a surface analysis but instead a volume analysis. This is important for evaluating thin films as thi depth is often larger than the

thickness of the thin film. That means that elements from the substrate will be detected and must be accounted for. Second, the peaks produced by EDS must be evaluated with care. Figure 15 is a typical EDS spectrum. In this example, it is a spectrum taken from a ZnO thin film on a glass substrate. The x-axis represents the measured energy level and the y-axis is the count of that energy, of the amount of that element present. These peaks are fairly broad as opposed to being exactly at the energy level of the X-ray produced [216]
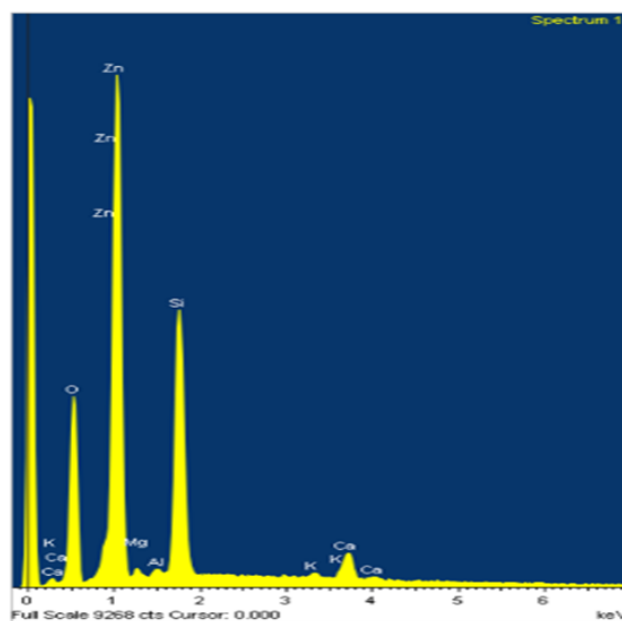
Figure II.13. EDS spectrum of ZnO thin film on a glass substrate

II.3.4 Atomic Force Microscope

Atomic Force Microscopy (AFM) is a non-destructive method for visualizing the three-dimensional morphology of a material's surface at the nanometric scale. The principle of AFM, as shown in **Figure II.14**, is based on the interaction between the surface of the sample to be analyzed and a nanometric probe. The tip of the probe is fixed under a flexible or cantilever micro-lever of given stiffness. The tip scans the surface and follows the topography of the sample, giving a three-dimensional image of the material being analyzed.

The sample is placed on the piezoelectric ceramic controlling the movements in the 3 directions X, Y and Z. As the sample is approached to the tip, the tip / sample interaction forces cause the micro-lever to deflect proportional to the intensity of the force. A laser beam, reflected on the rear face of the microlever, is directed onto a 4 quadrant photodiode which makes it possible to measure this deflection.

Historically, the first operating mode developed for atomic force microscopy is the contact mode. The tip attached to the end of the lever arm sweeps the surface, while remaining in

permanent contact with it. In this mode of operation, the main drawback lies in the large frictional forces. These forces can lead to damage to the tip or the observed sample.
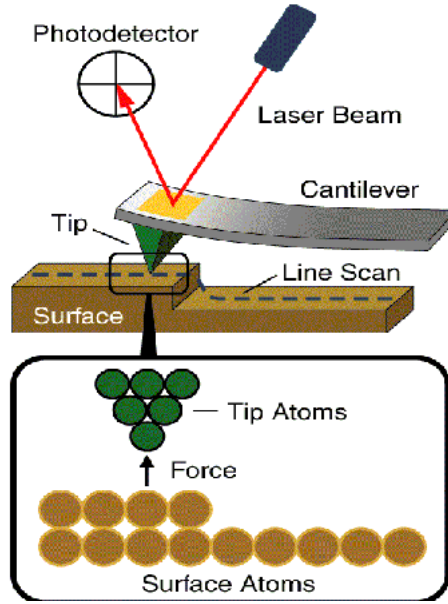
Figure II.14. Principle of Atomic Force Microscope.

If the tip only generates an attractive force with the sample without touching it, then this is called non-contact mode.

From the topological image, it is possible to evaluate the roughness of the sample:

➤ Ra (Arithmetic Roughness): This is the average deviation of all points of the roughness profile from an average line over the evaluation length [218] :

$$Ra = \frac{\sum_{i=1}^{N}(Z_i - \hat{Z})}{N} \qquad (4)$$

➤ Root mean square roughness Rms or Rq: Root mean square of the height deviations over the evaluation length and measured with respect to the mean line:

$$Rq = \sqrt{\frac{\sum_{i=1}^{N}(Z_i - \hat{Z})^2}{N}} \qquad (5)$$

Where:

Z_i: is the height value for a given point i of the scan surface.

$\hat{Z}$: is the arithmetic mean height in the scanned area. $\hat{Z} = \frac{\sum_{i=1}^{N}(Z_i)}{N}$

N: is the number of points in the scanned area.

In this work, the surface topography images and roughness values of the studied samples were determined using an AFM (**Fig.II.15**), MFP-3D Asylum Research with a Herzan TS-150 active vibration isolation table with lateral resolution of ~ 0.1 nm which is available at the Laboratory of Chemistry, Molecular Engineering and Nanostructures, university Ferhat Abbas-Setif 1.
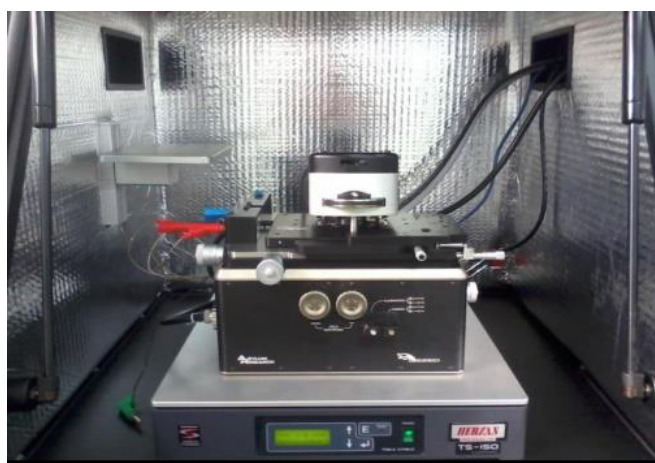
Figure II.15. *The Atomic Force Microscopy equipment.*

II.3.5 Raman spectroscopy

The phenomenon of inelastic scattering of light by matter was first observed experimentally by C.V. Raman, an Indian physics professor, and his collaborator K.S. Krishnan in1928 (Raman and Krishnan 1928) [219]. In 1930, he won the Nobel Prize in physics for his work on the scattering of light and for the discovery of the effect named after him. Raman spectroscopy is a non-destructive material analysis method, which provides additional information on diffraction techniques. It also makes it possible to detect the presence of impurities in small quantities and also the characterization of crystallized or amorphous materials at room temperature. The mechanism for Raman scattering lies in the change of the rotational or vibrational quantum states of molecules being illuminated. When monochromatic light is scattered from a surface 99.99% of it will be elastically scattered - i.e. it will have the same wavelength upon scattering. This is known as Rayleigh Scattering. It is considered elastic scattering because there is no net energy transfer between the incident photons and the lattice vibrations. (**Figure II.16**). However, for the Raman scattering, the energy of the scattered light is different from the incident one. If the light beam loses energy during the interaction, the phenomenon is called Stokes scattering, whereas it is

referred to as anti-Stokes scattering in the inverse case. The difference between the scattered and incident light can be used to identify the sample in terms of the characteristic vibrational modes.

A typical Raman spectrum of bulk ZnO is presented in **Figure II.17** [220]. The Raman peaks and the corresponding vibration modes are listed in **Table II.2**.

Table II.2: Optical phonon modes and their corresponding Raman shift, from [221]

Optical phonon modes	Raman shift (cm^{-1})
E2(low)	99
A1(TO)	378
E1(TO)	410
E2(high)	438
A1(LO)	574
E1(LO)	590
E2(high)- E2(low)	330
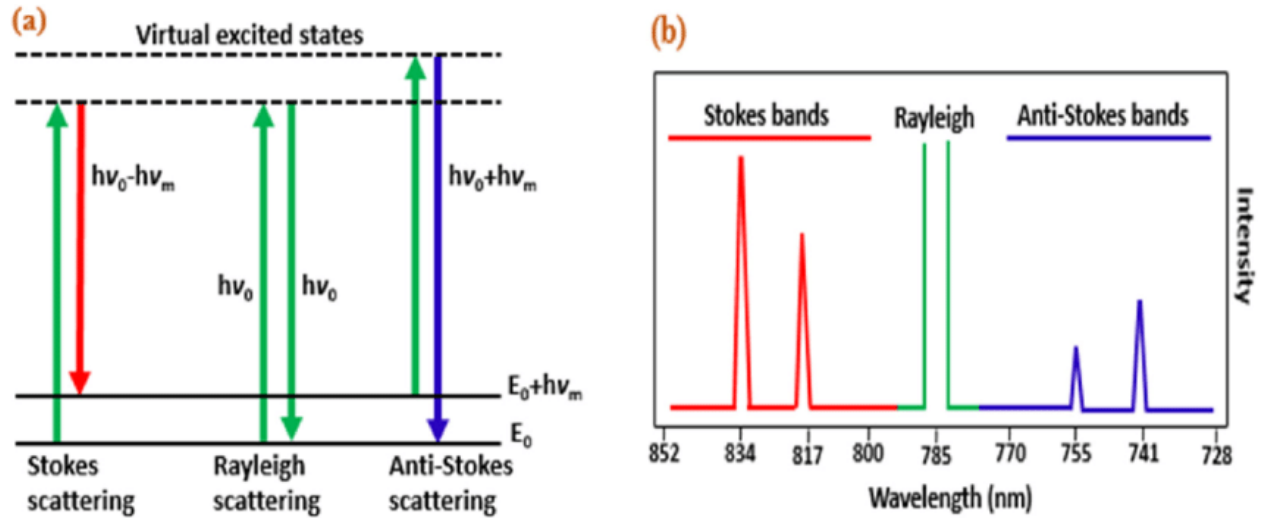
Figure II.16. (a) Schematic representation of Rayleigh and Raman scattering. v_0 indicates laser frequency (green: no energy difference), Stokes scattering (red: incident photon loss energy), and anti-Stokes scattering (blue: incident photon gain energy). (b) present illustrative diagram of resulting Raman spectrum (The frequency difference between the incident and scattered radiation is called Raman shift) [222]
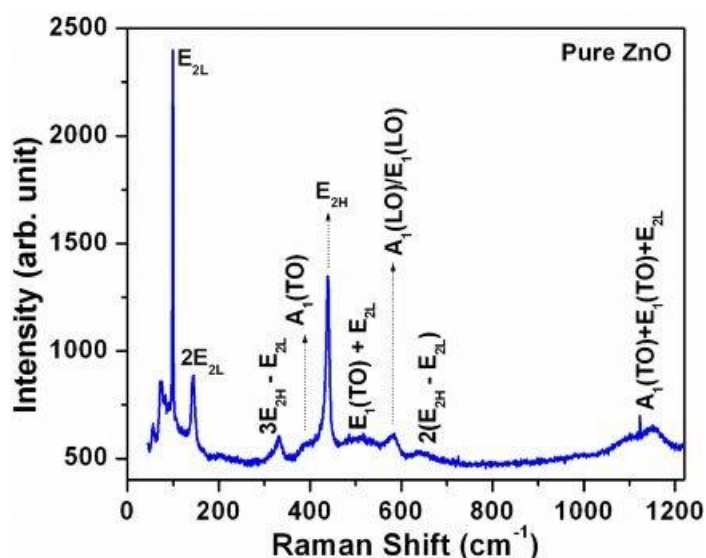
Figure II.17. *Micro Raman spectra of pure ZnO nanoparticles for 0.05 M zinc precursor [223].*

The measurements were performed using a Raman spectroscopy measurements were performed in a Senterra Bruker micro Raman system employing the 325 nm excitation line in the backscattering geometry configuration. of the University Mentouri-Constantine.

II.3.6 Fourier-transform infrared spectroscopy

Each chemical bond, in solids or molecules, has specific (quantized) vibrational modes. These modes, acting as oscillators, can absorb photons of energy corresponding to the oscillator transition. The absorption spectrum is thus "a picture" of the chemical bonds present in the sample, provided that they are IR active, i.e. having a dipole moment, capable of absorbing the electromagnetic radiation. Fourier Transform-Infrared Spectroscopy (FTIR) is an analytical technique used to identify organic (and in some cases inorganic) materials. This technique measures the absorption of infrared radiation by the sample material versus wavelength. The infrared absorption bands identify molecular components and structures. When a material is irradiated with infrared radiation, absorbed IR radiation usually excites molecules into a higher vibrational state. The wavelength of light absorbed by a particular molecule is a function of the energy difference between the at-rest and excited vibrational states. The wavelengths that are absorbed by the sample are characteristic of its molecular structure. [224].

IR absorption spectroscopy can be performed using either a monochromatic source or a broad spectrum IR source. Before the incident light arrives at the sample, it is divided by a beam splitter into two light beams and reflected by a stationary and a movable mirror, respectively. The two reflected light beams then recombine and undergo interference which is normally called the

Michelson interferometer, as shown in **Figure II.18**. The recombined light illuminates the studied samples, and the transmitted or deflected light is detected. The transmittance spectrum can be obtained from the collected signal and the interferogram is treated by the Fourier transform. The absorption spectrum can also be converted from the transmittance spectrum using programs integrated in the FTIR instrument. The method using the broad band IR source has the advantage of being faster and more sensitive than the simpler one using a monochromatic source [225].
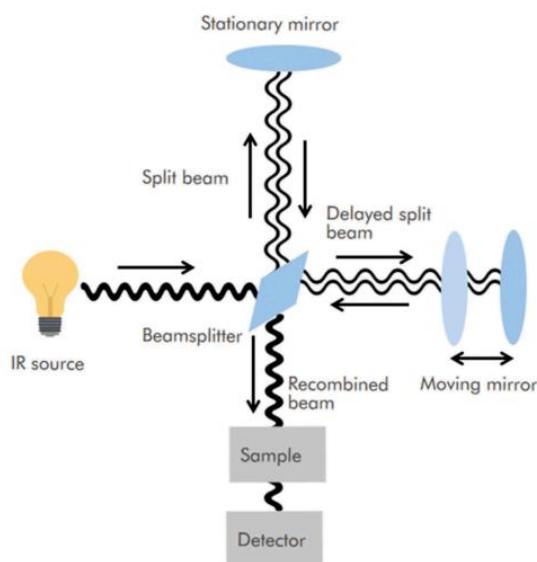
Figure II.18. Schematics of a Michelson interferometer used in modern FTIR instruments [226].

A common Fourier Transform Infrared Spectroscopy (FTIR) is able to cover a long range of electromagnetic spectrum regions: the near-infrared (0.8–2.5 µm), mid-infrared (2.5–25 µm) and far infrared (25–1000 µm).
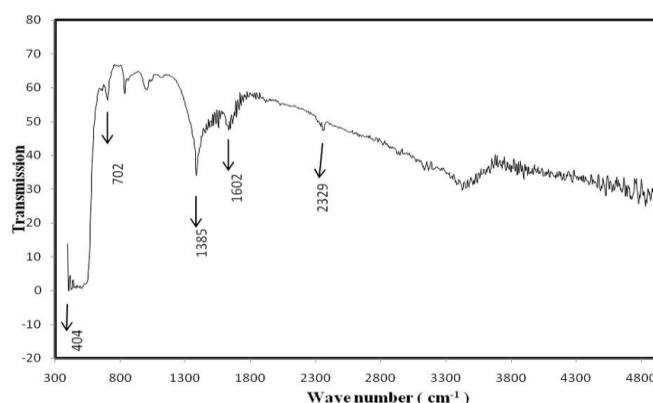
Figure II.19. FT-IR spectrum of thin films of ZnO showing Zn–O bonding at 428.12 cm^{-1} [227].

A typical IR spectrum of bulk ZnO is shown in **Figure II.19**. Metal oxides generally give transmission bands in the fingerprint region below 1000 cm^{-1} , arising from inter-atomic vibrations . Peaks in the range 400-700 cm-1 have been observed in IR spectra of ZnO and they are attributed to wurzite crystalline Zn-O stretching mode [228].
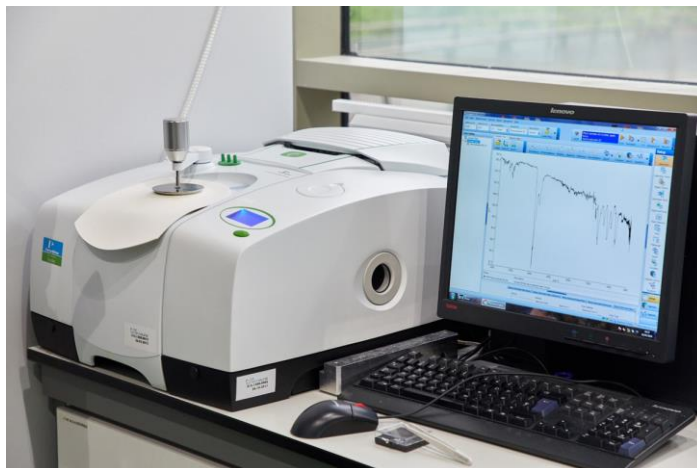
Figure II.20. FTIR Spectrometer PerkinElmer equipment.

The FTIR analysis was recorded using Perkin Elmer spectrometer in the range of 3500–300 cm^{-1} (**Figure II.20**) light source and the transmittance detection mode were used.

II.3.7 UV –Visible spectroscopy

Optical transmission measurements are used to evaluate and test certain optical constants of materials that are critical for system fabrication and analysis. Among these optical constants: the absorption coefficients, the bandgap energy, dielectric index, refractive index and and Urbach energy, it can also provide information on the thickness of the sample. Furthermore, optical transmission or absorption measurements are used to detect certain impurities present in a material as some impurities have characteristic absorption lines. The most common type of spectrophotometer is a double beam one as shown in **Figure II.21**, A spectrum of monochromatic wavelengths is continuously shone into a sample during a transmission measurement, and the emitted light is regularly measured as a function of the incident wavelength. A transmission spectrum is generated by plotting the relative intensity of the transmitted light to the incident light as a function of the wavelength [229].

The beam is split into two beams; one is directed to the sample while the other passes through a blank control (substrate). The path lengths over which the split beams travel are equal. The detector then compares the intensity of the two beams and calculates a transmittance for the film with respect to the substrate. Since the comparison between the

sample and reference beams is made simultaneously, the instrument compensates for beam fluctuations [230]

The transmitted light is continuously recorded as a function of the incident wavelength thus a transmission spectrum is generated by plotting the relative intensity of the transmitted light to the incident light as a function of the wavelength. From the transmission data the optical bandgap *Eg* can be easily determined using the Tauc relation which is given by [231]:
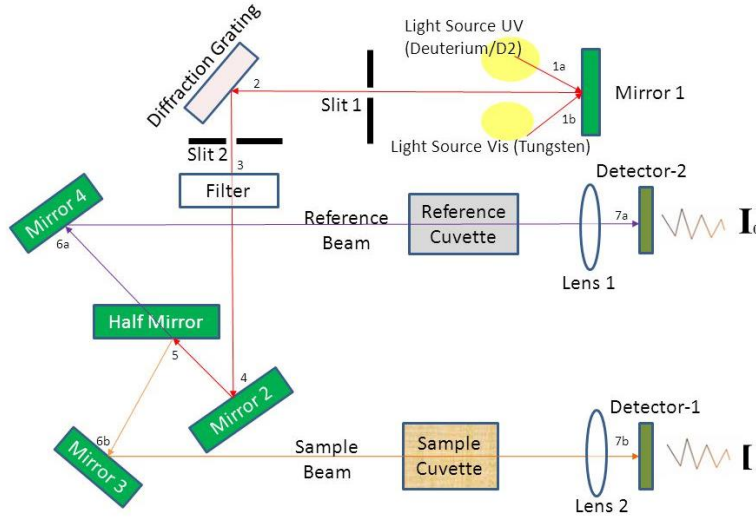
Figure II.21. Basic Double-beam UV-Vis spectrophotometer set-up.

The intensity of light after it passes through the cuvette, can be related it to transmittance (T). Transmittance is the fraction of light that passes through the sample. This can be calculated using the equation [232]:

$$T = \frac{I}{I_0} \qquad (6)$$

Where I is the light intensity after the beam of light passes through the cuvette and Io is the light intensity before the beam of light passes through the cuvette. Transmittance is related to absorption (A) by the expression:

$$A = -\log(T) = -\log\left(\frac{I}{I_0}\right) \qquad (7)$$

The absorption coefficient α of ZnO films was determined from transmittance measurements. The films' absorption coefficient was calculated using the following expression [233]:

$$T = e^{-\alpha d} \qquad (8)$$

$$\alpha = -\frac{1}{d}\ln(T) \qquad\qquad (9)$$

Where T is the normalized transmittance, d is the film thickness.

Swanepoel [234] is without a doubt the most well-known model to calculate the optical parameters such as: dielectric index, refractive index and thickness. multiple reflections of light (interference fringes) occur between the lower surface in contact with the substrate and the free surface of the layer, it is the envelope method which is based on the creation of an upper and lower envelope of the transmission spectrum beyond the absorption limit.

The thickness "t" of a thin film is given by the following equation [235] :

$$t = \frac{\lambda_1\lambda_2}{2[n(\lambda_1)\lambda_2 - n(\lambda_2)\lambda_1]} \qquad\qquad (10)$$

With n (λ1) and n (λ2) are the refractive index of the layer for two maxima adjacent ones corresponding to wavelengths λ1 and λ2.

The refractive index n at different wavelengths was calculated using the envelope curve for Tmax and Tmin in the transmission spectra (**Figure II.22**). The expression for refractive index is given by [236]:

$$n = \left[N + (N^2 - n_s^2)^{1/2}\right]^{1/2} \qquad\qquad (11)$$

$$N = \frac{(n_s^2 + 1)}{2} + 2n_s\frac{(T_{max} - T_{min})}{(T_{max}T_{min})} \qquad\qquad (12)$$

Where ns is the refractive index of the substrate. Tmax and Tmin are maximum and minimum transmittances at the same wavelength in the fitted envelope curves on the transmittance spectrum.

The extinction coefficient can be also calculated by the following equations [237]:

$$k = \frac{\alpha\lambda}{4\pi} \qquad\qquad (13)$$

Where α is the absorption coefficient and d is the film thickness. λ is the wavelengths.

$$\alpha = \frac{\ln(^1/_T)}{t} \qquad\qquad (14)$$

The optical properties of an insulator or semiconductor are always described in terms of complex dielectric function ε (ω), the latter is an intrinsic property fundamental of the material considered. It is given by the relation [238]:

$$\varepsilon(\omega) = \varepsilon_r(\omega) + \varepsilon_i(\omega) \tag{15}$$

With ε_r (ω) and ε_i (ω) are respectively the real part and the imaginary part of the function dielectric ε (ω), these functions are related to the refractive index n (λ) and the coefficient extinction k (λ) by the equations [239]:

$$\varepsilon_r = n^2 - k^2 \tag{16}$$

$$\varepsilon_i = 2nk \tag{17}$$
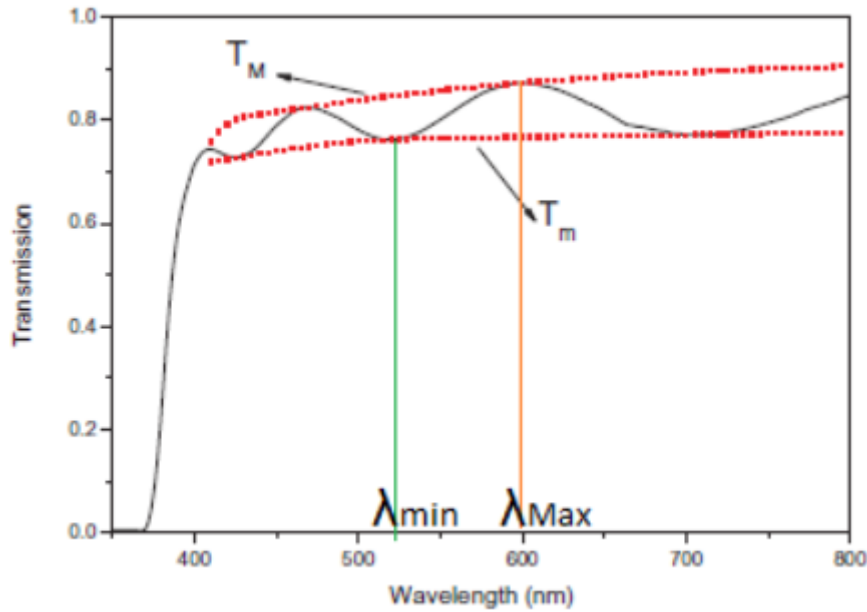
Figure II.22. UV/VIS/NIR transmission curve of ZnO film.

The optical energy band gaps Eg of the films were calculated using the Tauc's relationship as follows [240]:

$$\alpha h v = A\big(hv - E_g\big)^n \tag{18}$$

Where: α is absorption coefficient, A is constant, h is Planck's constant v is photon frequency and n is 1/2,2,3/2 and 3 for allowed direct, allowed indirect, forbidden direct and forbidden indirect band gap semiconductors, respectively. Since ZnO is a direct band gap semiconductor, value of n was selected to be 1/2.

An extrapolation of linear region of a plot $(\alpha h\upsilon)^2$ on y axis versus photon energy (hυ) on X axis gives the value of the band gap energy. The direct band gap of ZnO films was estimated by from extrapolation of linear portion of graph $(h\upsilon\alpha)^2=0$ as shown in Figure II.23.
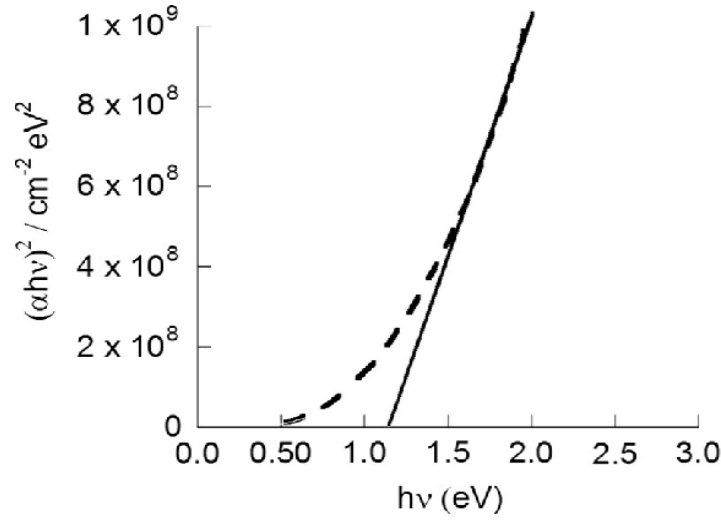
Figure II.23. band gap energy determination using an linear region extrapolation of a plot (αhυ)2 as a function of photon energy for a ZnO thin film doped by Al at 3 at%

The degree of structural disorder present in the film is calculated by a quantity called Urbach energy (Eu). In semiconductors, there is an exponential increase of the fundamental absorption near the band gap energy. The width of the exponential absorption edge is called the Urbach energy [241], which can be obtained using [242]:

$$\alpha = \alpha_0 exp\left(\frac{h\upsilon}{E_u}\right) \qquad\qquad (19)$$

Where *hv* and α₀ are constants, E_u is the Urbach energy. The plot of logarithm of absorption coefficient against the photon energy allowed getting E_u value, which is the reciprocal of the slope of the linear portion of the graph.

Chapter III :

Results & discussion

III.1 Introduction

sol-gel as Chemical techniques, can efficiently control the nucleation, growth of particles in a solution, providing for the synthesis of appropriate precursor particles with a variety of parameters to control the solid formation process [243]. A tremendous challenge to develop a high-quality material and control its structural, optical, and electrical properties. A clear mastering of the experimental procedures allows to change the material's physical properties to satisfy the expectations of a chosen application. using suitable impurity material has a paramount importance that can have significant effect on ZnO thin films properties. In the following section, we present the experimental processes used for the production of thin films of ZnO undoped and doped with Rare Earth Element (REE). The elaboration methods used are the Sol-Gel While the deposit techniques chosen is Dip-Coating. The aim of this work is to enhance ZnO nanostructures properties by REE ions dopants. The choice and preparation of substrates and precursor solutions are then described. Finally, in the main To get a deep understanding of the impact of REE ions on the morphological, structural and optical properties of the deposited films. several characterizing techniques were used viz: X-ray diffraction, atomic force microscopy scanning electron microscopy, Raman and FTIR spectroscopy and UV-visible spectroscopy.

III.1.1 Films preparation and processing

ZnO is a unique material that exhibits multiple properties, i.e.,semiconducting, piezoelectric and pyroelectric. ZnO thin films are being widely studied for their interesting optical properties and uses as solar cell window materials due to its Non-toxicity, abundance in nature and excellent properties which make it one of the most suitable materials today for a wide range of technological applications [244,245]. Among all deposition techniques, sol gel method presents several advantages such as low cost, large-scale deposition and low-temperature processing, it is mainly used to deposit most of the thin layers of metal oxides such as ZnO due to the simplicity of the equipment, the homogeneity of the layers, with high surface quality [246]

III.1.1.1 Substrat pre-treatement

In order to prepare a high quality ZnO thin films some specific material are needed, among these required materials, suitable substrate type has a paramount importance. The substrate is very important for the growth of thin films in terms of the lattice and thermal mismatching between it and the film because it commonly leads to the development of stress in the deposited film. The choice of substrate affects crystalline quality as well as optical and electrical properties of ZnO film [247]. In the present work, undoped and RE ions doped ZnO thin films were deposited in a

microscopy slide glass substrates in a size of 1.5×1.5 cm$^2 \times 0.1$ cm. The choice of glass as substrate was due to three reasons, for economic reasons, to perform a good optical characterization of our films and to minimize the stresses because the two materials constituting the sample (glass + zinc oxide) have a very close expansion (dilatations) Coefficients (α_{glass}=8,5 10^{-6} K^{-1}, α_{ZnO}=7,2 10^{-6} K^{-1}) [248-250].

Clean microscopy slide glass substrates prevent contamination without damage to the substrate, allow for correct deposition of materials. The primary function of this step is to provide a strategy to remove everything from a glass substrate surface. This would effectively make the used slides function as if they were new slides. While cleaning, the bond between the substrates is broken and contaminants are set free from the substrates. Contaminants such as fingerprints, dust, oil, and lint particles are expected. Those undesired contamiants affect directly morphology, nucleation and the the substrate film interface [251]. Initially, These glass substrates were cleaned ultrasonically by acetone, ethanol and deionised water each for 15 min and Substrates were rinsed with methanol after the sonication. Finally they were dried under hot flow air to evaporate residuals water drops. Before use, all cleaned substrates passed through a visual control in order to check the absence of scratches, streaks and other defects that will affect the properties after deposition of thin films. Cycle presented in **Fig.III.1.**

1) **Sonicated for 15 minutes in acetone ethanol and Di-ionized water**   2) **rinsed with methanol**   3) **drying**
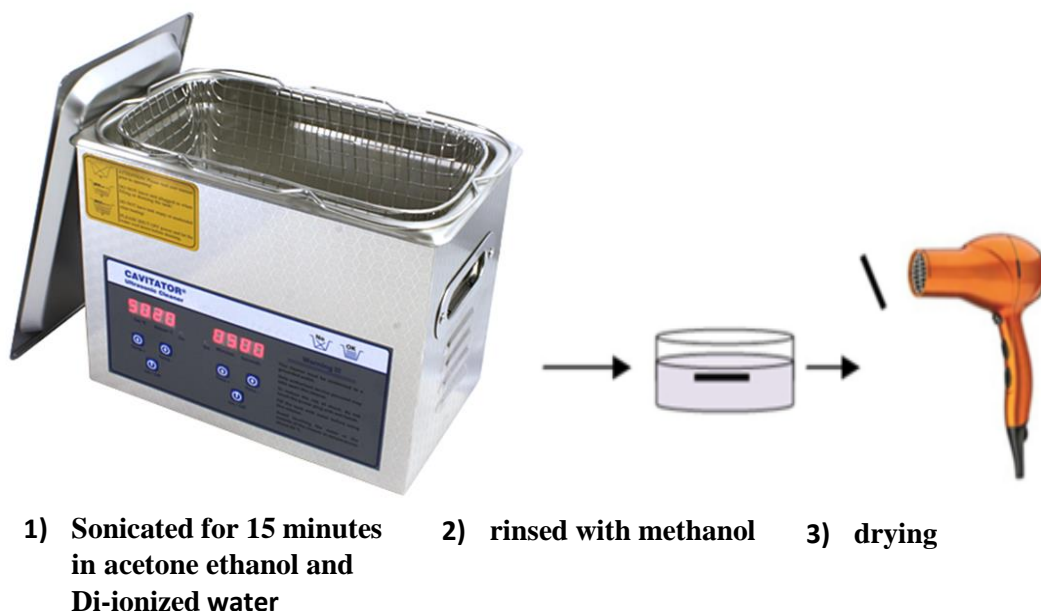
Figure III.1. Schematic illustration of the Cleaning Process of the substrates.

III.1.1.2 Preparation of the pure solution

Undoped ZnO nanostructures were synthesized using sol gel dip coating route onto glass substrates. As starting materials, Zinc-acetate-dehydrate (Zn(CH3COO)2.2H2O, Sigma Aldrich product-99.99% purity). The undoped ZnO samples was obtained by dissolving 2.5 g of zinc acetate dehydrate in 50 ml of isopropanol as a solvent. Under continuous magnetic stirring at 60 °C for 30 min, Monoethanolamine MEA (H2N-CH2CH2OH, Sigma Aldrich product-99.99% purity) was added drop by drop as a sol stabilizer, it was also used to control pH of condensation reaction in sol–gel solution and the further addition of MEA leads to change sol condition from acidic to alkaline. The pH was maintained at 9 for all prepared sols. The as-prepared solutions was stirred at 60 °C for 2 h to yield a lucent and homogeneous solution. The mixture was then served as the coating solution after aging in dark for more than 72 h.

III.1.1.3 Preparation of the doped solution (Er and Yb)

Erbium and Ytterbium doped ZnO nanostructures with various doping concentration were synthesized using the same method. As a dopants source, Erbium (III) Nitrate Pentahydrate and Ytterbium (III) Nitrate Pentahydrate were used. The concentration of Erbium/Ytterbium as a dopants atom were (1wt%, 3wt% and 6wt%) and the EZO/YZO doped samples were named respectively as EZO1, EZO3, EZO6. YZO1, YZO3, YZO6.

III.1.1.4 Deposition process of pure and doped ZnO thin films

The sol gel deposition of pure and doped ZnO thin films was carried out using a dip-coater device (**Figure III.2**) available in the ENMC research laboratory (Laboratory for the Elaboration of New Materials and their Characterizations) at the university Ferhat Abbes, Sétif 1.

Figure III.2. Sol Gel Dip-Coating Device.

The aged solution was dropped on cleaned glass substrates with a dip speed of 80 mm/min, and for the evaporation of all solvents, the as-deposited samples were then preheating at 300°C for 10 min, this dipping to preheating procedure was repeated 16 times in order to obtain the desired thickness. Finally, all deposited samples were annealed at temperature of 500°C for 90 min in a tube furnace.

The structural properties were studied by X-ray diffractometer (Siemens D5000 diffractometer) with CuKα (λ = 1.5406 Å) radiation in the Bragg-Brentano geometry in the range (10º < 2θ < 80º), Crystalline phases were identified using the JCPDS database. Scanning electron microscope SEM (Bruker Quanta 650) and Atomic force microscope AFM were used to characterize the morphological properties of the obtained nanostructures. Elemental compositional analysis was carried out with X-Ray dispersive Energy (EDX). Raman spectroscopy measurements were performed in a Senterra Bruker micro Raman system employing the 325 nm excitation line in the backscattering geometry configuration. The FTIR analysis was recorded using Perkin Elmer spectrometer in the range of 3500–300 cm^{-1}. The optical properties were investigated with a double beam SHIMADZU-330 spectrophotometer.

III.2 Results and Discussion

III.2.1 Part one: Erbium doping effect

In the present section, the structural, morphological and optical properties of zinc oxide thin films were studied as a function of Er doping concentration in order to find out the influence of Er^{3+} doping rate on zinc oxide thin film properties.

III.2.1.1 Structural Characterization

Figure III.3 shows the X-ray diffraction patterns of the undoped and Er doped ZnO nanostructures grown on glass substrate with different concentrations (1wt%, 3wt% and 6wt%), All samples exhibited different diffraction peaks at 2θ ≈ 31.80°, 34.50°, 36.36°, 47.60°, 47.59°, 51.33°, 56.74°, 62.94°, 68.13°and 72.60° corresponding to hexagonal wurtzite ZnO planes of (100), (002), (101), (102), (110), (103), (112) and (004) respectively, a pure phase of ZnO wurtzite structure was indicated by the appearance of those XRD peaks: (100), (002), and (101) [252]. The high intensity and sharp peaks are attributed to the high pH value, S.S. Alias et al [253] showed that at pH 9 a high ZnO peaks intensity were obtained indicating high crystalline quality, because when increasing pH, the number of hydroxides (OH-) increase which enhance ZnO growth. K Sivakumar et al [254] reported that alkaline environment promotes the formation of ZnO with enhancing in grains growth. All the samples are well matched with the Joint Committee on Powder

Diffraction Standards file (JCPDS card no. 36-1451). As seen from the Fig. 1, the (002) is the most sharp and intense peak located at 2θ ≈ 34.50° for all patterns, this indicates a good crystalline quality. It can be seen from Figure III.3 that the (002) peak intensity decrease when increasing doping concentration, this may be due to the larger ionic radius of Er^{2+} ions with respect to that of Zn^{2+}. We note that phases due to Er_2O_3 was not observed in all patterns which suggests that Er^{2+} are well incorporated into Zn^{2+} lattice sites without altering the ZnO structure.
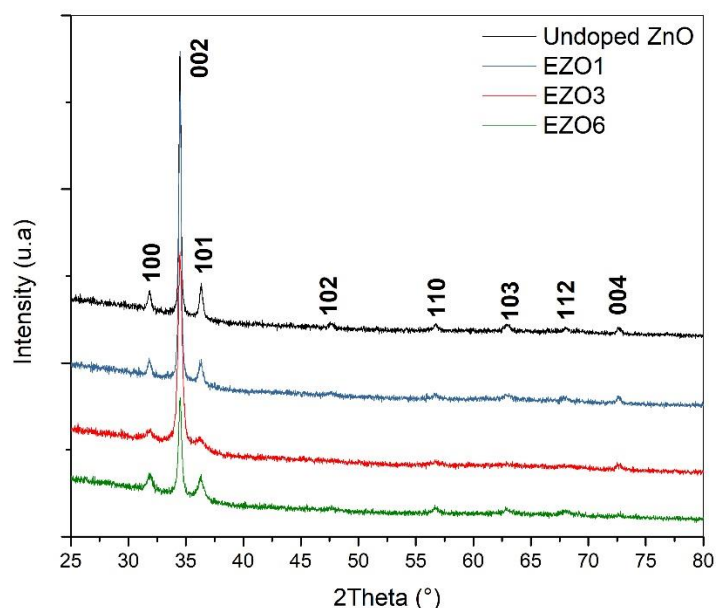
Figure III.3 *XRD pattern of Er-doped ZnO thin films with varying doping concentrations of Er under alkaline conditions (pH 9).*

Figure III.4 shows the variation of Undoped and Er doped ZnO crystallite size as a function of doping concentration. As expected, the crystallite size decreases with increasing in doping concentration and this due to the substitutions of Er^{3+} ions in the sites of Zn^{2+} ions, also the large difference between the ionic radius of RE element (Er^{3+} with 0.88 Å) and Zn^{2+} with 0.74 Å [255]. beside this, RE ions acts as nucleation centers when they incorporate in the ZnO matrix [256,257].

As we can see from Figure III.4, the variation of the lattice parameters c shows a double behavior, when doping between 1 and 3wt%, "c" increases as compared with undoped samples, but when the doping concentration exceed 3wt %, "c" decreases rapidly. The first behavior can be explained by the fact that Er^{3+} ions have been entered and well substituted the Zn^{2+} ions sites. When the second behavior can be related to the limit solubility of RE element [257].
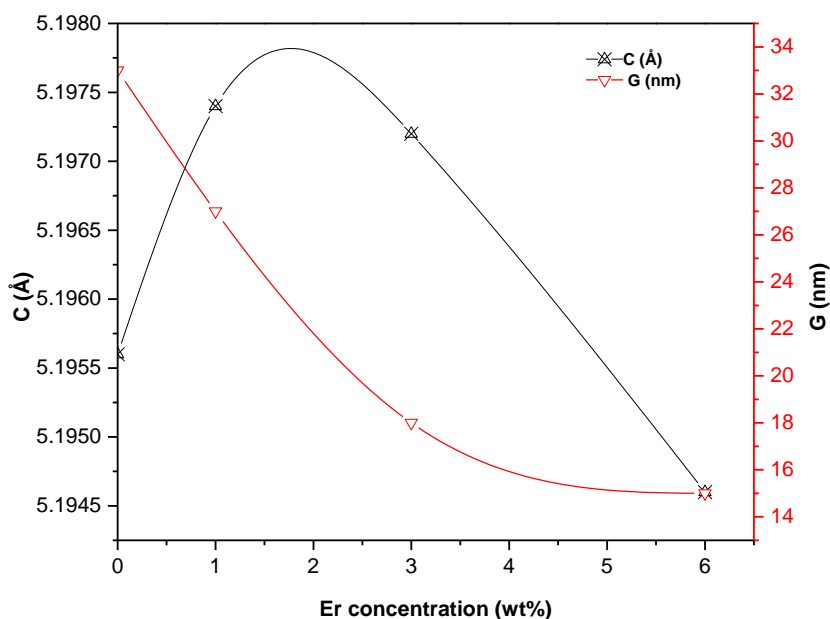
***Figure III.4**. Variation of grain size and lattice parameters "C" of ZnO thin films as a function of Er doping concentration.*

Figure III.5 shows the variation of stress in the ZnO matrix and the position of (002) peak as a function of Er doping concentration. It can be seen that there is a proportional relationship between strain and (002) peak's position. The shift of (002) peak position is indicated by the existence of strain in the ZnO matrix, this stress is caused by the incorporation of dopant agent (Er3+) [258], and maybe the dissimilarity of thermal expansion coefficient between substrates and EZO films [259]. (002) peak is found to be displaced to the lower diffractive angle compared to the pure ZnO films, but with further increase in Er concentration (up to 3 wt%) the peak move to the larger angle.

The crystallite sizes G, the values of β, The plane spacing and the lattice parameters of all samples are presented in Table III.1.
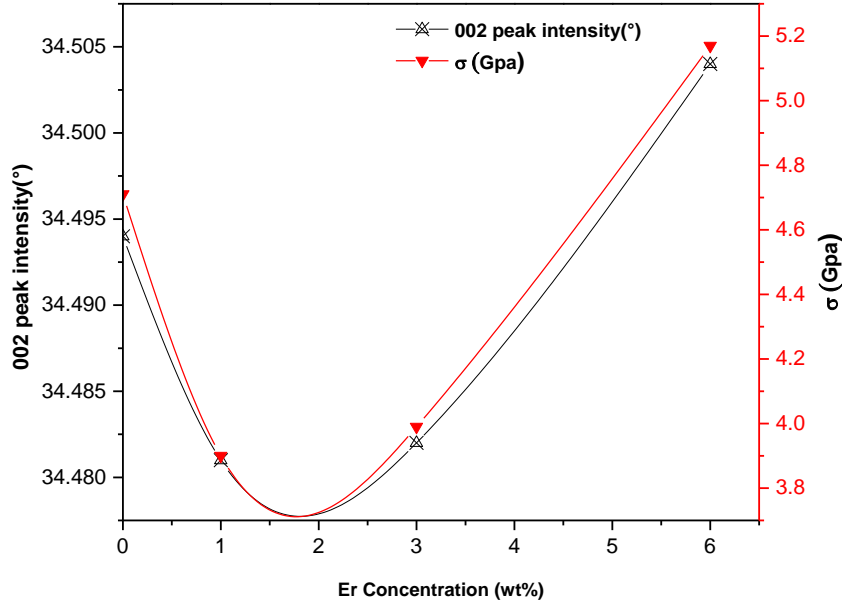
Figure III.5: *Variation of stress in the ZnO matrix and 002 peack's position of ZnO thin films as a function of Er doping concentration.*

Table III.1*: Structural parameters evaluated by XRD data for deposited undoped ZnO and EZO thin film.*

Samples	2θ (°)	β(°)	c (Å)	a (Å)	d (Å)	G (nm)	Ϭ (GPa)	RMS (nm)
Undoped ZnO	34.494	0.25	5.1956	3.1816	2.5978	33	4.71	6.25
EZO1	34.481	0.31	5.1974	3.1827	2.5987	27	3.90	4.98
EZO3	34.482	0.47	5.1972	3.1826	2.5986	18	3.99	3.86
EZO6	34.504	0.54	5.1946	3.1810	2.5973	15	5.17	2.68

III.2.1.2 Surface Morphology

III.2.1.3 Atomic force microscopy

In order to have a deeper insight into the surface morphology properties and the influence of the Er doping concentration under alkaline environment (pH 9), Atomic force microscopy (AFM) has been used, the scanning area was 1 μm×1 μm. Figure III.6 shows the 2D and 3D AFM micrographs of pure ZnO and Er doped ZnO with different concentration. It can be seen from Figure III.6 that undoped ZnO films micrograph exhibits homogenous, dense and granular morphology nanostructures, composed of small grains without regular shape in a uniform distribution on the entire glass substrate. The insertion of Er atoms leads to the modification of surface morphology. Effectively, when doped with 1wt% of Er (sample EZO1) the crystallite size decreases with keeping the same homogenous, dense and granular morphology, and for further

increasing of doping concentration (3 wt% for EZO3 and 6 wt% for EZO6) the crystallite grains get more and more small. Moreover, all AFM micrographs present a smooth surface with no crack and voids. The smoothness of surface is indicated by the Root Mean Square (RMS), it is a very important parameters that gives us a clear insight to compare the topography of all elaborated nanostructures. The surface roughness (RMS) of all films estimated from AFM micrographs is given in Table III.1. It can be noted that all samples show a smooth surface with a low roughness value which decreases when increasing Er doping concentration (from ~ 6 nm for pure ZnO to ~ 2 nm for EZO6). Note that alkaline conditions are favourable to get smooth surface [254] The low value of surface roughness makes EZO films less dispersive of light, consequently, the transmittance increases. R. Ashiri et al. reported that the low values of surface roughness (RMS) indicate that the entire surface is uniform [260].

Pure ZnO

EZO1

EZO3

EZO6
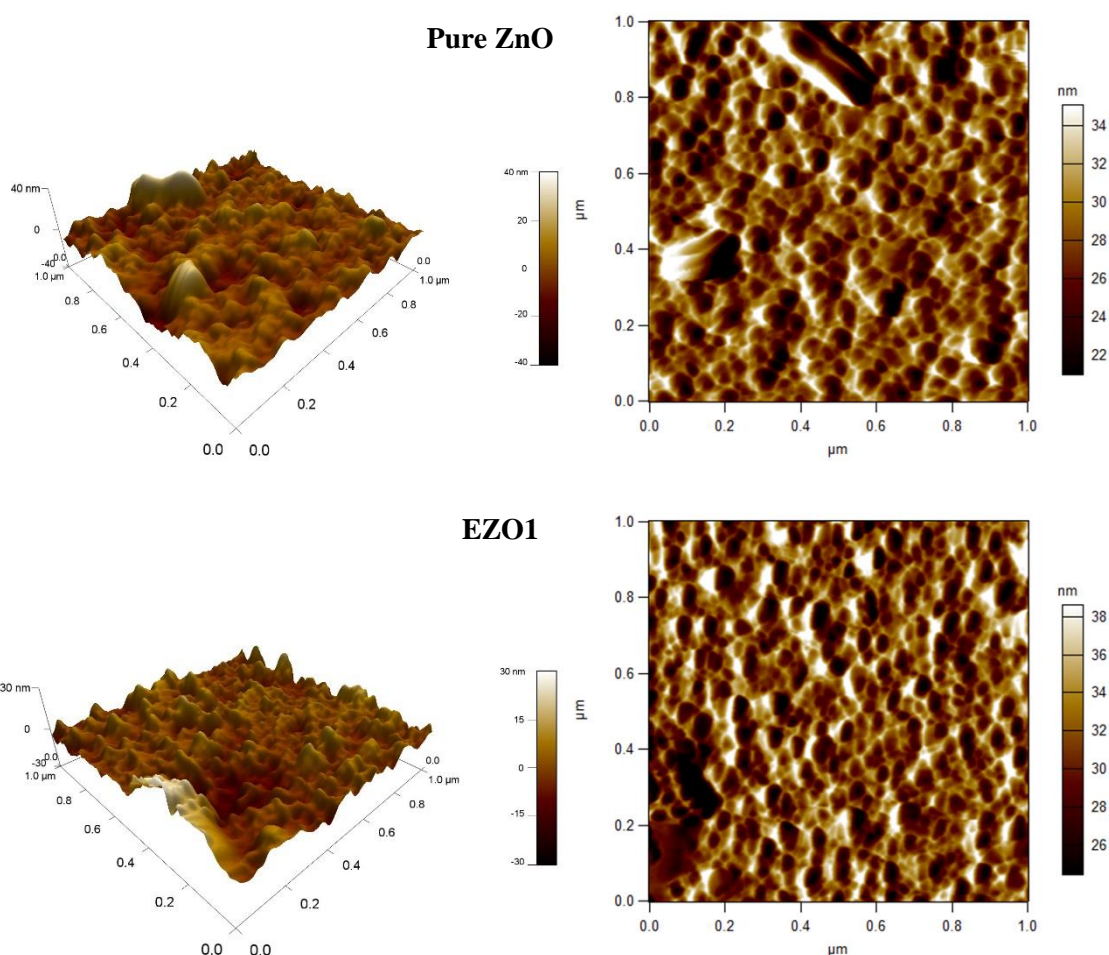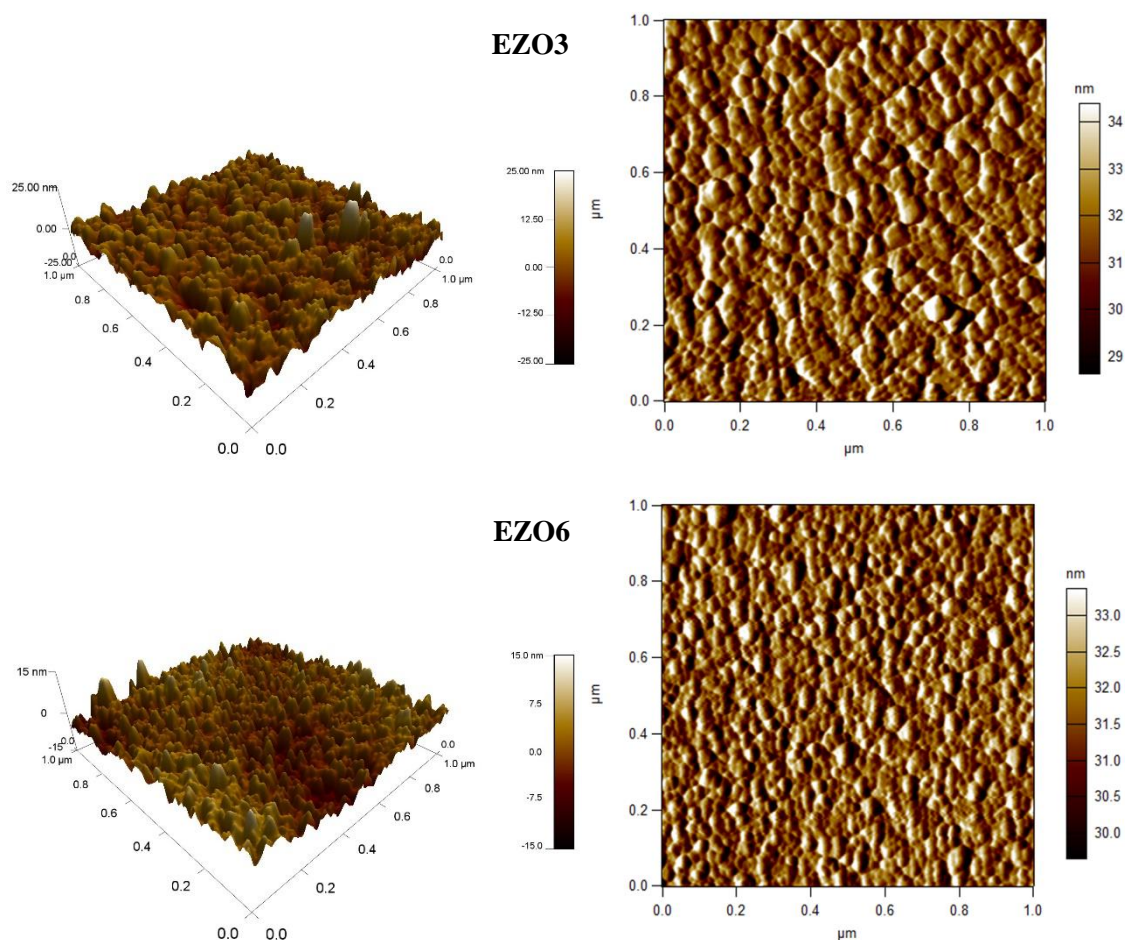
Figure III.6: 2D-3D AFM micrographs of ZnO and Er-doped ZnO with different doping concentrations

III.2.1.4 Scanning electron microscopy

Figure III.7 shows the observed SEM images of prepared undoped and Er doped ZnO nanostructures namely: pure ZnO, EZO1, EZO3 and EZO6. The morphology of all samples exhibits homogenous, dense, smooth and a uniform distribution of small crystalline grains without cracks and voids. In fact, this homogeneity is attributed to the high pH value which leads to regular growth of crystalline grains [261]. because, the access amount of OH- improve the nucleation and the growth of ZnO nanocrystalline [262]. It can be observed that the insertion of RE element (Er+3) in the ZnO crystal lattice affect the morphology of crystalline grains. Effectively, the undoped ZnO thin films pattern shows a dense packing granular structure formed by an agglomeration of a small nanocrystals without a regular shape. After, by increasing the dopant concentration the grains become more and more small. This systematic change of crystallites size indicates the successful incorporation of Er ions in the Zn lattice, i.e. more the dopant concentration increases more the Er ions create a nucleation center [8]. It can be seen that the observation from SEM images is in close agreement with the results obtained from XRD analysis.
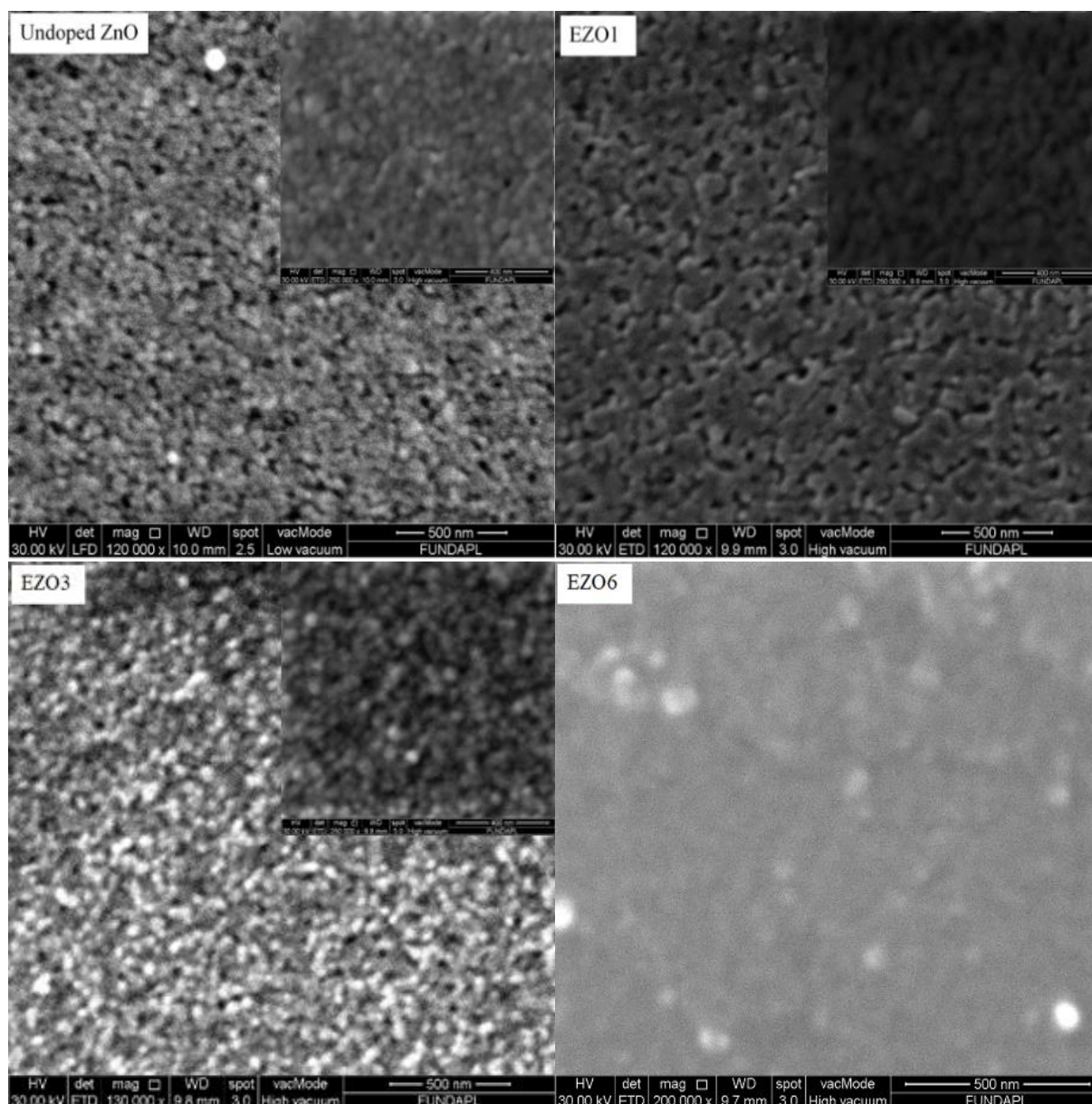
Figure III.7: SEM images for undoped ZnO and Er doped ZnO nanoparticles.

III.2.1.5 Elemental analysis (Energy Dispersive Spectroscopy)

Elemental compositional analysis was carried out with X-Ray dispersive Energy (EDX) in order to prove the presence of Er ions in the Zn lattice. Figure III.8 shows the EDX spectrum of all prepared samples, from later spectrum the successful substitution of Zn atoms by Er atoms in the ZnO crystal lattice was confirmed. However, we found that the estimated percentage of Er atoms is less than the real concentration of Er2O3 added during the deposition process. This mismatch can be explained in two ways: first way, the difference in ionic radius between RE element (Erbium) and Zn. Second way, is when Erbium with 3 positive charge (Er3+) tends to substitute Zinc with 2 positive charge (Zn2+) this leads to create a charge imbalance [263].
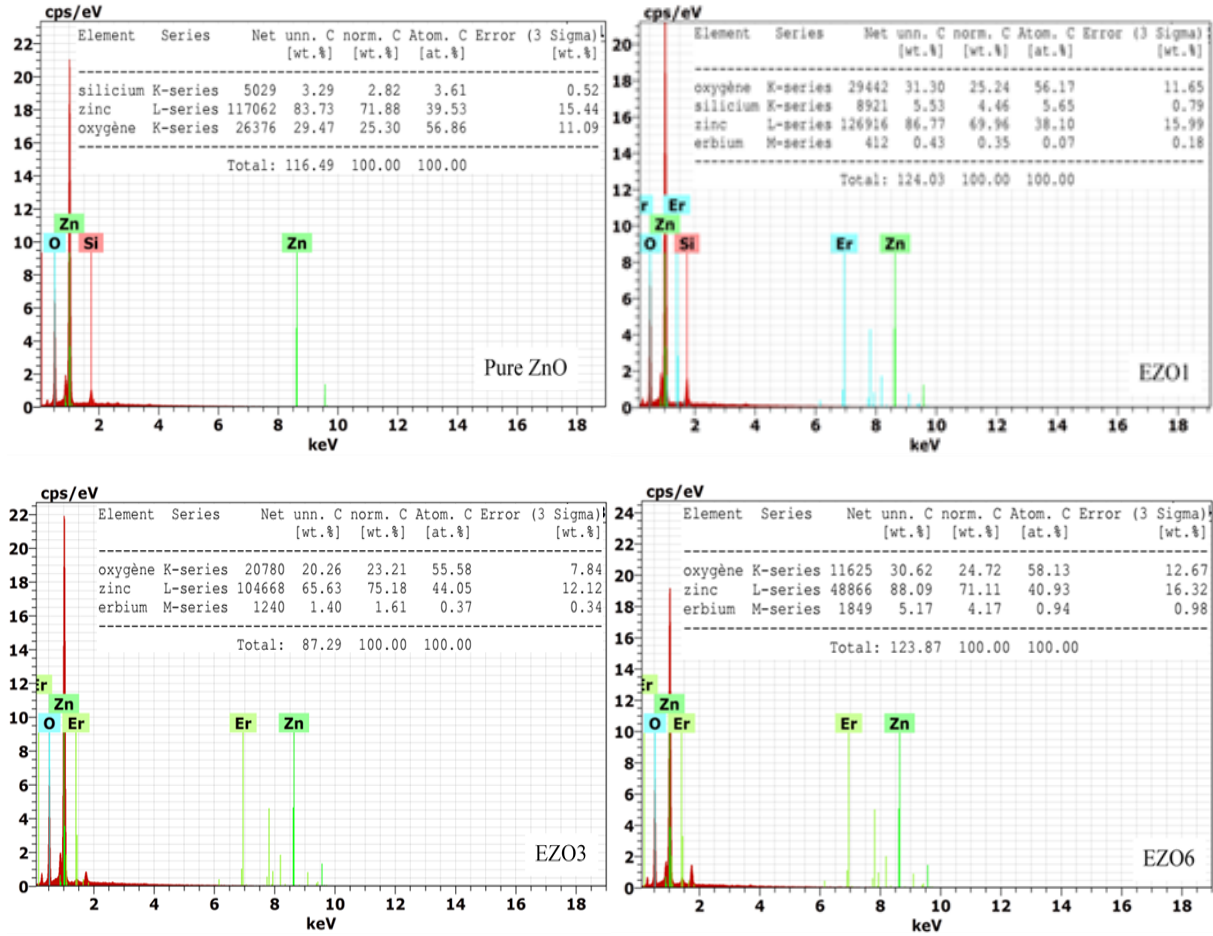
Figure III.8: EDX spectrum at various Er doping concentrations.

III.2.1.6 Raman spectroscopy

Because of the limit detection of XRD technique the possible secondary phases due to doping could not be detected [264]. That is why micro Raman spectroscopy was employed. Moreover, the high sensitivity to the crystallization and defects in crystals make Raman scattering the most important technique to reveal the existence of secondary phases of dopants atoms in the ZnO lattice.

Figure III.9, displays micro Raman spectra of undoped ZnO and Er doped ZnO thin films at room temperature in four different scattering configurations. It is well known that ZnO with wurtzite hexagonal structure belongs to the P63cm symmetry group, according to the group theory, there is eight optical phonons at the Γ point of the Brillouin zone [265], the following equation represents the optical phonons of ZnO:

$$\Gamma_{opt} = A_1 + E_1 + 2E_2 + 2B_1 \tag{5}$$

Where: $2B_1$ are Raman silent modes, E1 and A1 are both infra-red (IR) active ad Raman active, while E2 is a Raman active only. Further, A1 and E1 modes split into two optical branches (Transverse optical "TO" and Longitudinal optical "LO") because of the polar symmetry [266].

In the present work, all Raman spectrum of Pure ZnO and Er doped ZnO exhibit the same number of vibrational modes, except for the samples doped with 6 wt% of Erbium (EZO6), which has two extra-peaks, this indicate that Er did not affect too much the ZnO lattice. The four common peaks are centered at 93, 370, 439 and 571 cm^{-1}, those peaks are attributed to: E2 (low), A1(TO), E2(high) and A1(LO) respectively. The E2 (low) is associated with the vibration on Zn sub-lattice [256], while E2 (high) is the result of oxygen atom motions and it is the characteristic mode of ZnO wurtzite crystal structure [29]. A1 (LO) could be attributed to the Zn interstitials [267]. Table III.2 lists the observed Raman peaks and their assignments compared to literature, it is clear that the obtained results are close to those reported in previous works [267,268].
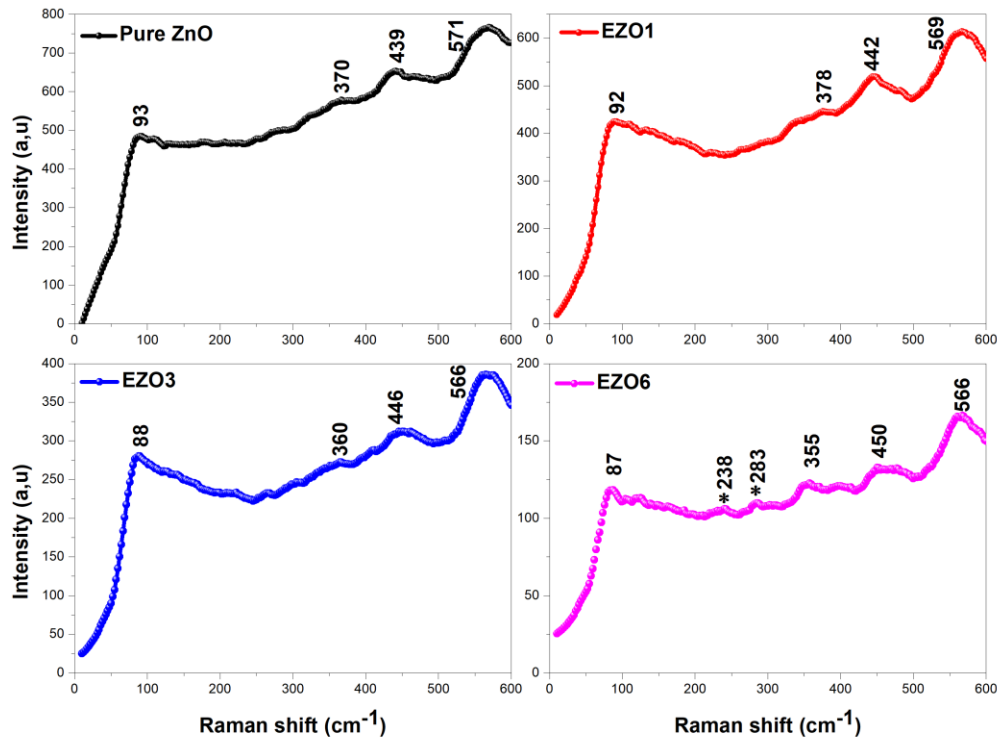
Figure III.9: Raman spectra for ZnO and Er-doped ZnO with different doping concentrations
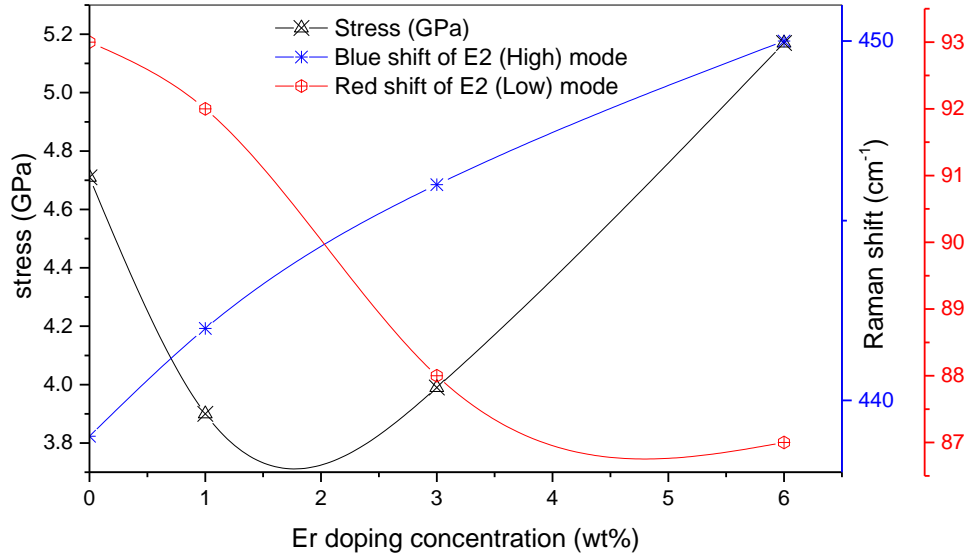
Figure III.10: Variation of stress in the EZO lattice and the Raman shift of the two characteristic modes "E2 (High) blue shifted" and "E2 (low) red shifted" as a function of Er doping concentration.

Table III.2: Raman phonon modes of all prepared samples compared to literature.

Raman Modes	Raman assignment of the present work (cm^{-1})				Ref [267]	Ref [268]
	Pure ZnO	**EZO1**	**EZO3**	**EZO6**		
E2 (low)	93	92	88	87	100	97
A1 (TO)	370	378	360	355	375	377
E2 (High)	439	442	446	450	435	437
A1 (LO)	571	569	566	566	576	580

Figure III.10 shows that the E2 (high) mode is blue shifted with increasing in Er doping concentration, while E2 (low) is red shifted. This shift towards low and high frequencies can be attributed to compressive stress [269]. Furthermore, the shift could be attributed to the intense local heating induced by laser in the ZnO nanocrystals. Alim et al [253] found that the redshift of the LO-phonon peak in the ZnO nanocrystals increases with laser power; it reaches 10 cm^{-1} for the laser power of 20 mW (UV laser). The broad band appears on the Raman peaks could be associated with oxygen vacancies in the ZnO films [270]. Er doping has a visible effect on the Raman spectra of the ZnO films, it can be noted that the intensity of all detected vibrational modes decreses by increasing Er doping concentration, this effect is related to the crystallinity. The results obtained from Raman analysis confirm the XRD results.

III.2.1.7 Fourier-transform infrared spectroscopy

To investigate deeply the Er doping effect on the synthesis of ZnO nanostructures obtained via sol gel method, Fourier Transformation infrared spectroscopy (FT-IR) spectra was employed at room temperature, in the range of 3500–300 cm−1. FT-IR spectrum gives information about chemical composition of prepared nanostructures. The FT-IR spectra of pure ZnO and ZnO: Er films are presented in **Figure III.11**. The spectra of undoped sample exhibits three band regions, first band is located between ~ 300 - 700 cm-1, this band is attributed to Zn-O stretching, which confirms the formation of ZnO wurtzite hexagonal structure [271]. The second band is located between ~ 1600 - 1800 cm-1 and its attributed to C=O bonds [262]. The third band region is situated between ~ 2300 - 2500 cm-1 and its associated with the O=C=O bonds [272]. As we can see that the effect of RRE (Er) on the ZnO FTIR spectrum is clear. Effectively, in addition of the three regions observed in pure ZnO spectrum, there is two additional bands which are located between (~ 1000 - 1300 cm-1) and (~ 3000 - 3300 cm-1) and it's assigned to C-O-C bonds and O-H stretching mode of vibration for Er doped ZnO nanocrystals [267] respectively. S.S. Alias et al [262] observed that at high pH value the O-H peaks become narrower. Furthermore, we observe that the broad peaks of Zn-O stretching and C=O bonds become narrower by increasing Er atoms concentration. As mentioned above, all prepared samples are annealed at 500°C, and this is not enough to disappear the organic residual bands. R. Salhi et al [273] reported that high annealing temperature is required to make all organic contaminations disappear. The FTIR results was found very consistent with XRD and Raman spectroscopy results.
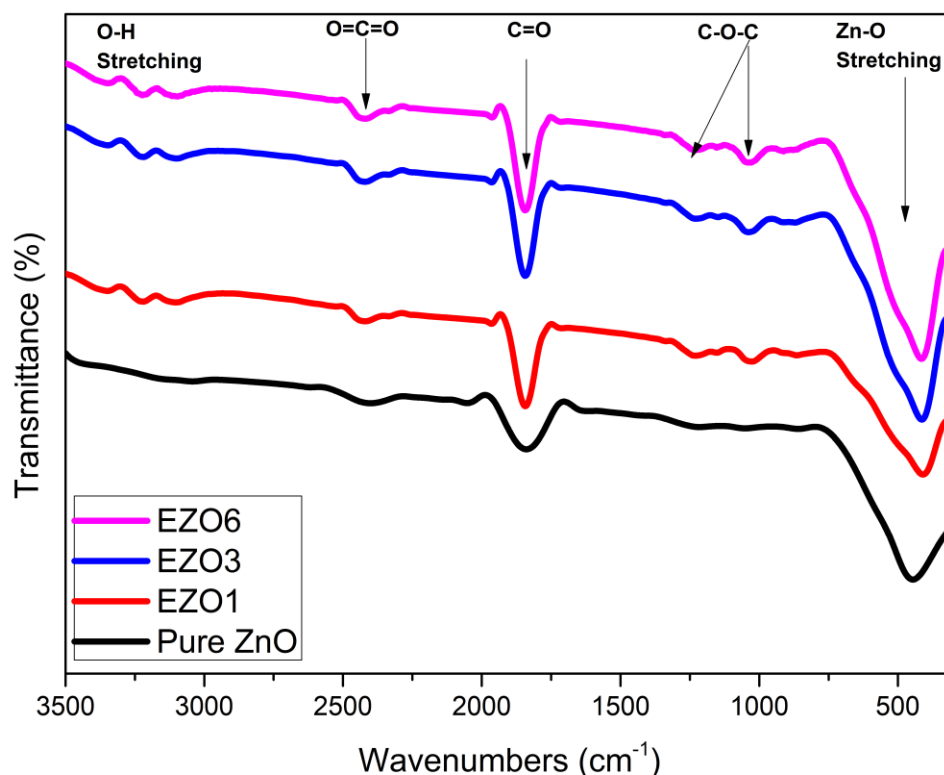
Figure III.11: *FTIR spectra for ZnO and Er-doped ZnO with different doping concentrations.*

III.2.1.8 Optical characterization (UV-Vis)

The UV-VIS spectroscopy technique provides useful information about the optical properties such as transmittance and absorption. The optical transmittance of Er doped ZnO nanostructures with various doping concentrations were recorded in the wavelength range of 200 nm–1100 nm which are shown in **Figure III.12**. it could be noticed that the samples show an average optical transmittance of about 85% in the visible region, and exhibit a sharp fall near the absorption edge seen approximately between 370 – 400 nm and this indicate the high crystallinity quality and the direct band gap nature [8]. The transmittance of all doped samples is higher than undoped samples, which means that Er ions have a great effect on the optical transmittance of ZnO nanostructures, because when increasing Er concentration the crystallites get more and more smaller, consequently the surface roughness value (RMS) decreases and for this EZO films become more transparent [274].
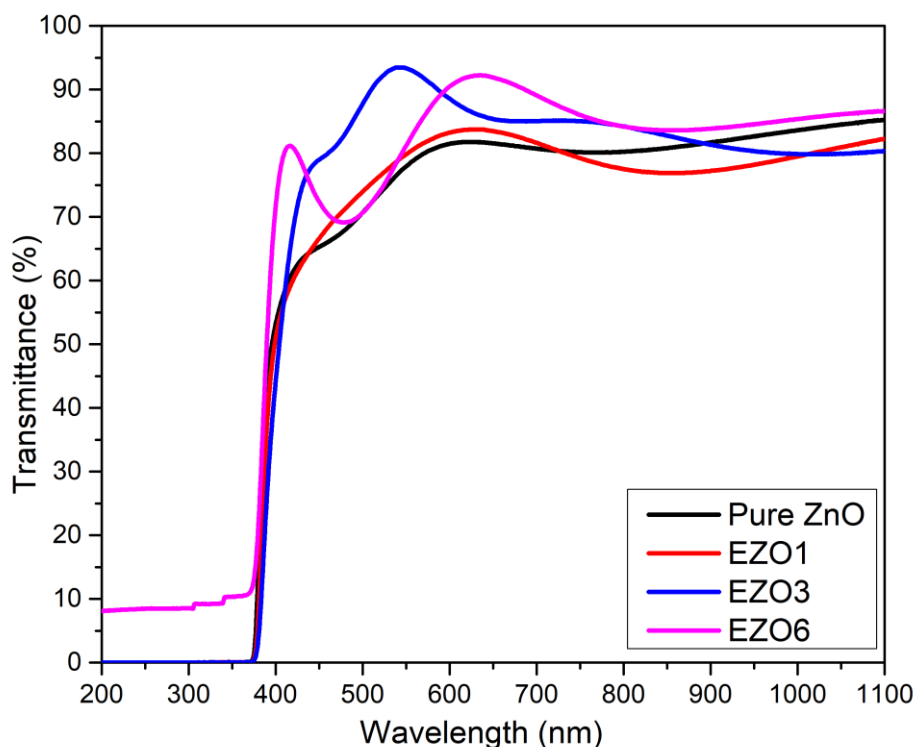
Figure III.12 *Optical transmittance spectra of undoped ZnO and EZO films at different concentration of Er.*

III.2.1.9 Band gap energy

Figure III.13 shows the Tauc's plot of ZnO and Er doped ZnO films. Eg is estimated by the extrapolation of the linear portion of $(\alpha h\nu)2$ curve downwards the hν axis it intersects the hν axis then got the value of Eg [275] . The optical band gap decreased with an increase in the Er doping concentrations from 3.25 eV for the undoped samples to approximately 3.20 eV for the doped samples. The low Eg of ZnO based nanostructures as compared to the ZnO bulk (3.37 eV) is associated with the high pH value (pH 9) [262,254]. The shrinkage of the band gap can be explained by the introduction of new impurity levels bands of RRE (Er) in the ZnO hosts matrix which leads to the modification of the crystallinity of ZnO nanostructures. The same results were reported elsewhere [276,256]. The low optical gap energy makes Er doped ZnO based thin films suitable to be used in dye-sensitized solar cell (DSSC) as a working electrode [277].
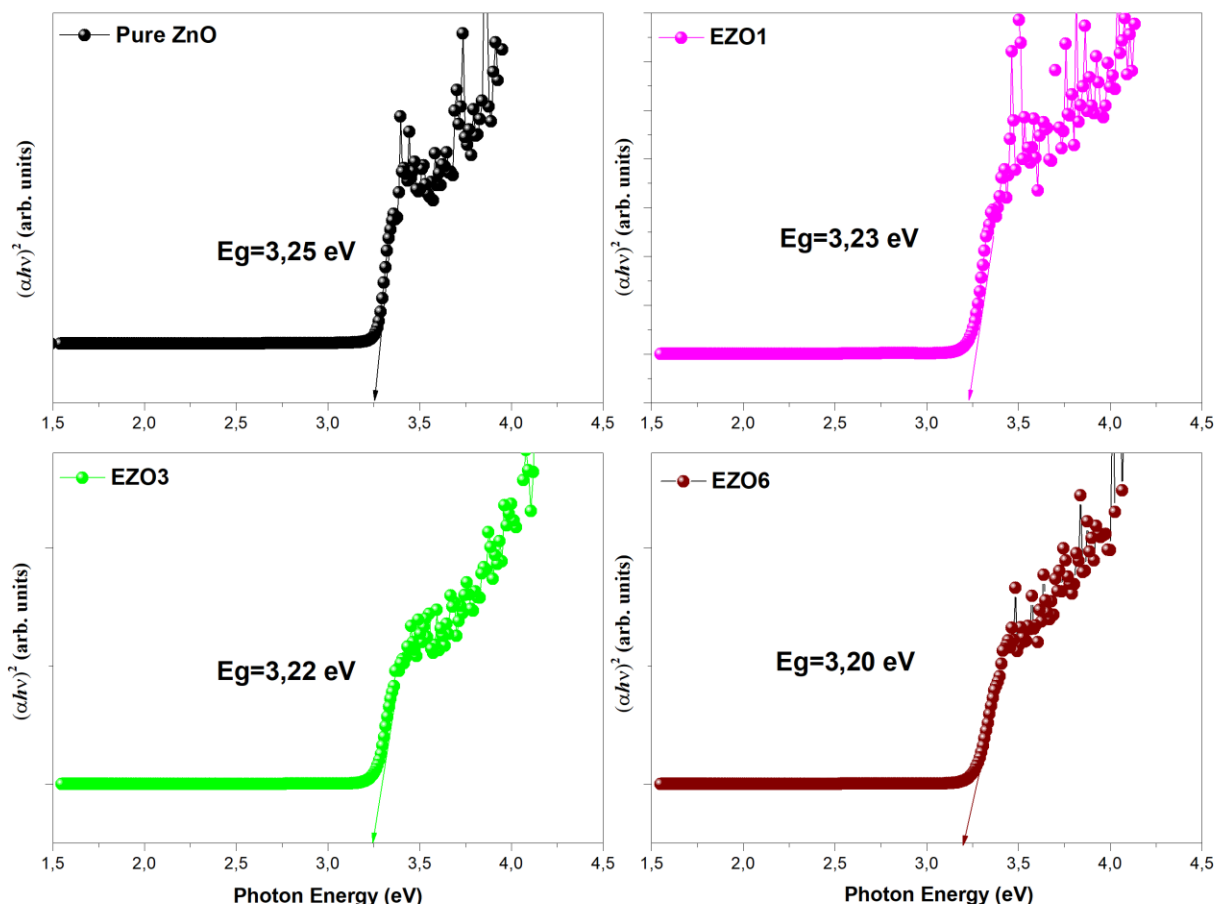
Figure III.13: Band gap variation of undoped ZnO and EZO films as the function of Er concentration

III.2.2 Part two : Ytterbium doping effect

III.2.2.1 Structural Characterization

Figure III.14 depict the typical XRD pattern of Yb-doped ZnO nanopencils with various doping concentrations (1wt%, 3wt% and 6wt%), which revealed various well-defined diffraction peaks which are corresponding to the wurtzite hexagonal phase of ZnO [278,279]. Further, the observed diffraction peaks are consistent with the reported literature and JCPDS card No. 36–1451 [280]. Diffraction peaks situated at $2\theta \approx 31.76°$, 34.45°, 36.35°, 47.66°, 56.69°, 63.01°, 68.08° and 72.69° are corresponding to the (100), (002), (101), (102), (110), (103), (112) and (004) diffraction planes of ZnO wurtzite respectively. The diffraction pattern shows that all films have a strong texture along the (002) direction. The three main diffraction peak : (100), (002), and (101) indicate the presence of a pure phase of ZnO wurtzite structure [252]. It is clearly seen that only the peaks corresponding to the ZnO wurtzite structure are observed. The samples are polycrystalline with no diffraction peaks from Yb2O3 or other impurities are found in any of the samples within the detection limit of XRD, which suggests that Yb3+ are well incorporated into Zn2+ lattice sites .

The sharp diffraction peaks, frequently observed, indicate the good crystallinity of the prepared films. The diffraction peaks correspond to (002) planes indicate that the film have preferential c-axis orientations. In essence, in zinc oxide films, preferred orientation effects are common.and the crystallites tend to stack in the c direction along the (002) axis, whch is Zinc oxide's most energetically stable crystal plane, and it is known to be the result of self-ordering effect caused by the minimization of the crystal surface free energy of each plane as well as by the interaction between the deposit material and the substrate surface. With an increase in the film's cohesive energy to the substrate, this phenomenon becomes more pronounced. Basically, all of the processes that influence grain size have an effect on grain orientation distribution. and also production processes and environments have a major impact on it. During film formation and subsequent processing, the grain orientation distribution emerges and can be regulated. If surface energy minimization contributes to the driving force for grain boundary motion at the surface of the film, the crystallographic texture of the grains at the surface of the film will evolve as grains with high energy surfaces are eliminated or occluded during thickening [281-284]. Furthermore, for applications requiring crystallographic anisotropy, an ordered c-axis orientation of ZnO crystallites perpendicular to the substrate surface is preferable [285]. As we mentioned above, all ZnO:Yb was deposited under basic environement, which promotes the formation of ZnO with enhancing growth quality [253,254], because when increasing pH, the number of hydroxides (OH-) increase which enhance ZnO growth. As seen from the **Figure III.14**, the (002) is the most sharp and intense peak located at $2\theta \approx 34.45°$ for all patterns, this indicates a high crystalline quality. the deposited films were found to change with Yb doping. All diffractions peaks intensity decreases when increasing Yb doping concentration, this may be due to the larger ionic radius of Yb3+ ions with respect to that of Zn2+.
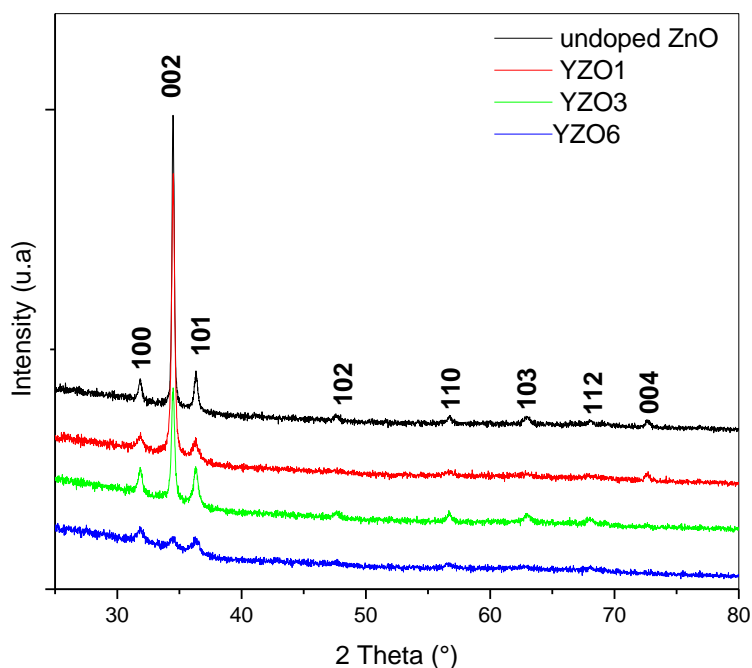
Figure III.14: *XRD pattern of Yb-doped ZnO thin films with varying doping concentrations.*

In order to attain the detailed structure information, the grains sizes were calculated. This size calculated from the (002) diffraction line using the Scherrer's formula. **Figure III.15** shows the variation of Undoped and Yb doped ZnO crystallite size as a function of doping concentration. as can be seen, The size decreases rapidly from 33 to 19 nm when the Yb concentration increases to 6 wt%. Besides the solubility limit of Yb in ZnO, this suggests that Yb acts as nucleation centers as long as Yb substitutes Zn ions in the ZnO matrix, and other cause is that the large difference between the ionic radius of RE element (Yb^{3+} with 1.008 Å) and Zn^{2+} with 0.74 Å [108].

As we can see from **Figure III.15**, the slight variation of the lattice parameters c shows a double behavior, when doping between 1 and 3wt%, "c" decreases as compared with undoped samples, but when the doping concentration exceed 3wt %, "c" increases in contrary with Erbium case. But it still just a slight variation, Due to this low solubility limit [286].
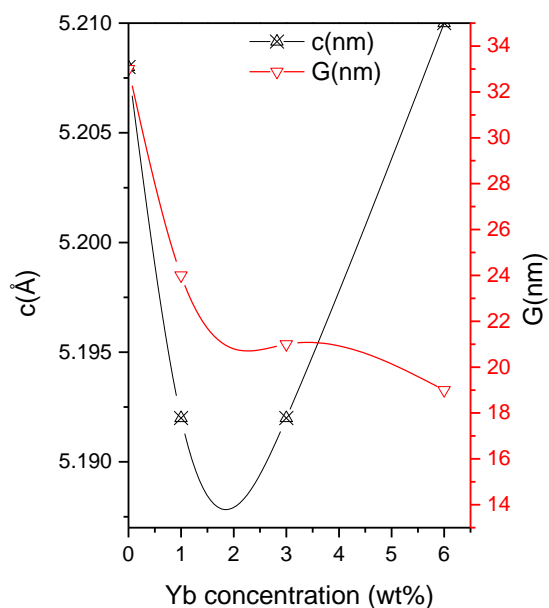
Figure III.15: *Variation of grain size and lattice parameters "C" of ZnO thin films as a function of Yb doping concentration.*

The crystallite sizes G, the values of β, The plane spacing and the lattice parameters of all samples are presented in Table III.3.

Table III.3*: Structural parameters evaluated by XRD data for deposited undoped ZnO and YZO thin film.*

Samples	2 θ (°)	β(°)	c (Å)	a (Å)	d (Å)	G (nm)	Ϭ (GPa)	RMS (nm)
Undoped ZnO	34.41	0.25	5.208	3.195	2.604	33	-8.94	6.25
YZO1	34.51	0.35	5.192	3.185	2.596	24	62.60	5.00
YZO3	34.51	0.40	5.192	3.185	2.596	21	62.60	3.48
YZO6	34.40	0.42	5.21	3.196	2.605	19	-17.88	2.98

III.2.2.2 Surface Morphology

III.2.2.3 Atomic force microscopy

In order to have a deeper insight into the surface morphology properties and the influence of the Yb doping concentration under alkaline environment (pH 9), the film surface morphology and surface roughness were studied using an AFM technique. **Figure III.16** displays 2D-3D AFM micrograph in tapping mode of ZnO thin films deposited under alkaline conditions with different Yb dopant concentration. The micrograph of undoped ZnO films shows homogeneous, compact, and granular morphology nanostructures, consisting of small grains of irregular shapes distributed uniformly around the entire glass substrate with the absence of cracks and pinholes. As can be

seen from doped ZnO micrographs, The incorporation of Yb atoms changes the surface morphology. When doped with 1 wt% Yb, the crystallite grains decrease while maintaining the same homogeneous, dense, and granular morphology, and as the doping concentration increases (3 wt% and 6 wt%), the crystallite grains get smaller and smaller. Furthermore, all AFM micrographs exhibit a smooth surface with no crack, pinholes and voids. The Root Mean Square (RMS), is a very important parameters which indicates the smoothness of a surface and gives us a clear insight to compare the topography of all elaborated nanostructures. The root-mean square (RMS) of average surface roughness for all samples was determined for scanning area of 1µm x 1µm (see table III.3). the undoped ZnO sample exhibits a granular structure with spherical shaped grains and smooth surface with an RMS of 6.25 nm. But after the insertion of Yb ions, doped films exhibit a different surface roughness which appears to be dependent on Ytterbium doping. Indeed, with the increase in concentration of Yb, the surface of the films is more or less rough with a clear and visible change in morphology. And the RMS value decrease drasticaly from 5 to 2.98 nm.

It can be noted that all samples show a smooth surface with a low roughness value which decreases when increasing Yb doping concentration (from ~ 6 nm for pure ZnO to ~ 3 nm for YZO6). It's worth noting that alkaline environments are ideal for achieving a smooth surface [254]. The low roughness value of the films surface indicates that the thickness of the prepared samples is uniform over the entire surface of the substrate [260]. Moreover, The reduction of the roughness of the films makes it possible to reduce the dispersion of the light, which increases optical transmission

Pure ZnO

YZO1

YZO3

YZO6
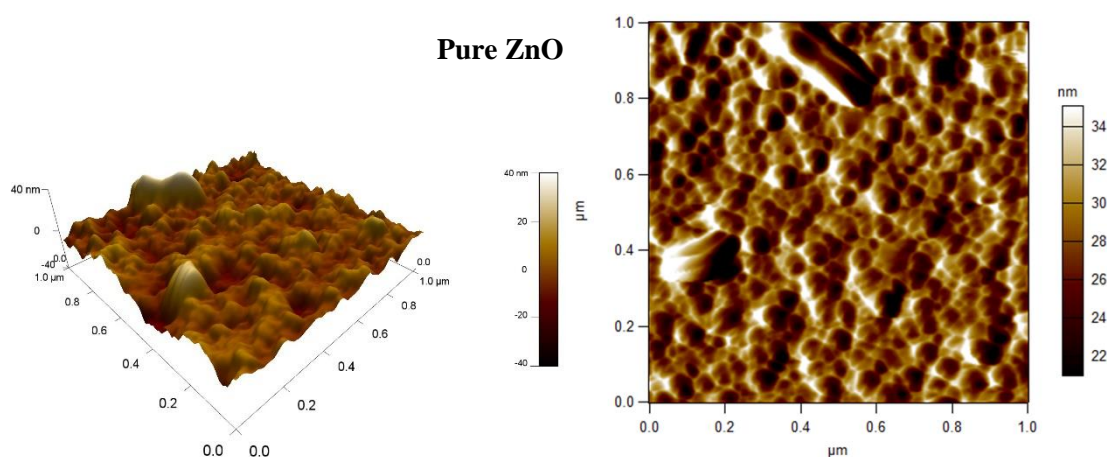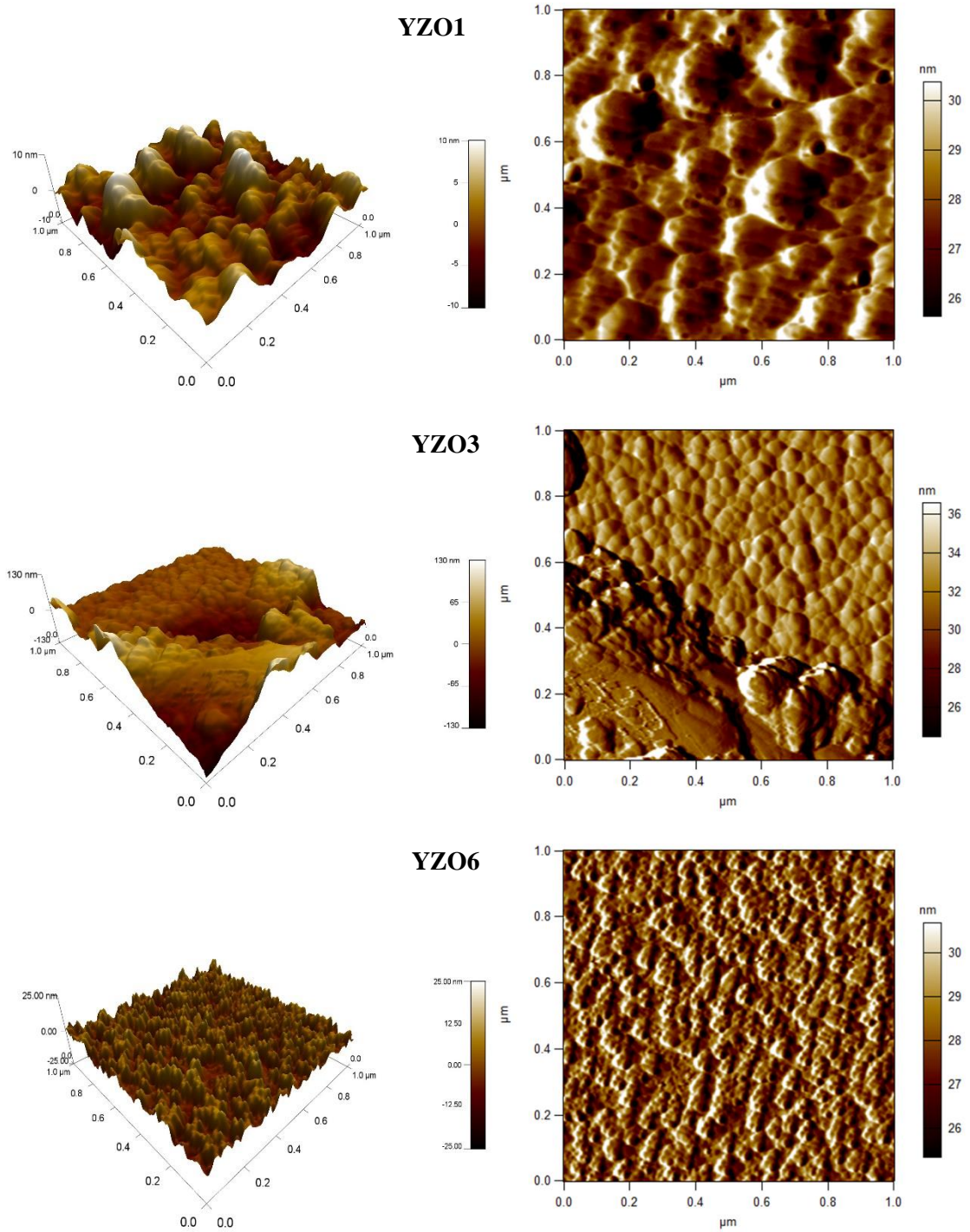
Figure III.16: *2D-3D AFM micrographs of ZnO and Yb-doped ZnO with different doping concentrations*

III.2.2.4 Scanning electron microscopy

Figure III.17 shows the surface morphologies of pure ZnO and Yb-doped ZnO deposited by Sol Gel dip coating technique. Scanning microscopy observations were used to analyze morphology of the studied samples. The micrographs show a very good crystallization and a homogenous, dense, smooth and a uniform distribution of small crystalline grains without cracks and voids. with a well-defined hexagonal character for the whole samples. As we have seen before,

the insertion of RE element (Yb+3) in the ZnO matrix affect the morphology of crystalline grains. The morphology of undoped ZnO thin films reveals a dense packing granular structure formed by agglomerations of tiny nanocrystals with irregular shapes. The increase of Ytterbium doping rate clearly influences the size and the shape of the particles. This is because the grains become entangled with each other and the particle size gradually decreases. This systematic change in crystallite size as compared with undoped samples suggests that REE ions have been successfully incorporated into the Zn lattice, i.e. more the dopant concentration increases more the Yb ions create a nucleation center [8]. In particular, the high pH value is responsible for the homogeneity, as it promotes the normal growth of crystalline grains [261]. since increased OH-access improves in the nucleation and the growth of ZnO nanocrystalline [262]. The results from SEM images are consistent with the observations from XRD.
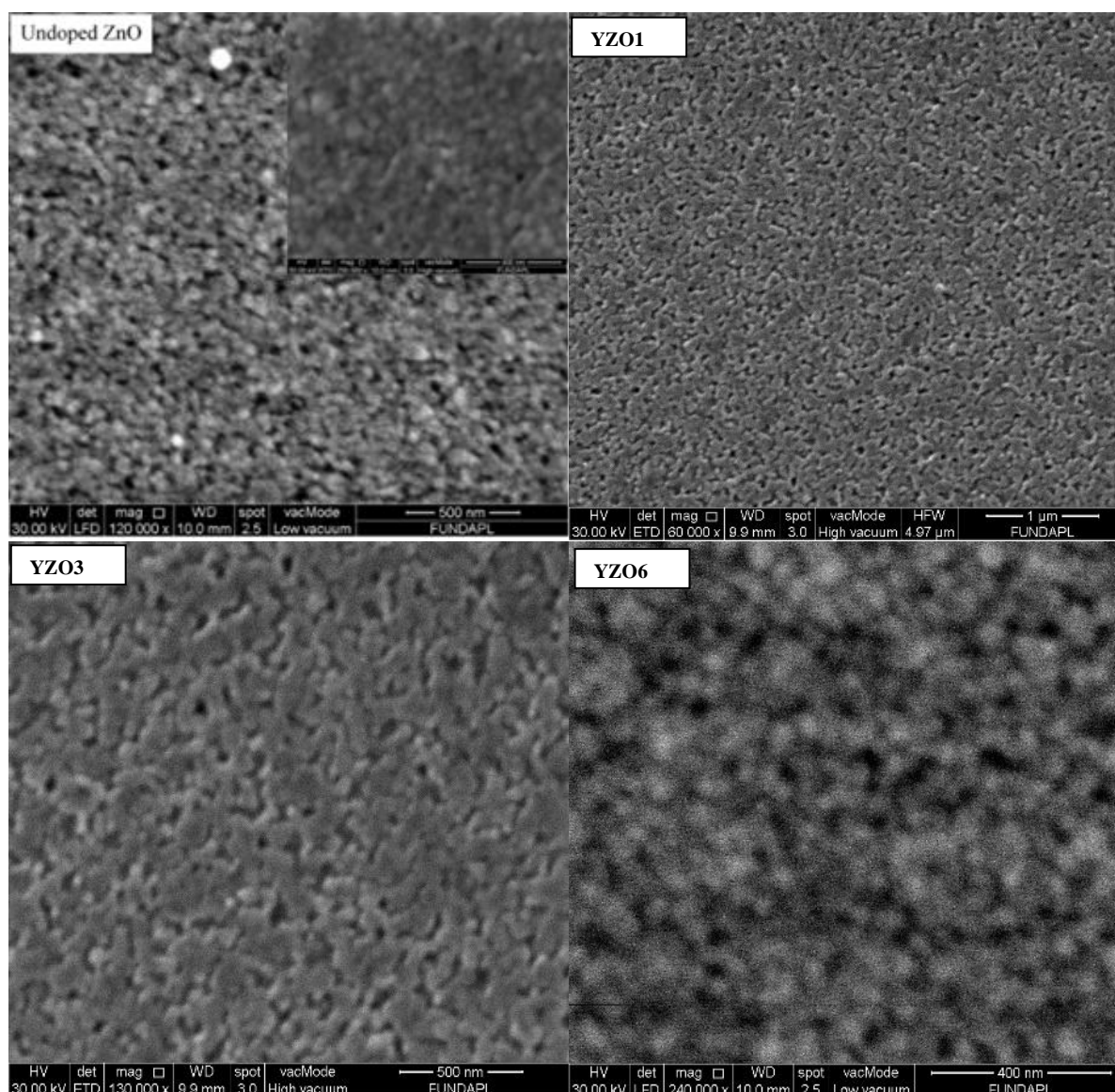
Figure III.17: SEM images for undoped ZnO and Yb doped ZnO nanoparticles.

III.2.2.5 Raman spectroscopy

The Raman signals are usually very sensitive to the structure of crystal as well as to the defects in the crystal structure. The Raman-scattering spectra of the as grown ZnO and Yb doped ZnO structures at room temperature are shown in Figure III.18.

It is obvious that all Raman spectrum of Pure ZnO and Yb doped ZnO show the same number of vibrational modes, except for the samples doped with 3 and 6 wt% of Yb, The four common peaks are centered at ~ 90, 360, 450 and 560 cm^{-1}, those peaks are attributed to: E2 (low), A1(TO), E2(high) and A1(LO) respectively. The main dominant sharp peak labeled as A1(LO) (at 571 cm-1for Undoped ZnO, 564 cm-1 for YZO1, 567 cm-1 for YZO3 and 560 cm-1 for YZO6) was observed and could be attributed to the Zn interstitials [267]. Other peaks are also usually observed, i.e. the E2(high) (at 439 cm-1for Undoped ZnO, 466 cm-1 for YZO1, 455 cm-1 for YZO3 and 468 cm-1 for YZO6) was observed and is known as Ramanactive optical phonon mode, which is the characteristic of wurtzite hexagonal phase ZnO and it is the result of oxygen atom motions [264]. the peak at ~90 cm-1 known as E2(Low), is associated with the vibration on Zn sub-lattice [256], and the peak at 360 cm-1 labeled as A1(TO) is the second-order Raman spectrum, originating from the zone boundary phonons 3E2H–E2L [287].

Table III.4 gives a comparison of the Raman peak with the theoretical values reported reported in previous works [267,268].
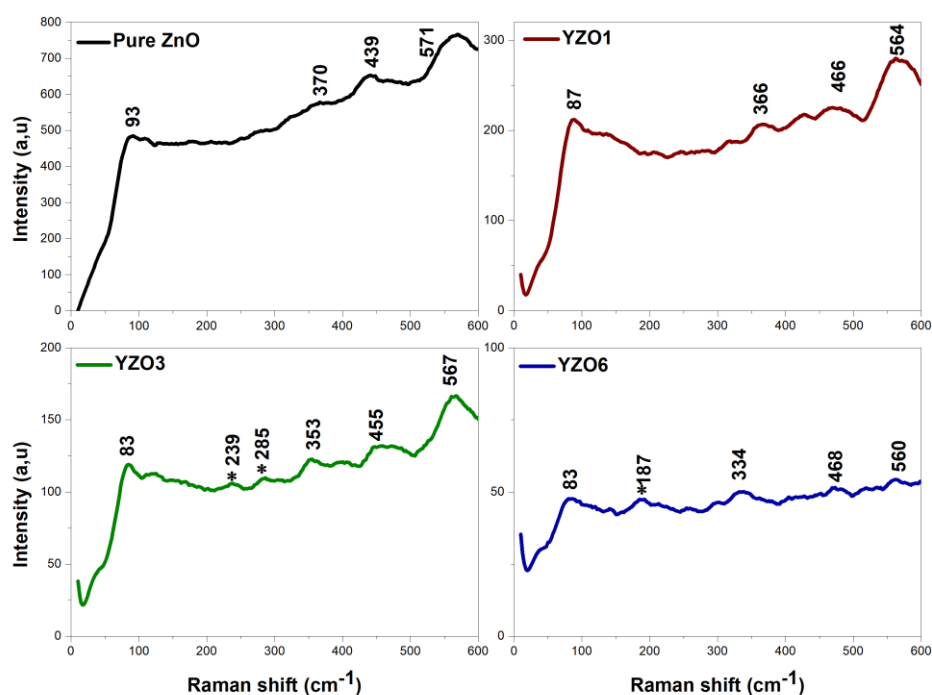
Figure III.18: Raman spectra for ZnO and Yb-doped ZnO with different doping concentrations

Table III.4: Raman phonon modes of all prepared samples compared to literature.

	Raman assignment of the present work (cm⁻¹)					
Raman Modes	**Pure ZnO**	**YZO1**	**YZO3**	**YZO6**	**Ref [267]**	**Ref [268]**
E2 (low)	93	87	83	83	100	97
A1 (TO)	370	366	353	334	375	377
E2 (High)	439	466	455	468	435	437
A1 (LO)	571	564	567	560	576	580

III.2.2.6 Fourier-transform infrared spectroscopy

In order to have a deeper understanding about the Ytterbium effect on the chemical properties of EnO nanostructures, Fourier Transformation infrared spectroscopy (FT-IR) spectra was employed at room temperature, in the range of 3500–300 cm−1. As mentioned before, the chemical composition of prepared nanostructures can be determined using the FT-IR spectrum.

The FTIR spectra of pure and RE (Yb)-doped ZnO films synthesized via sol gel route are presented in Figure III.19. We can note that all FT-IR spectra of of pure ZnO and Yb doped ZnO films exhibits three band regions which located at ~ [300 - 700 cm-1], ~ [1600 - 1800 cm-1] and

~ [2300 - 2500 cm-1] those bands are attributed to Zn-O stretching, C=O bonds and O=C=O bonds respectively [288,289]. The appearance of this bands confirms the formation of ZnO wurtzite hexagonal structure.

Furthermore, It can be noticed that the incorporation of Yb dopants has a direct impact on the ZnO bands. Effectively, the two peaks appearing in the spectrum of the doped ZnO samples, in addition of the three regions observed in pure ZnO spectrum, which are located between (~ 1000 - 1300 cm-1) and (~ 3000 - 3300 cm-1) and it's assigned to C-O-C bonds and O-H stretching mode [261] respectively. as previously stated , The O-H peaks become narrower as the amount of hydroxides increases [262]. Moreover, we perceive that when the doping rate increase the broad peaks such as Zn-O stretching and C=O bonds become narrower.The FTIR results was found very consistent with XRD and Raman spectroscopy results.
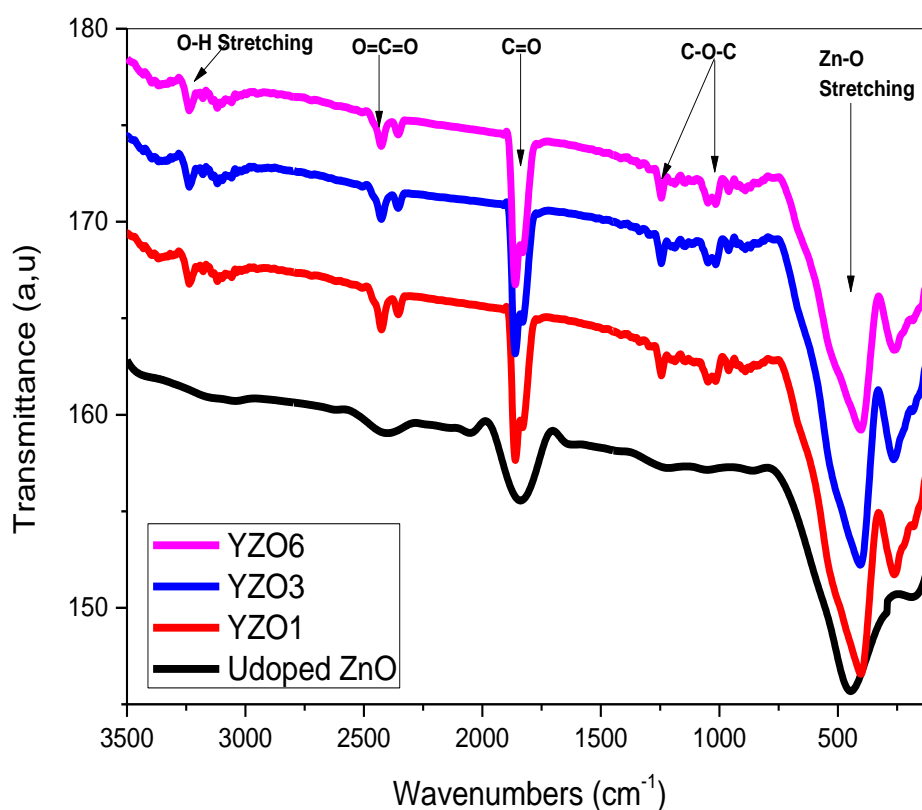
Figure III.19. FTIR spectra for ZnO and Yb-doped ZnO with different doping concentrations.

III.2.2.7 Optical characterization (UV-Vis)

Optical parameters such as the transmittance, absorption coefficient and bandgap are important because they govern the properties of a material for many applications. UV-visible-IR measurements were performed using a spectrophotometer (Shimadzu UV-1700) belonging to the department of chemistry and process engineering (UFAS Sétif 1). The wavelength scan was

performed between 200nm and 1100nm. **Figure III.20** represents the optical transmission spectra (T%) of undoped and Ytterbium doped ZnO, In order to investigate the effect of REE (Yb) on the optical transmittance of the prepared samples. we notice that all samples have high transparency in the visible region and also the presence of interference fringes due to the multiples reflections on the two interfaces of the film. The average optical transmittance in the visible region is around 85 % for non-doped films and around 90% for Yb-doped films, which mean that the Yb doping improves the optical transmission of ZnO thin films. This high transparency is attributed to the low surface roughness and also indicate the high crystallinity quality and the direct band gap nature [8,274]. In addition, all the deposited films show sharp absorption band edges at approximately 370 nm. This edge implies a good crystalline structure with minimum lattice strain, and thus it is very appropriate for optoelectronics, photovoltaics, solar cells and sensor devices [290,291].
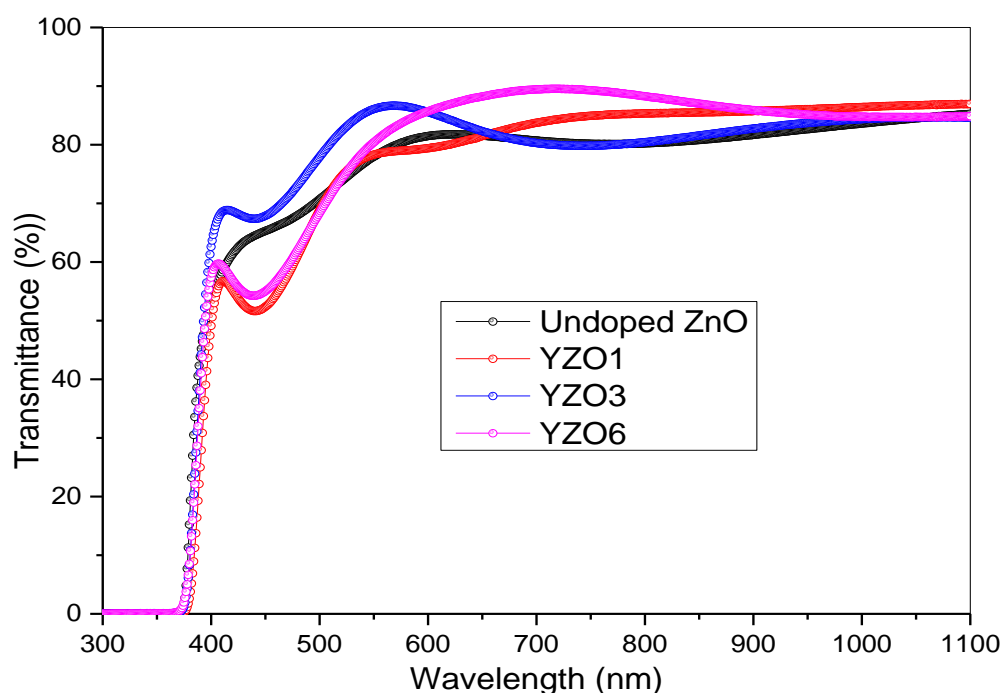
Figure III.20*: Optical transmittance spectra of undoped ZnO and YZO films at different concentration*

III.2.2.8 Band gap energy

The electronic structure of the deposited films is revealed by the optical band gap. It describes the energetic transitions allowed between the valence band and the conduction band. **Figure III.21** shows the determination of the optical band gap energy by extrapolation of the linear portion of $(\alpha h\nu)2$ curve as a function of hν for thin films of undoped and Yb-doped ZnO. The optical band gap energy of undoped ZnO films was around 3.25 eV, while that of Yb doped ZnO films was in the range of (3.24-3.23) eV. Moreover, It is clear that there is a slight decrease in band gap energy of ZnO films.

This variation of the band gap energy may explained by the introduction of new impurity levels bands of RRE (Yb) in the ZnO lattice which leads to the modification of the crystallinity of ZnO nanostructures. Furthermore, Different factors, such as the film's crystalline quality, grain size, strain, dopant, and defects, are found to affect the band gap energy of the ZnO film. [292]. This reduction in energy band gap with doping concentration may be explained by Burstein–Moss (BM) effect [293]. When ZnO is heavily doped the Fermi level will be inside the conduction band the absorption edge in this case should have a blue shift because the filled states would block thermal or optical excitations, according to Burstein [64,294]. Therefore, the observed shift in band gap energy with Yb doping can be attributed to both: the BM effect and film defects. [54]. The low Eg of ZnO-based nanostructures in comparison to ZnO bulk (3.37 eV) is related to the high pH value (pH 9) [254,262].the same results were reported elsewhere [295,296].
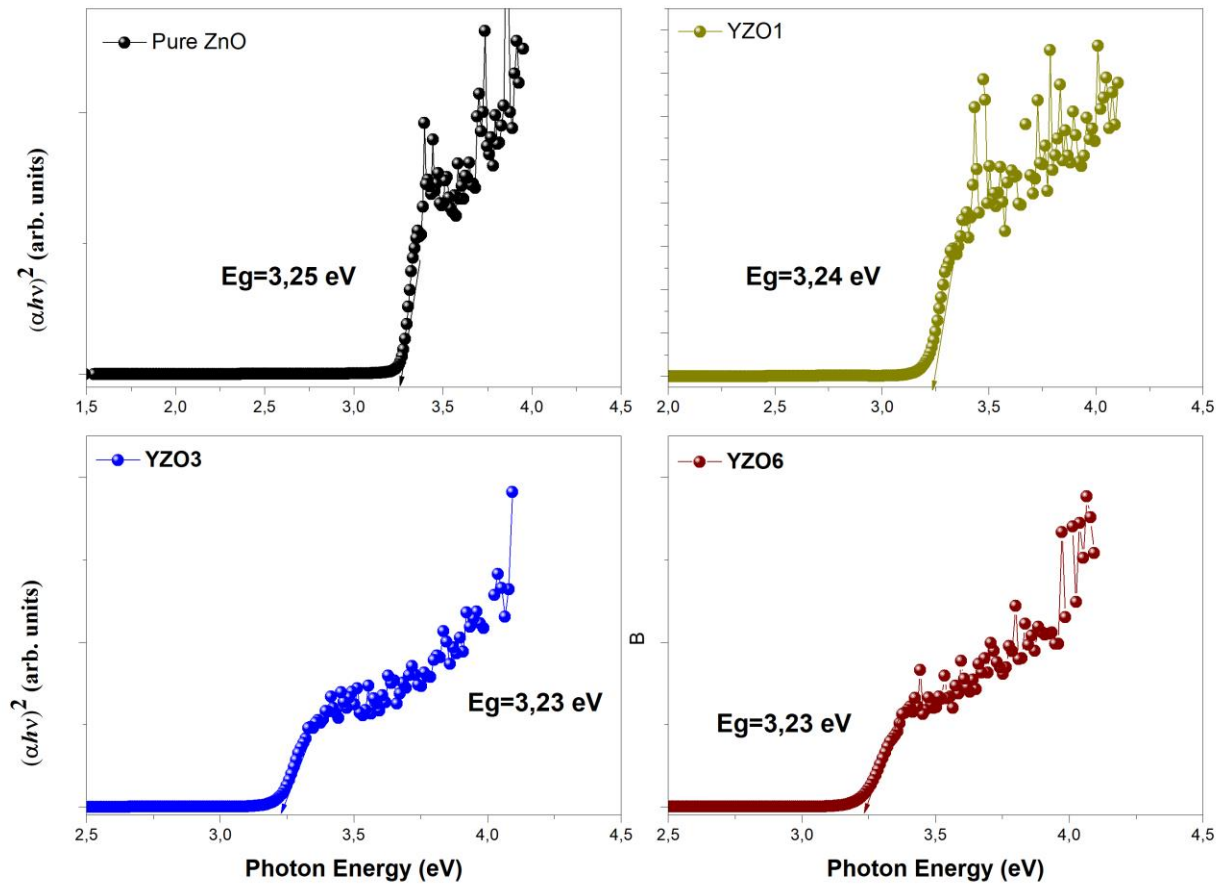
***Figure III.21:** Band gap variation of undoped ZnO and YZO films as the function of Yb concentration*

General conclusions

The main aim of this thesis work is to focus on the synthesis process and characterization of rare earth elements (REEs) doped Zinc oxide thin films under alkaline conditions using sol gel dip coating route as a low-cost deposition technique. In line with this, Erbium and Ytterbium ions (Er3+, Yb3+) have been successfully introduced in the ZnO lattice using dip coating technique with different concentrations (1 wt%, 3%wt and 6%wt), under alkaline conditions (pH 9). The structural, morphological and optical properties of prepared Er doped ZnO based thin films were considered. The doping rate effect on the structural, morphological and structural was studied.

The XRD spectra of (Er3+, Yb3+) doped ZnO showed that all samples exhibit a polycrystalline hexagonal wurtzite structure without extra peak, The high intensity and sharp peaks are attributed to the high pH value. It was found that the (002) peak is the most sharp and intense peak located at 2θ ≈ 34.50° for all patterns approximately, this indicates a good crystalline quality and a preferential c-axis orientations. As the doping rate increase, the intensity of those peaks decreases due to the large ionic radius of REEs with respect to that of Zn2+.

The morphological investigations carried out via SEM-EDX and AFM showed that all prepared REEs doped ZnO exhibit Homogenous, dense and granular morphology nanostructures. The successful substitution of Zn atoms by (Er, Yb) atoms in the ZnO crystal lattice was confirmed by EDX measurement. all samples show a low roughness value which decreases when increasing Er doping concentration.

Raman spectroscopy confirms the formation of ZnO wurtzite structure, which indicated by the appearance of Four vibrational mode (E2 (low), A1(TO), E2(high) and A1(LO)).

The FTIR results was found very consistent with XRD and Raman spectroscopy results.

It was found that a suitable amount of RE dopant is significantly crucial for obtaining a high transparent films. Effectively, the optical transmittance was found to be enhanced by RRE (Er3+, Yb3+). REEs ions have a great effect on the optical transmittance of ZnO nanostructures, because when increasing (Er3+, Yb3+) concentration the crystallites get more and more smaller, consequently the surface roughness value (RMS) decreases and for this ZnO films become more transparent. Hence, all the films showed an average of optical transparency of about 85% in the visible range, then the decreasing trend of the optical band gap lead an enhancement in the optical transmittance.

Furthermore, the band gap energy was decreased when increasing (Er3+, Yb3+) doping rate from 3.25 to approximately 3.20 eV, and this low value was associated with the alkaline environment (pH 9).

Finally, we find that doping concentration is one of the most significant factors in obtaining the optimum characteristics, this brings us to choose an appropriate concentration rate values. Moreover, based on the results analyzed above, the RE (Er, Yb) Doped ZnO films synthesized by dip coating route exhibit promising structural and optical characteristics, and they have an advantage over the others due to high stability at acceptable temperatures and low manufacturing costs, which make RE doped ZnO based thin films very suitable for solar cells applications as down converting layers and can be implemented to improve the efficiency of photovoltaic cells, especially in the field of thin film PV structures.

REFERENCES:

[1] Bayda S, Adeel M, Tuccinardi T, Cordani M, Rizzolio F. The History of Nanoscience and Nanotechnology: From Chemical-Physical Applications to Nanomedicine. Molecules. 2019;25(1):112. Published 2019 Dec 27. doi:10.3390/molecules25010112

[2] D Brabazon, Nanostructured Materials, Dublin City University, Dublin, Ireland – 2016. doi:10.1016/B978-0-12-803581-8.04103-5

[3] R. Asmatulu, Toxicity of nanomaterials and recent developments in lung disease, in: P. Zobic (Ed.), Bronchitis, InTec, 2011, pp. 95–108 (Chapter 6).

[4] C. Kumar, Nanomaterials: Toxicity, Health and Environmental Issues, Wiley-VCH, 2006.

[5] Jayaraman, Theerthagiri & Salla, Sunitha & Senthil, & Palaniyandy, Nithyadharseni & Kumar, Madan & Arunachalam, Prabhakarn & Maiyalagan, T & Kim, Hyun-Seok. A Review on ZnO Nanostructured Materials: Energy, Environmental and Biological Applications. Nanotechnology (2019).

[6] R. Kripal, AK. Gupta, RK. Srivastava, SK. Mishra, Spectrochim. Acta, Part A, 79(5) (2011) 1605-1612.

[7] S.S. Alias, A.B. Ismail, A.A. Mohamad, J. Alloys Compd, 499 (2010) 231–237.

[8] V. Kumari, V. Kumar, B.P. Malik, R.M. Mehra, D. Mohan, Opt. Commun, 285 (2012) 2182–2188.

[9] Z. Z. Gui, X. H. Liu, S. Q. Ming, J. Y. Zhang, Q. M. Xie, T. Chen, H. Q. Wang, Organic Electronics, 53 (2018) 296-302.

[10] S. M. Liu, F. Q. Liu, H. Q. Guo, Z. H. Zhang and Z. G. Wang, Phys. Lett. A, 271 (2000) 128-133..

[11] L. Tang, B. Zhou, Y. Tian, F. Sun, Y. Li, Z. Wang, Synthesis and surface hydrophobic functionalization of ZnO nanocrystals via a facile one-step solution method. Chem. Eng. J. 139 (3) (2008) 642-648.

[12] C. Chen, P. Liu, C. Lu, Synthesis and characterization of nano-sized ZnO powders by direct precipitation method. Chem. Eng. J. 144(3) (2008) 509-513.

[13] D. Perednis, L. J. Gauckler, Thin film deposition using spray pyrolysis. J. Electroceram. 14(2) (2005) 103-111.

[14] Q. Zhao, X.Y. Xu, X.F. Song, X.Z. Zhang, D.P. Yu, C.P. Li, L. Guo, Appl. Phys. Lett. 88 (2006) 033102.

[15] W. Water, S.Y. Chu, Mater. Lett. 55 (2002) 67.

[16] GUO, H.G.; ZHOU, J.Z.; LIN, Z.G. ZnO nanorod light-emitting diodes fabricated by electrochemical approaches. Electrochemistry Communications, 2008. Vol. 10, No. 1, p. 146-150.

[17] ZHANG, Q.F.; DANDENEAU, C.S.; ZHOU, X.Y.; CAO, G.Z. ZnO Nanostructures for Dye-Sensitized Solar Cells. Advanced Materials, 2009. Vol. 21, No. 41, p. 4087-4108.

[18] Zinc Oxide: Fundamentals, Materials and Device Technology. Edited by Hadis Morkoç and Ümit Özgür Copyright 2009 WILEY-VCH Verlag GmbH & Co. KGaA, Weinheim, ISBN: 978-3-527-40813-9

REFERENCES

[19] Ü. Özgür, Y.I. Alivov, C. Liu, A. Teke, M. Reshchikov, S. Doğan, V. Avrutin, S.-J. Cho, H. Morkoc, A comprehensive review of ZnO materials and devices, Journal of applied physics, 98 (2005) 11.

[20] D.R. Lide, Handbook of organic solvents, CRC Press, 1994

[21] A. Wander, F. Schedin, P. Steadman, A. Norris, R. McGrath, T. S. Turner, G. Thornton, N. M. Harrison, Phys. Rev. Lett. 86 3811 (2001).

[22] V. Staemmler, K. Fink, B. Meyer, D. Marx, M. Kunat, S. G. Gil, U. Burghaus, C. Woll Phys. Rev. Lett. 90 106102 (2003).

[23] Y. Ding, X. Y. Kong, Z. L. Wang, Phys. Rev. B 70 235408 (2004).

[24] Z. R. Dai, Z. W. Pan, Z. L. Wang, Adv. Funct. Mater. 13 9 (2003).

[25] M. H. Huang, Y. Y. Wu, H. Feick, N. Tran, E. Weber, P. D. Yang, Adv. Mater. 13 113 (2001).

[26] R. S. Wagner, W. C. Ellis, Appl. Phys. Lett. 4 89 (1964).

[27] C. Jagadish, S. J. Pearton, Thin Films and Nanostructures Processing, Properties and Application, Elsevier (2006)

[28] Jin, B.J., S. Im, and S.Y. Lee, Violet and UV luminescence emitted from ZnO thin films grown on sapphire by pulsed laser deposition. Thin Solid Films, 2000. 366(1-2): p. 107-110.

[29] J. R. Chelikowsky, Solid State Commun. 22 (1977) 351.

[30] D. Vogel, P. Krüger, J. Pollmann, Phys. Rev. B 52 (1995) R14316.

[31] A.Abdulla "Density Functional Theory investigation of structural, electronic and optical properties of Erbium Zinc Oxide alloys" doctorat thesis, Abou bekr belkaid university- tlemcen 2016.

[32] Akira Onodera and Masaki Takesada, Materials Science: Advances in Ferroelectrics, chapite 11, Edition: Aimé Peláiz Barranco (2012).

[33] Li, Z., Hu, Z., Liu, F., Hang, H., Zhang, X., Wang, Y., Jiang, L., Yin, P. and Guo, L. (2012). Lateral growth and optical properties of ZnO microcrystal on sapphire substrate. Optical Materials, 34(11), pp. 1908-1912.

[34] Djurisic, A. and Leung, Y. (2006). Optical properties of ZnO nanostructures. Small, 2(8-9), pp. 944-961.

[35] Chen, L., Hu, H. and Xiong, Z. (2013). A role of Eu-doping on electronic structure and optical properties of ZnO from first-principles. Applied Physics Frontier, 1(2), pp. 22-26.

[36] S. Xu, Z. L. Wang, One-dimensional ZnO nanostructures: solution growth and functional properties. Nano Res. 4(11) (2011) 1013-1098.

[37] N. Mir, M. Salavati-Niasari, F. Davar, Preparation of ZnO nanoflowers and Zn glycerolate nanoplates using inorganic precursors via a convenient rout and application in dye sensitized solar cells. Chem. Eng. J. 181 (2012) 779-789.

[38] N. Han, L. Chai, Q. Wang, Y. Tian, P. Deng, Y. Chen, Evaluating the doping effect of Fe, Ti and Sn on gas sensing property of ZnO. Sensor. Actuat. B-Chem. 147(2) (2010) 525- 530.

[39] H. Hartnagel, Semiconducting transparent thin films, CRC Press, 1995.

[40] P. H. Kasai, Electron spin resonance studies of donors and acceptors in ZnO, Phys. Rev. 130 (1963) 989-995..

[41] K. Vanheusden, W. L. Warren, C. H. Seager, D. R. Tallant, J. A. Voigt, and B. E. Gnade, Mechanisms behind green photoluminescence in ZnO phosphor powders, J. Appl. Phys. 79 (1996) 7983-7990.

[42] S. Yamauchi, Y. Goto, and T. Hariu, Photoluminescence studies of undoped and nitrogen-doped ZnO layers grown by plasma-assisted epitaxy, J. Cryst. Growth 260 (2004) 1-6.

[43] M. Liu, A. H. Kitai, and P. Mascher, Point defects and luminescence centres in zinc oxide and zinc oxide doped with manganese, J. Lumin. 54 (1992) 35-42.

[44] E. G. Bylander, Surface effects on the low-energy cathodoluminescence of zinc oxide, J. Appl. Phys. 49 (1978) 1188-1195.

[45] X. Yang, G. Du, X. Wang, J. Wang, B. Liu, Y. Zhang, D. Liu, D. Liu,H. C. Ong, and S. Yang, Effect of post-thermal annealing on properties of ZnO thin film grown on c-Al2O3 by metal-organic chemical vapor deposition, J. Cryst. Growth 252 (2003) 275-278.

[46] J. Zhong, A. H. Kitai, P. Mascher, and W. Puff, The Influence of Processing Conditions on Point Defects and Luminescence Centers in ZnO, J. Electrochem. Soc. 140 (1993) 3644-3649.

[47] K. Johnston, M. O. Henry, D. M. Cabe, T. Agne, and T. Wichert, Proceedings of the Second Workshop on "SOXESS European Network on ZnO, 27-30 October 2004, Caernarfon, Wales, UK.

[48] R. Dingle, Luminescent transitions associated with divalent copper impurities and the green emission from semiconducting zinc oxide, Phys. Rev. Lett. 23 (1969) 579-581.

[49] O. Lupan, S. Shishiyanu, V. Ursaki, H. Khallaf, L. Chow, T. Shishiyanu, V. Sontea, E. Monaico, S. Railean, Synthesis of nanostructured Al-doped zinc oxide films on Si for solar cells applications, Sol. Energy Mater. Sol. Cells 93 (2009) 1417.

[50] O. Lupan, L. Chow, G. Chai, L. Chernyak, O. Lopatiuk-Tirpak, H. Heinrich, Focused-ion-beam fabrication of ZnO nanorod-based UV photodetector using the in-situ lift-out technique, Phys. Stat. Sol. A 205 (2008) 2673.

[51] G. Chai, O. Lupan, L. Chow, H. Heinrich, Crossed zinc oxide nanorods for ultraviolet radiation detection, Sens. Actuators A: Phys. 150 (2009) 184.

[52] G.C. Yi, C.R. Wang, W.I. Park, ZnO nanorods: synthesis, characterization and applications, Semicond. Sci. Technol. 20 (2005) S22–S34.

[53] O. Lupan, G. Chai, L. Chow, A single ZnO tetrapod-based sensor, Sens. Actuators B: Chem. 141 (2009) 511;

[54] Z.L. Wang, Nanodevice, nanosensors and nanocantilevers based on semiconducting oxide nanobelts, in: Z.L. Wang (Ed.), Nanowires and Nanobelts–materials, properties and devices. Vol. II. Nanowires and Nanobelts of Functional Materials, Kluwer Academic Publisher, 2003.

[55] A. Janotti, C.G. Van de Walle, Fundamentals of zinc oxide as a semiconductor, Reports on progress in physics, 72 (2009) 126501.

REFERENCES

[56] S.T. Pantelides, Deep centers in semiconductors, CRC Press, 1992.

[57] A. Alkauskas, M.D. McCluskey, C.G. Van de Walle, Tutorial: Defects in semiconductors—Combining experiment and theory, Journal of Applied Physics, 119 (2016) 181101.

[58] Fahad Azad, Electrical, optical and Magnetic properties of erdoped zno grown by pulsed Laser deposition, Ph.D THESIS, The University Of Hong Kong, 2017.

[59] M. Lannoo, J. Bourgoin, Point Defects in Semiconductors I—Theoretical Aspects, volume 22 of Springer Series in Solid-State Sciences, in, Springer, Berlin, 1981.

[60] Francis Otieno Otieno, Investigation of ZnO, AZnO and Rare earth doped ZnO thin films for spectral conversion and application to solar cells, Ph.D THESIS , University of the Witwatersrand Johannesburg – South Africa, 2018.

[61] A. Janotti and C. G. Van de Walle, Physical Review B, (2007) 76(16).

[62] Yi, G. (2012). Semiconductor nanostructures for optoelectronic devices. 1st ed. Heidelberg: Springer.

[63] Chen, L., Hu, H. and Xiong, Z. (2013). A role of Eu-doping on electronic structure and optical properties of ZnO from first-principles. Applied Physics Frontier, 1(2), pp. 22-26.

[64] Sara Marouf, Propriétés Optiques des Nanostructures d'Oxyde de Zinc (ZnO), Ph.D Thesis, Université Ferhat Abbas Sétif 1 2017.

[65] Agura, H., Low resistivity transparent conducting Al-doped ZnO films prepared by pulsed laser deposition. Thin Solid Films, 2003. 445(2): p. 263-267.

[66] Chen, K.J., F.Y. Hung, and S.J. Chang. Structural Characteristic, Raman Analysis and Optical Properties of Indium-Doped ZnO Nanoparticles Prepared by Sol-Gel Method. 2007. Fayetteville, AR: Amer Scientific Publishers.

[67] Joanna Podporska-Carroll, Adam Myles, Brid Quilty, Declan E.McCormack, Rachel Fagan, Steven J.Hinder, Dionysios D.Dionysiou, Suresh C.Pillai, Anti-bacterial properties of F-doped ZnO visible light photocatalyst, Journal of Hazardous Materials. 2015.12.038

[68] R. Yousefi, F. Jamali-Sheini / Ceramics International 38 (2012) 5821–5825

[69] S. Rafique, A.K. Kasi, Aminullah, J.K. Kasi, M. Bokhari, Zafar shakoor, Fabrication of Br doped ZnO nanosheets piezoelectric nanogenerator for pressure and position sensing applications Current Applied Physics,2020.10.004.

[70] Y.-Z. Zheng et al. Electrochimica Acta 157 (2015) 258–265

[71] K. K. Kim, H. Tampo, J. O. Song, T. Y. Seong, S. J. Park, J. Lee, S. W. Kim, S. Fujita, and S. Niki, Jpn. J. Appl. Phys., (2005) 44 p. 4776.

[72] H. J. Ko, Y. F. Chen, H. Wenisch, T. Yao, and D. C. Look, Appl. Phys. Lett., (2000) 77 p. 3761.

[73] S. M. Park, T. Ikegami, and T. Ebihara, Thin Solid Films, (2006) 513 p. 90.

[74] H. Q. Le and S. J. Chua, J. Phys. D Appl. Phys., (2011) 44 p. 125104.

[75] K. W. Seo, H. S. Shin, L. J. H., K. B. Chung, and H. K. Kim, Vacuum, (2014) 101 p.250

REFERENCES

[76] B.K. Meyer et al. Superlattices and Microstructures 38 (2005) 344–348

[77] W.W. Liu, B. Yao, Z.Z. Zhang, W.F. Li, B.H. Li, C.X. Shan, J.Y. Zhang, D.Z. Shen, X.W. Fan, Doping efficiency, optical and electrical properties of nitrogen-doped ZnO films, J. Appl. Phys. 109 (9) (2011) 093518

[78] F.X. Xiu, Z. Yang, L.J. Mandalapu, J.L. Liu, Donor and acceptor competitions in phosphorus-doped ZnO, Appl. Phys. Lett. 88 (15) (2006) 152116.

[79] S. Limpijumnong, S.B. Zhang, S.H. Wei, C.H. Park, Doping by large-size-mismatched impurities: the microscopic origin of arsenic-or antimony-doped p-type zinc oxide, Phys. Rev. Lett. 92 (15) (2004) 155504

[80] B.K. Singh, S. Tripathi , Journal of Luminescence 198 (2018) 427–432

[81] I. Kaskow, P. Decyk, I. Sobczak, The effect of copper and silver on the properties of AuZnO catalyst and its activity in glycerol oxidation, Applied Surface Science.2018.02.285

[82] Gupta, C.K. and N. Krishnamurthy, Extractive metallurgy of rare earths. 2005, Boca Raton, Florida.: CRC Press.

[83] Masaed M. Almotari, Fabrication and Characterisation ofZinc Oxide Thin Films Singly doped With Trace amounts of Rare Earth Materials, Ph.D THESIS, University of Canterbury, 2013

[84] Accorsi, G., Trivalent Lanthanide Ions: Luminescence and Applications, in Chemical Sciences 2007, The University of Bologna: Bologna, Italy.

[85] Becker, P.C., N.A. Olsson, and J.R. Simpson, Erbium-doped fiber amplifiers: fundamentals and technology. Optics and photonics. 1999, San Diego: Academic Press

[86] A. J. Kenyon, Recent developments in rare-earth doped materials for optoelectronics. Prog. Quant. Electron. 26 (4) (2002) 225-284.

[87] H. L. Voncken, The Rare Earth Elements: An Introduction, Springer, (2015)

[88] Digonnet, M.J.F., Rare earth doped fiber lasers and amplifiers. 1993, New York: Marcel Dekker.

[89] Wybourne, B.G., Spectroscopic properties of rare earths. 1965, New York: Interscience Publishers.

[90] S. Cotton, Lanthanide and actinide chemistry, John Wiley & Sons Ltd, (2006)

[91] Gschneidner Jr, K.A., V.K. Pecharsky, and J.-C. Bunzli, Handbook on the Physics and Chemistry of Rare Earths. Vol. 37. 2007, Amesterdam: Elsevier.

[92] J. C. G. Bünzli, C. Piguet, Taking advantage of luminescent lanthanide ions. Chem. Soc. Rev. 34(12) (2005)1048-1077.

[93] P. Kumar, S. Singh, B. K. Gupta, Future prospects of luminescent nanomaterial-based security inks: from synthesis to anti-counterfeiting applications. Nanoscale, 8(30) (2016) 14297-14340

[94] P. Hänninen, H. Härmä, Lanthanide luminescence: photophysical, analytical and biological aspects (Vol. 7). Springer Science & Business Media. (2011).

[95] Dieke, G., Spectra and energy levels of rare earth ions in crystals. 1968, New York,USA: John Wiley & Sons, Inc.

REFERENCES

[96] Shulin Ji, Liangliang Yin, Guodong Liu, Lide Zhang, and Changhui Ye, the Journal of Physical Chemistry C 2009 113 (37), 16439-16444 DOI: 10.1021/jp906501n

[97] Toma, M.; Selyshchev, O.; Havryliuk, Y.; Pop, A.; Zahn, D.R.T. Optical and Structural Characteristics of Rare Earth-Doped ZnO Nanocrystals Prepared in Colloidal Solution. Photochem 2022, 2, 515-527.

[98] Stwertka, A., A guide to the elements. 2002, New York: Oxford University Press.

[99] Levine, A.K. and F.C. Palilla, A new, highly efficient red-emitting cathodoluminescent phosphor (YVO4:Eu) for color television. Applied Physics Letters, (1964). 5(6): p. 118-120

[100] Chrisey, D.B. and G.K. Hubler, Pulsed Laser Deposition of Thin Films. 1994: John Wiley & Sons.

[101] German, R.M., Sintering theory and practice. 1996, New York: Wiley.

[102] Rahaman, M.N., Ceramic processing and sintering. 1995, New York: M. Dekker.

[103] Lee, W.E. and W.M. Rainforth, Ceramic microstructures : property control by processing. 1994, London: Chapman & Hall.

[104] Emsley, John (2001). "Erbium". Nature's Building Blocks: An A-Z Guide to the Elements. Oxford, England, UK: Oxford University Press. pp. 136–139. ISBN 0-19- 850340-7.

[105] Balygin, A. A., et al. "Use of Uranium-Erbium and Plutonium-Erbium Fuel in Rbmk Reactors." Safety Issues Associated with Plutonium Involvement in the Nuclear Fuel Cycle. Springer Netherlands, 1999. 121-130.

[106] Hammond, C. R. (2000). The Elements, in Handbook of Chemistry and Physics (81st ed.). CRC press. ISBN 0-8493-0481-4.

[107] John Emsley, Nature's Building Blocks: An A-Z Guide to the Elements, Oxford University Press, New York, 2nd Edition, 2011.

[108] W. M. Haynes, ed., CRC Handbook of Chemistry and Physics, CRC Press/Taylor and Francis, Boca Raton, FL, 95th Edition, Internet Version 2015.

[109] Lee, C.-T. Fabrication Methods and Luminescent Properties of ZnO Materials for Light-Emitting Diodes. Materials 2010, 3, 2218-2259.

[110] S. Flickyngerova, V. Tvaro¡zek, and P. Ga¡spierik; Zinc Oxide—A ́ unique material for advanced photovoltaic solar cells; J. Elect. Eng. 61, 291 (2010)

[111] M. Berginiski, J. Hupkes, M. Schutle, G. Schope, H. Stiebig, and M. Wuttig; The effect of front ZnO:Al surface texture and optical transparency on efficient light trapping in silicon thin-film solar cells; J. Appl. Phys. 101, 074903 (2007).

[112] V.S. Bhati, M. Hojamberdiev and M. Kumar, Enhanced sensing performance of ZnO nanostructures-based gas sensors: A review. Energy Reports (2019),

[113] P. Sharma et al. Journal of Magnetism and Magnetic Materials 282 (2004) 115–121

[114] Rajendra K Saroj et al 2018 Semicond. Sci. Technol. 33 125012

REFERENCES

[115] Y.Q. Fu, J.K. Luo, X.Y. Du, A.J. Flewitt, Y. Li, G.H. Markx, A.J. Walton, W.I. Milne, Recent developments on ZnO films for acoustic wave based bio-sensing and microfluidic applications: a review, Sensors and Actuators B: Chemical,Volume 143, Issue 2,2010,606-619,

[116] F. Gao, M. M. Morshed, S. B. Bashar, Y. Zheng, Y. Shi and J. Liu, 'Electrically Pumped Random Lasing Based on Au-ZnO Nanowire Schottky Junction', Conference on Lasers and ElectroOptics, San Jose, USA, 10th–15th May 2015, Paper SM1F.7, The Optical Society, Washington, DC, USA

[117] D. J. Rogers, F. H. Teherani, P. Bove, R. McClintock, M. Razeghi, Improved LEDs and photovoltaics by hybridization and nanostructuring. SPIE Newsroom, 10(2.1201206), 004238.(2012)

[118] H. Colder, E. Guilmeau, C. Harnois, S. Marinel, R. Retoux, E. Savary, Preparation of Ni-doped ZnO ceramics for thermoelectric applications, Journal of the European Ceramic Society, Volume 31, Issue 15,2011,Pages 2957-2963,

[119] Manuel Toledano, Monica Yamauti, María Estrella Ruiz-Requena, Raquel Osorio, A ZnO-doped adhesive reduced collagen degradation favouring dentine remineralization, Journal of Dentistry, Volume 40, Issue 9, 2012, Pages 756-765,

[120] Yalan Li, Hao Sun, Yangyang Zhang, Min Xu, Sheldon Q. Shi, The three-dimensional heterostructure synthesis of ZnO/cellulosic fibers and its application for rubber composites, Composites Science and Technology,Volume 177,2019,Pages 10-17

[121] C. Jagadish and S. Pearton, Zinc Oxide Bulk Thin Films and Nanostructures, book published by Elsevier, 1st Edition, 2006.

[122] K. L. Chopra, P. D. Paulson and V. Dutta, Prog. Photovoltaics Res. Appl., 2004, 12, (23), 69

[123] Sumit Vyas , A Short Review on Properties and Applications of Zinc Oxide Based Thin Films and Devices , Johnson Matthey Technol. Rev., 2020, 64, (2), 202–218

[124] Ü. Özgür, Y. I. Alivov, C. Liu, A. Teke, M. A. Reshchikov, S. Doğan, V. Avrutin, S.-J. Cho and H. Morkoç, J. Appl. Phys., 2005, 98, (4), 041301

[125] H. Ohta and H. Hosono, Mater. Today, 2004, 7, (6), 42

[126] D. J. Rogers, F. H. Teherani, A. Yasan, K. Minder, P. Kung and M. Razeghi, Appl. Phys. Lett., 2006, 88, (14), 141918

[127] S. F. Chichibu, T. Ohmori, N. Shibata, T. Koyama and T. Onuma, Appl. Phys. Lett., 2004, 85, (19), 4403

[128] A. B. Djurišić, X. Chen, Y. H. Leung, A. M. C. Ng, ZnO nanostructures: growth, properties and applications. J. Mater. Chem. 22(14) (2012) 6526-6535.

[129] Liu, W., Bian, J., Hu, L., Liang, H., Zang, H., Sun, J., Zhao, Z., Liu, A., Du, G.: Electroluminescence from a ZnO homojunction device grown by pulsed laser deposition. Solid state Commun. 142, 655–658 (2007)

[130] Tsukazaki, A., Ohtomo, A., Onuma, T., Ohtani, M., Makino, T., Sumiya, M., Ohtani, K., Chichibu, S.F., Fuke, S., Segawa, Y.: Repeated temperature modulation epitaxy for p-type doping and light-emitting diode based on ZnO. Nat. Mater. 4, 42–46 (2004)

REFERENCES

[131] Lim, J.H., Kang, C.K., Kim, K.K., Park, I.K., Hwang, D.K., Park, S.J.: UV electroluminescence emission from ZnO light emitting diodes grown by high temperature radiofrequency sputtering. Adv. Mater. 18, 2720–2724 (2006)

[132] A. B. Djurišic, X. Liu, and Y. H. Leung, phys. Status Solidi RRL, 8 (2014) 123-132.

[133] P. Rai, S. Raj, K.-J. Ko, K.-K. Park, Y.-T. Yu, Synthesis of flower-like ZnO microstructures for gas sensor applications. Sens. Actuators B: Chem. 178, 107–112 (2013).

[134] T. Hübert, L. Boon-Brett, G. Black, U. Banach, Hydrogen sensors – A review, Sensors and Actuators B: Chemical, Volume 157, Issue 2, 2011, Pages 329-352,

[135] Vijendra Singh Bhati, Mirabbos Hojamberdiev, Mahesh Kumar, Enhanced sensing performance of ZnO nanostructures-based gas sensors: A review, Energy Reports, Volume 6, Supplement 4, 2020,Pages 46-62,

[136] P.-S. Cho, K.-W. Kim and J.-H. Lee, J. Electroceramics, 2006, 17, (2–4), 975

[137] Q. Al-zaidi, A. Suhail and W. Al-azawi, Appl. Phys. Res., 2011, 3, (1), 89

[138] T. Pustelny, P. Struk, Opto-Electron. Rev. 20, 201 (2012)

[139] Ü. Özgür, D. Hofstetter and H. Morkoç, Proc. IEEE, 2010, 98, (7), 1255

[140] A. Z. Sadek, S. Choopun, W. Wlodarski, S. J. Ippolito and K. Kalantar-zadeh, IEEE Sensors J., 2007, 7, (6), 919

[141] L. N. Balakrishnan, S. Gowrishankar and N. Gopalakrishnan, IEEE Sensors J., 2013, 13, (6), 2055

[142] L. Znaidi, G.J.A.A. Soler Illia, S. Benyahia, C. Sanchez, A.V. Kanaev, Oriented ZnO thin films synthesis by sol–gel process for laser application,Thin Solid Films,Volume 428, Issues 1–2,2003,Pages 257-262,

[143] Z. K. Tang, G. K. L. Wong, P. Yu, M. Kawasaki, A. Ohtomo, H. Koinuma and Y. Segawa, Appl. Phys. Lett., 1998, 72, (25), 3270

[144] Ü. Özgür, A. Teke, C. Liu, S.-J. Cho, H. Morkoç and H. O. Everitt, Appl. Phys. Lett., 2004, 84, (17), 3223

[145] H.-C. Chen, M.-J. Chen, M.-K. Wu, Y.-C. Cheng and F.-Y. Tsai, IEEE J. Select. Topics Quantum Electron., 2008, 14, (4), 1053

[146] H. Cao, Y. G. Zhao, H. C. Ong, S. T. Ho, J. Y. Dai, J. Y. Wu and R. P. H. Chang, Appl. Phys. Lett., 1998, 73, (25), 3656

[147] A.-S. Gadallah, K. Nomenyo, C. Couteau, D. J. Rogers and G. Lérondel, Appl. Phys. Lett., 2013, 102, (17), 171105

[148] Y.-L. Wang, F. Ren, H. S. Kim, D. P. Norton and S. J. Pearton, IEEE J. Select. Topics Quantum Electron., 2008, 14, (4), 1048

[149] A. Tsukazaki, A. Ohtomo, T. Onuma, M. Ohtani, T. Makino, M. Sumiya, K. Ohtani, S. F. Chichibu, S. Fuke, Y. Segawa, H. Ohno, H. Koinuma and M. Kawasaki, Nature Mater., 2005, 4, (1), 42

REFERENCES

[150] Y. Ryu, T.-S. Lee, J. A. Lubguban, H. W. White, B.-J. Kim, Y.-S. Park and C.-J. Youn, Appl. Phys. Lett., 2006, 88, (24), 241108

[151] J.-H. Lim, C.-K. Kang, K.-K. Kim, I.-K. Park, D.- K. Hwang and S.-J. Park, Adv. Mater., 2006, 18, (20), 2720

[152] A. Strohm, L. Eisenmann, R.K. Gebhardt, A. Harding, T. Schlötzer, D. Abou-Ras, H.W. Schock, ZnO/InxSy/Cu(In,Ga)Se2 solar cells fabricated by coherent heterojunction formation, Thin Solid Films, Volumes 480–481, 2005, Pages 162-167,

[153] Ayman M. Mostafa, Eman A. Mwafy, Synthesis of ZnO and Au:ZnO core/shell nano-catalysts by pulsed laser ablation in different liquid media, Journal of Materials Research and Technology, Volume 9, Issue 3, 2020, Pages 3241-3248,.

[154] Hiroyuki Kato, Michihiro Sano, Kazuhiro Miyamoto, Takafumi Yao, Growth and characterization of Ga-doped ZnO layers on a-plane sapphire substrates grown by molecular beam epitaxy, Journal of Crystal Growth, Volumes 237–239, Part 1, 2002, Pages 538-543,

[155] Jeong Chul Lee, Ki Hwan Kang, Seok Ki Kim, Kyung Hoon Yoon, I Jun Park, Jinsoo Song, RF sputter deposition of the high-quality intrinsic and n-type ZnO window layers for Cu(In,Ga)Se2-based solar cell applications, Solar Energy Materials and Solar Cells, Volume 64, Issue 2, 2000, Pages 185-195,

[156] D. P. Ludwig, J. Gauckler, Journal of Electroceramics, 14 (2005) 103-111.

[157] J. Orava, T. Kohoutek, T. Wagner, Deposition techniques for chalcogenide thin films, book published by Woodhead, 2014

[158] Walle, A. J. (2009). Fundamnetals of zinc oxide as a semiconductor. Institute of physics.

[159] Peter M. Martin "Handbook of Deposition Technologies for Films and Coatings, Third Edition: Science, Applications and Technology", Published by Elsevier Inc.2009, ISBN–13: 978-0-8155-2031-3.

[160] JANKOWSKI A AND HAYES J, 'The evaporative deposition of aluminum coatings and shapes with grain size control', Thin Solid Films, (2004) 447–448, 568–574.

[161] T. Minami, S. Ida, T. Miyata, Y. Minamino, "Transparent conducting ZnO thin films deposited by vacuum arc plasma evaporation", Proceedings of the 3rd International Symposium on Transparent Oxide Thin films for Electronics and Optics, Thin Solid Films, 445 (2003) 268-273.

[162] Sabrina Blackwell, Roger Smith,Modelling the growth of ZnO thin films by PVD methods and the effects of post-annealing, J. Phys. Condens. Matter 25 (2013)12

[163] R. Prabu, S. Ramesh, M. Savitha, M. Balachandar, Proc. Of the International Conference on Sustainable Manufacturing, 427, 2013

[164] Chrisey, D.B. and G.K. Hubler, Pulsed Laser Deposition of Thin Films. 1994: John Wiley & Sons.

[165] R. J. Martín-Palma and A. Lakhtakia, Vapor-Deposition Techniques, book published by Elsevier Inc (chapter 15), 2013.

[166] Eason, R. Pulsed Laser Deposition of Thin Films. New Jersey: John Wiley and Sons (2007).

[167] M. M. Almotari, PhD thesis, Fabrication and Characterisation of Zinc Oxide Thin Films Singly doped With Trace amounts of Rare Earth Materials, University of Canterbury, (2013).

REFERENCES

[168] Song, Chongmyeong & Kwon, Hyuk-Jun. (2021). Ferroelectrics Based on HfO2 Film. Electronics. 10. 2759. 10.3390/electronics10222759.

[169] Barranco A, Borras A, Elipe ARG, Palmero A. Perspectives on oblique angle deposition of thin flmsDZ From fundamentals to devices. Progress Mater. Sci. 2016;76:59–153.

[170] Angusmacleod H. Recent developments in deposition techniques for optical thin flms and coatings. In: Piegari A, Flory F, editors. Optical Thin Films and Coatings from Materials to Applications. Oxford: Woodhead Publishing Series; 2013. p. 3–-25.

[171] D. Wang, Fabrication and Characterization of ZnO Related Materials Thin Films for Optical Device Application, doctoral thesis, University of Technology Kochi Japan, 2012

[172] Sputtering Sources, Matthew M. Waite, West Chester University of Pennsylvania, West Chester,Pennsylvania; S. Ismat Shah, University of Delaware, Newark, Delaware;David A. Glocker, Isoflux Incorporated, Rochester, New York

[173] Pierson, H. O. (1999). Handbook of Chemical Vapor Deposition. New York: Noyes Publication. Q. A. Drmosh, S. (n.d.)

[174] N. D. Khan, An Investigation of the Performance and Stability of Zinc Oxide Thinfilm Transistors and the Role of High-k Dielectrics, doctoral Thesis, Montfort University, 2010.

[175] Ajit Behera, P. Mallick, S.S. Mohapatra, Nanocoatings for anticorrosion: an introduction, Corrosion Protection at the Nanoscale, chapter 13 (2020).

[176] I.V. Shishkovsky, P.N. Lebedev, Chemical and physical vapor deposition methods for nanocoatings, in: Nanocoatings and Ultra-Thin Films, 2011, pp. 57e77 (Chapter 3).

[177] A. Richardt, A.M. Durand. Les interactions ions énergétiques-solides: Editions IN FINE, Paris, France, (1997). 383

[178] Ebelmen M. Recherches sur les combinaisons des acides borique et silicique avec les éthers. Ann Chim Phys 1846;16:12966

[179] Graham T. On the properties of silicic acid and other analogous colloidal substances. J Chem Soc1864;17:31827.

[180] N. V. Kaneva, C. D. Dushkin, ZnO thin films preparation on glass substrates by two different sol-gel methods, Bulgarian Chemical Communications, Volume 44 (2012) 63–69

[181] H. Kösea; A.O. Aydina, Sol–Gel Synthesis of Nanostructured SnO2 Thin Film Anodes for Li-Ion Batteries, Acta Physica Polonica A, Vol. 121 (2012) 227-229

[182] Marcelo M. Viana, Tarik D., Nanocrystalline Titanium Oxide thin Films Prepared by Sol-Gel Process, Brazilian Journal of Physics, vol. 36, (2006) 1081-1083

[183] Sue-min Chang, Ruey-an Doong, ZrO2 thin films with controllable morphology and thickness by spincoated sol–gel method, Thin Solid Films 489 (2005) 17– 22.

[184] Klein LC, Ann Rev Mater Sci 15 (1985) 227

[185] Hench LL, West JK, Chem Rev 90 (1990) 33

REFERENCES

[186] Aragon-Santamaria P, Santos-Delgado MJ, Maceira-Vidan A, Polo-Diez LM, J Mater Chem 1(3) (1991) 409

[187] Zayat, D. L. (2015). The Sol-gel Handbook part one. In D. L. Zayat, The Sol-gel Handbook (pp. 3-27). Weinheim: Wiley-VCH.

[188] M. Hu, E. P. (2000). Sol–Gel and Ultrafine Particle Formation via Dielectric Tuning of Inorganic Salt– Alcohol–Water Solutions. Journal of Colloid and Interface Science volume 222, 20-36.

[189] Pierre, A. C. (1998). Introduction to Sol-Gel Processing. New York: Springer.

[190] J. Livage, D. G. (2001). Sol-gel electrochromic coatings and devices: a review. Solar Energy and Materials and Solar Cells volume 68, 365-381.

[191] Znaidi, L. (2010). Sol-gel deposited ZnO thin films: A review. Material Science and Engineering B

[192] M. Ohyyama, H. K. (1997). Sol-gel preparation of ZnO films with extremely preferred orientation along (002) plane from zinc acetate solution. Thin Solid films volume 306, 78-85.

[193] M.N. Kamalasanan, S. C. (1996). Sol-gel synthesis of ZnO thin films. Thin Solid Films volume 288, 112-115.

[194] H. Bahadur, A. K. Srivastava, Morphologies of Sol–Gel Derived Thin Films of ZnO Using Different Precursor Materials and their Nanostructures, Nanoscale Res Lett. Vol. 2 (2007) 469–475.

[195] X. Zhou, T. Jiang, Investigation on Temperature Sensing of Nanostructured Zinc Oxide Synthesized via Oxalate Route. Actuators B: Chem. Vol. 123 (2007) 299–305.

[196] A.M.P. Santos, Edval J. P. Santos, High quality c-axis oriented thin ZnO film obtained at very low preheating temperature, Materials Letters. Vol. 61 (2007) 3432-3435.

[197] M. Wang, J. Wang, Effect of Preheating and Annealing Temperatures on Quality Characteristics of ZnO Thin Film Prepared by Sol–gel Method, Materials Chemistry and Physics, 97 (2006) 219-225.

[198] S. Hwangbo, Y.J. Lee, K.S. Hwang, Photoluminescence of ZnO layer on commercial glass substrate prepared by sol–gel process, Ceramics International. Vol. 34 (2008) 1237–1239

[199] B. K. Choi, D. H. Chang, Optical characterization of ZnO thin films deposited by Sol-gel method, J. Mater Sci: Mater Electron. Vol. 17 (2006) 1011–1015.

[200] N. Kumar, R. Kaur, R.M. Mehra, Photoluminescence studies in sol–gel derived ZnO films, Journal of Luminescence. Vol. 126 (2007) 784–788.

[201] R.E. Marotti, C.D. Bojorge, E. Broitman, Characterization of ZnO and ZnO:Al thin films deposited by the sol–gel dip-coating technique, Thin Solid Films. Vol. 517 (2008) 1077-1080.

[202] C. Richard, A. Renaudin, V. Aimez, P. Charette, An integrated hybrid interference and absorption filter for fluorescence detection in lab-on-a-chip devices, journal of Lab on a Chip devices, 9 (2009) 1371–1376.

[203] N. Kim, J.F. Stebbins, NMR results for sol-gel and ion-beam-sputtered materials, Chemistry of Materials, 23 (2011) 3460–3465.

REFERENCES

[204] M.F. Al-Kuhaili, S.M.A. Durrani, Enhancement of the refractive index of sputtered zinc oxide thin films through doping with Fe2O3, Journal of Alloys and Compounds, 690 (2017) 453-460

[205] L.E. Scriven, Physics And Applications Of Dip Coating And Spin Coating, Article Review, j. Mater. Res., 121 (1998) 717-729.

[206] J. K. Kim, S. Thomas, P. Saha, Multicomponent Polymeric Materials, book published by Springer Media Dordrecht, 2016.

[207] Sánchez-Herencia, Antonio. (2007). Water Based Colloidal Processing of Ceramic Laminates. Key Engineering Materials - KEY ENG MAT. 333. 39-48.

[208] M. A. Aegerter and M. Mennig, Sol-gel technologies for glass producers and users, book published by Springer Media New York, 2004.

[209] Xie, K. & Fu, Qiang & Qiao, Greg & Webley, Paul. (2018). Recent progress on fabrication methods of polymeric thin film gas separation membranes for CO2 capture. Journal of Membrane Science. 572. 10.1016

[210] A. T. Wee, Selected topics in nanoscience and nanotechnology. World Scientific Publishing Co. Pte. Ltd. (2009).

[211] D. Bimberg, Semiconductor nanostructures. Springer-Verlag Berlin Heidelberg, (2008)

[212] C. Jin, Growth and Characterization of ZnO and ZnO-Based Alloys MgxZn1-xO and MnxZn1-xO, doctoral thesis, North carolina State University, 2003

[213] Cao G, Nanostructures and Nanomaterials: Synthesis, Properties & Applications, 6th edition, London, (2004)

[214] M. A. Moram, M. E. Vickers, X-ray diffraction of III-nitrides. Rep. Prog. Phys. 72(3) (2009) 036502.

[215] B. Fultz, J. Howe, Transmission Electron Microscopy and Diffractometry of Materials, Springer-Verlag Berlin Heidelberg, (2013).

[216] T. R. Prasada, M.C. S. Kumar, S. A. Angayarkanni and M. Ashok, J. Alloys Compd, 485 (2009) 413–417.

[217] Leng, Y. (2013). In Y. Leng, Materials Characterization: Introduction to Microscopic and Spectroscopic Methods (pp. 47-82). Weinheim: Wiley-VCH.

[218] Leng, Y. X-ray Spectroscopy for Elemental Analysis.b(pp. 191-219). Weinheim: Wiley-VCH, (2013).

[219] G. N. Dar, PhD thesis, Metal Oxide Nanostructures and Their Applications, University of Patras Greece, (2015)

[220] Nano-RTM, AFM User's Manual, Pacific Nanotechnology, Inc. (2003).

[221] RAMAN, C., KRISHNAN, K. A New Type of Secondary Radiation. Nature 121, 501–502 (1928).

[222] Cuscó R., Alarcón-Lladó E., Ibáñez J., Artús L., Temperature dependence of Raman scattering in ZnO. Physical Review B, 2007, vol. 75, p. 165202/1-11.

REFERENCES

[223] Yuvaraj D., Ra K. N., Optical and electrical properties of ZnO films deposited by activated reactive evaporation. Vacuum, 2008, vol. 82, p. 1274-1279..

[224] Lohumi, Santosh & Kim, moon seok & Qin, Jianwei & Cho, Byoung-Kwan. (2017). Raman imaging from microscopy to macroscopy: Quality and safety control of biological materials. TrAC Trends in Analytical Chemistry. 93. 10.1016/j.trac.2017.06.002.

[225] SILAMBARASAN, Murugesan & Shanmugam, Saravanan & Soga, Tetsuo. (2015). Raman and Photoluminescence Studies of Ag and Fe-doped ZnO Nanoparticles. International Journal of ChemTech Research. 7. 1644-1650.

[226] Helmut Günzler; Alex Williams, Handbook of analytical techniques, Weinheim; New York : Wiley-VCH, 2001.

[227] Valand R, Tanna S, Lawson G, Bengtström L. A review of Fourier Transform Infrared (FTIR) spectroscopy used in food adulteration and authenticity investigations. Food Addit Contam Part A Chem Anal Control Expo Risk Assess. 2020 Jan;37(1):19-38.

[228] Albert S, Keppler Albert K, Quack M. 2011. Handbook of high-resolution spectroscopy. Vol. 2. doi:10.1002/9780470749593.

[229] Kayani, Zohra & Iqbal, Maryam & Riaz, Saira & Zia, Rehana & Naseem, Shahzad. (2014). Fabrication and properties of zinc oxide thin film prepared by sol-gel dip coating method. MATERIALS SCIENCE-POLAND. 33. 10.1515/msp-2015-0085.

[230] Yao ZHU, Nanoparticules de ZnO pour couches luminescentes "down-shifting" de cellules solaire, PhD Thesis, Institut des Nanotechnologies de Lyon de l'INSA de LYON, 2015.

[231] A. J. C. Fiddes, Deposition of zinc oxide by spray pyrolysis, doctoral thesis, Durham University, 1993.

[232] F. M. Sanda, M. E. Victor, T. A. Monica, C. Alina, Base Theory For Uv-Vis Spectrophotometric Measurements, Article review, University of Oradea Romania, 2012.

[233] A. Hafdallah, F. Yanineb, M.S. Aida, N. Attaf, Journal of Alloys and Compounds, 509 (2011) 7267–7270

[234] R. Swanepoel, Determination of the thickness and optical constants of amorphous silicon, J. Phys. V 17, (1984) 896.

[235] A.M. El Sayed,S.Taha,Tuning the structural, electrical and optical properties of tin oxide thin films via cobalt doping and annealing, Superlattices and Microstructures 95 (2016) 1-13.

[236] M. Caglar, Y. Caglar, S. Ilican, Journal Of Optoelectronics And Advanced Materials, 8 (2006) 1410-1413.

[237] V. Srikant and D. R. Clarke, J. Appl. Phys., 83(1998) 5447-5451.

[238] M.A. Omar, Elementary Solid State Physics, Addison-Wesley Publishing Company, New-York, 4th edition (1993).

[239] M. Kamruzzaman, Kamal Uddin Azad and Jiban Podder, Synthesis and Characterization of Zn1-xCdxS Thin Films Prepared by the Spray Pyrolysis Technique, Asian Journal of Applied Sciences, 7(2014) 607-620

REFERENCES

[240] B. V. Rajendra, V. Bhat, D. Kekuda, International Journal of Emerging Technology and Advanced Engineering, 3 (2013) 82-85.

[241] U. Chaitra, D. Kekuda, K. M. Rao, j.ceramint, 43 (2017) 7115-7122.

[242] F. Yakuphanoglu, S. Ilican, M. Caglar, Y. Caglar, Journal Of Optoelectronics And Advanced Materials, 9 (2007) 2180-2185.

[243] L. Wang, M. Muhammed, Synthesis of zinc oxide nanoparticles with controlled morphology. J. Mater. Chem. 9(11) (1999) 2871-2878.

[244] X. Zhou, T. Jiang, Investigation on Temperature Sensing of Nanostructured Zinc Oxide Synthesized via Oxalate Route. Actuators B: Chem. Vol. 123 (2007) 299–305.

[245] N. Mukherjee, Sk. F. Ahmed, K.K. Chattopadhyay and A. Mondal, Electrochim. Acta. 54 (2009) 4015-4024.

[246] M. Wang, J. Wang, Effect of Preheating and Annealing Temperatures on Quality Characteristics of ZnO Thin Film Prepared by Sol–gel Method, Materials Chemistry and Physics, 97 (2006) 219-225..

[247] A. Bedia, F.Z. Bedia, M. Aillerie, N. Maloufi, B. Benyoucef, Energy Procedia, 74 (2015) 529-538

[248] S. Abed, H. Bougharraf, K. Bouchouit, Z. Sofiani, B. Derkowska-Zielinska, M. S. Aida, B. Sahraoui, Superlattices and Microstructures, 85 (2015) 370-378.

[249] D. Miao, H. Hu, L. Gan, Journal of Alloys and Compounds, 639 (2015) 400-405

[250] S. Benramache, B. Benhaoua, O. Belahssen, Optik, 125 (2014) 5864-5868.

[251] A. I. Abd Ali, International Journal of Scientific & Engineering Research, 5 (2014) 2250-2256.

[252] Yu. Kai-sheng, S. Jian-ying, Zh. Zai-li, L. Yong-mei and Wei Liu, Journal of Nanomaterials, (2013) 1-5.

[253] K. A. Alim, V. A. Fonoberov, M. Shamsa, and A. A. Balandin, J. Appl. Phys, 97 (2005) 124313-124318.

[254] K Sivakumar, V. S. Kumar, N. Muthukumarasamy, M. Thambidurai and T S Senthil, Bull. Mater. Sci, 35(3) (2012) 327–331.

[255] G. Marris, V. Volotchaev and T.T. M. Palstra, New J. Phys, 6 (2004) 153-165.

[256]] K. Siraj, J. Z. Hashmi, S.Naseem, M. S. Rafique, S. Shaukat, Materials Today: Proceedings, 2 (2015) 5365 – 5372.

[257] P.P. Murmu, J. Kennedy, B.J. Ruck, J. Leveneur, Nucl. Instrum. Methods Phys. Res., Sect. B, 359 (2015) 1–4.

[258] N.K. Divya, P.P. Pradyumnan, Mater. Sci. Semicond. Process, 41 (2016) 428–435.

[259] R. Vettumperumal, S. Kalyanaraman, R. Thangavel, J. Lumin, 158 (2015) 493-500.

[260] R. Ashiri, A. Nematib, M. S.Ghamsaric, Ceram. Int., 40 (2014) 8613–8619.

[261] S. Bhatia, N. Verma, R.K. Bed, Opt. Mater, 62 (2016) 392-398.

REFERENCES

[262] S.S. Alias, A.B. Ismail, A.A. Mohamad, J. Alloys Compd, 499 (2010) 231–237..

[263] R. S. Sreedharan, R. R. Krishnan, R. J. Bose, V.S. Kavitha, S. Suresh, R. Vinodkumar, S.K. Sudheer, V.P. M. Pillai, J. Lumin, 184 (2017) 273–286.

[264] M. Ram, G. S. Arya, Kusum Parmar, R. K. Kotnala and N. S. Negi, International Journal of Advances in Engineering & Technology, 8(3) (2015) 329-336.

[265] J. Marquina, Rev. Mex. Fıs, S 53 (7) (2007) 170–173.

[266] B. Cao, W. Cai, H. Zeng, and G. Duan, J. Appl. Phys, 99 (2006) 073516.

[267] R. Zamiri, A. Kaushal, A. Rebelo, J.M.F. Ferreira, Ceram. Int., 40 (1-B) (2014) 1635-1639.

[268] R. Zamiri, A.F. Lemosa, A. Rebloa, H.A. Ahangarb, J.M.F. Ferreira, Ceram. Int., 40 (1-A) (2014) 523-529.

[269] N.K. Hassan, M.R. Hashim, M. Bououdina, Superlattices Microstruct, 62 (2013) 182–191.

[270] X.L. Xu, S.P. Lau, J.S. Chen, G.Y. Chen, B.K. Tay, J. Cryst. Growth, 223 (2001) 201–205.

[271] K.L. Foo, M. Kashif, U. Hashim, M.E. Ali, Curr. Nanosci, 9 (2013) 288-292.

[272] C. Pholnak, C. Sirisathitkul, S. Suwanboon, D. J. Harding, Materials Research, 17(2) (2014) 405-411.

[273] R. Salhi, R. Maalej, M. Fourati, Y. Guyot, O. Chaix-Pluchery, L. Rapenne, C. Jiménez, J. L. Deschanvres, J. Lumin, 131 (2011) 2311–2316.

[274] T. R. Prasada, M. C. Santhosh Kumar, J. Alloys Compd, 509 (2011) 8676– 8682.

[275] J. Tauc. Optical Properties of Solids 22, F. Abeles, Ed., North Holland Pub, Amsterdam, (1970).

[276] I. Soumahoro, G. Schmerber, A. Douayar, S. Colis, M. Abd-Lefdil, N. Hassanain,

[277] G. Boschloo, T. Edvinsson, A. Hagfeldt, Handbook of Nanostructured Materials for Solar Energy Conversion, T. Soga (editor), Elsevier B.V, Amsterdam, chapter 8 (2006) 227–254.

[278] A. Souissi, A. Boukhachem, Y. BenTaher, A. Ayadi, A. Mefteh, M. Ouesleti, S. Guermazi, M. Amlouk, Optik, 125 (2014) 3344-3349

[279] N. Renaut, M. Jimenez, J. Dutroncy, M. Traisnel, Thin Solid Films, 589 (2015) 161-164

[280] A. Umar, R. Kumar, G. Kumar, H. Algarni, and S. H. Kim, J. Alloys Compd. 648, 46 (2015)

[281] D. S. Bhachu, G. Sankar, I.P. Parkin, Aerosol assisted chemical vapor deposition of transparent conductive zinc oxide films, Chem. Mater. 24 (2012) 4704–4710.

[282] D. S. Bhachu, G. Sankar, I.P. Parkin, Aerosol assisted chemical vapor deposition of transparent conductive zinc oxide films, Chem. Mater. 24 (2012) 4704–4710.

[283] Bailin Zhu, Kun Lü, Jun Wang, Taotao Li, Jun Wu, Dawen Zeng, Changsheng Xie, J. Vac. Sci. Technol. A 31 (6) 061513 (2013)

[284] X. Jiang, C. L. Jia, B. Szyszka, Appl. Phys. Lett. 80 (2002) 3090

REFERENCES

[285] Nicola R. S. Farley, Christopher R. Staddon, Lixia Zhao, Kevin W. Edmonds, Bryan L. Gallagher, Duncan H. Gregory, J. Mater. Chem. 14 (2004) 1087-1092.

[286] Soumahoro, G. Schmerber, A. Douayar, J. Appl. Phys. 109, 033708 (2011).

[287] Aurangzeb Khan, J Pak Mater Soc 2010; 4(1).

[288] Kumar, H., Rani, R.: Structural and optical characterization of ZnO nanoparticles synthesized by microemulsion route. Int. Lett. Chem. Phys. Astron. 19, 26–36 (2013)

[289] Hernandez, A., Maya, L., S´anchez-Mora, E., S´anchez, E.M.: ´Sol-gel synthesis, characterization and photo-catalytic activity of mixed oxide ZnO-Fe2O3. J. Sol-Gel Sci. Technol. 42, 71–78 (2007)

[290] M.A. Rafea, N. Roushdy, Determination of the optical band gap for amorphous and nanocrystalline copper oxide thin films prepared by SILAR technique, J. Phys. D Appl. Phys. 42 (2009) 15413.

[291] K. Ravichandran, R. Mohan, N.J. Begum, S. Snega, K. Swaminathan, C. Ravidhas, B. Sakthivel, S. Varadharajaperumal, Impact of spray flux density and vacuum annealing on the transparent conducting properties of doubly doped (Sn þ F) zinc oxide films deposited using a simplified spray technique, Vacuum 107 (2014) 68–76.

[292] [52] R. S. Sreedharan, R. Vinodkumar, I. Navas, R. Prabhu, V. M. Pillai, Influence of Pr Doping on the Structural, Morphological, Optical, Luminescent and Non-linear Optical Properties of RF-Sputtered ZnO Films. J.O.M. 68(1) (2016) 341-350

[293] E. Burstein, Phys. Rev. 93 (1954) 632.

[294] S. Sharma, R. Vyas, N. Sharma, V. Singh, A. Singh, V. Kataria, B. K. Gupta, Y.K. Vijay, Highly efficient green light harvesting from Mg doped ZnO nanoparticles: Structural and optical studies, J. Alloys Compd. 552 (2013) 208–212.

[295] Mao, Caiying & Li, Wanjun & Wu, Fang & Dou, Yuanyao & Liang, Fang & Ruan, H. & Kong, C.. (2015). Effect of Er doping on microstructure and optical properties of ZnO thin films prepared by sol–gel method. Journal of Materials Science: Materials in Electronics. 26. 10.1007/s10854-015-3550-x.

[296] W.J. Li, C.Y. Kong, H.B. Ruan, G.P. Qin, L. Fang, X.D. Meng, H. Zhang, P. Zhang, Q. Xu, Investigation on the formation mechanism of In–N codoped p-type ZnCdO thin films: experiment and theory. J. Phys. Chem. C 118, 22799–22806 (2014)